A NEW MODEL OF THE IO-CONTROLLED JOVIAN DECAMETRIC RADIATION

A thesis presented in partial fulfillment of the requirements for the degree of Doctor of Philosophy of Rhodes University

by

CHRISTOPH K. GOERTZ Dipl. Phys. (Berlin)

Department of Physics,
Rhodes University,
G R A H A M S T O W N,
South Africa.

December, 1971.

Except where it is obvious that I am describing the work of others, the work presented in this thesis is my own.

TABLE OF CONTENTS

ACKNOWLEDGEMENTS

I would like to thank my supervisor Professor J.A. Gledhill, who has introduced me to this exciting field of astrophysics, for his interest in my work and for the many helpful discussions we have had. Also, I would like to thank Mr P. Deift for numerous stimulating and most productive hours and nights of debate.
Dr A.D.M. Walker and Professor E. Baart have always been willing to discuss certain aspects of this thesis in spite of the demands of their own commitments. I am very grateful to both of them. Dr A.D.M. Walker has also corrected certain stylistic errors.
I would also like to thank Dr G.M. Gruber, who has supplied me with many valuable experimental data and who has always taken a keen interest in this work.
Thanks also to Mr A. Haschick, Mr J. Greener and Mr C. Way-Jones for the computing they have done for me. Their patience has always been remarkable.
I would also like to thank Mrs M. Visser and Mrs M. Zimmerman for their expert typing which required as much ingenuity in deciphering my script as did my attempt to decipher Jupiter's decametric handwriting.
The assistance of Mr G. Walters in connection with the reproduction of this thesis is also very much appreciated.

Last but not least, I would like to thank my wife for her encouragement and patience with spells of bad temper when things did not work out as they should have.

1. INTRODUCTION

Jupiter, the largest planet in the solar system, is not only an emitter of thermal radiation like any other planet. Jupiter also emits relatively high-intensity non-thermal radiation in two bands, the decimetre wavelength range and the decametre wavelength range ($5\ \text{MHz} < f < 40\ \text{MHz}$). The decimetric radiation is believed to be due to synchrotron radiation of electrons trapped in a kind of Jovian "Van Allen belt". This thesis deals almost exclusively with the decametric radiation. Although the decametric radiation has been observed for 15 years since its discovery by Burke and Franklin in 1955, there is no generally accepted theoretical model of its generation to be found in the literature as yet. This is not surprising, as there are many complex and confusing aspects of the radiation. And since our knowledge of the Jovian ionosphere, magnetosphere and magnetic field is very limited indeed, every theoretical model must be based on some more or less well justified assumptions. It is, however, possible to draw some conclusions from the observed properties of the decimetric and decametric radiation.

1. The radiation in both bands is polarized. It has been shown that at least part of the polarization is an intrinsic property of the radiation source at Jupiter. This indicates the existence of a Jovian magnetic field. The magnitude and shape of the magnetic field, however, is open to discussion, although a dipole field does seem to be a good approximation at least for large distances from Jupiter. There are observations, both in the decametric and decimetric range, that can be interpreted to indicate an equatorial field strength B_E between 5 and 30 G.

2. The high intensity of the non-thermal decametric

radiation calls for some coherent radiation mechanism. (This argument is partly based on the small source size of the radiation.) There are basically three radiation mechanisms suggested to be responsible for the decametric radiation. Warwick (1961, 1964, 1967, 1970) believes that energetic electrons travelling along magnetic field lines emit Cerenkov radiation slightly below the local electron gyrofrequency. This model calls for a thin, low-density Jovian ionosphere. Ellis (1965) and also Goldreich and Lynden-Bell (1969) suggest Doppler-shifted cyclotron radiation as the radiation mechanism. Ellis' theory involves beaming due to refraction, thus calling for an extended dense ionosphere, whereas Goldreich and Lynden-Bell propose a radiation mechanism which provides for an intrinsic beaming without the need for refraction. A thin low density ionosphere seems to fit their model better than an extended one. Gledhill (1967), suggests transformation of plasma waves into electromagnetic waves, a possibility also mentioned by Zheleznyakov (1970). This model calls for a high-density ionosphere and, for reasons which will be described later, an extension of the ionosphere out to Jupiter's innermost Gallilean sattelite Io, which orbits Jupiter with a mean radius of $\approx 5.9\ R_J \simeq 400\ 000$ km (R_J = Jupiter Radius). All three mechanisms require the existence of a magnetic field in some way or other. The equatorial field intensity in the various models lies between 10 - 30 G. Even a crude comparison of these models, shows that the problem of the Jovian ionosphere and magnetosphere is one of great importance. A model of the Jovian ionosphere and magnetosphere will be described in detail in Chapter 3.

3. The most puzzling aspect of the decametric radiation is the strong control of Io over most of the higher frequency ($f > 20$ MHz) decametric radiation.

Some observations of this effect will be presented in Chapter 2. Gledhill (1967) suggests that the radiation is emitted in Io's vicinity. This meets with some difficulties which will be described later. If the radiation is generated in Jupiter's ionosphere, one faces the problem of explaining how such a relatively small satellite as Io can exert a strong influence over a distance about 150 times its own diameter. Except for Goldreich and Lynden-Bell (1969), who assume that Io acts as a sort of unipolar generator driving currents along field lines into the ionosphere, no serious attempt has been made to account for the influence of Io over such a large distance. This thesis is mainly concerned with this aspect. It is suggested that Io emits hydromagnetic waves of considerable amplitude travelling along the magnetic field lines into the Jovian ionosphere. It is known (Warwick, 1967 and Montgomery, 1958) that large amplitude hydromagnetic waves steepen into shock waves, an effect which is likely to occur in the Jovian magnetosphere. Part of the energy of these shock waves will be transformed into radio waves which can be received at earth. These processes will be described in more detail in Chapters 5 and 6.

In Chapter 6 it will be shown how the model can be applied to the explanation of a considerable number of observed properties of the decametric radiation. Although the proposed model is still based on a number of assumptions and some of the calculations only have approximative value, it is believed that the agreement between observations and theoretical predictions in some areas, as described in Chapter 6, is quite encouraging.

2. Some Observations of Jupiter's Decametric Radiation

In this chapter some of the observed properties of Jupiter's decametric radiation will be described. Since this thesis deals with a theoretical explanation of the Io-related radiation, only a limited selection of observations will be presented. Most of these have been published and extensively described by other authors. Thus only short descriptions and references to the original papers are believed to be sufficient. The selection of some aspects as the more important ones is, of course, open to prejudice. On the other hand, the collected data, are so numerous that some kind of selection must be done, to keep this purely descriptive chapter at a reasonable length.
For a more detailed review of experimental results the reader is referred to the excellent review articles by Warwick (1964, 1967, 1970) and Carr and Gulkis (1970).

2.1 Intensity and Source Size

Jovian decametric radiation has been observed between 5 MHz and 40 MHz. No storms have been detected above 42 MHz. The average power spectrum of the radiation from Jupiter is shown in figure (1). Although individual bursts involve much higher power densities, an average power density of 300 watts/Hz seems to be a fair estimate of the power density involved in a storm. The average bandwidth of a storm is about 1 MHz, giving a value of 3×10^8 W for the power involved in an average burst. Warwick (1964), assuming beaming of the radiation, derives a value of 10^7 W for an individual storm. In this thesis the average power will thus be taken as 10^8 W.

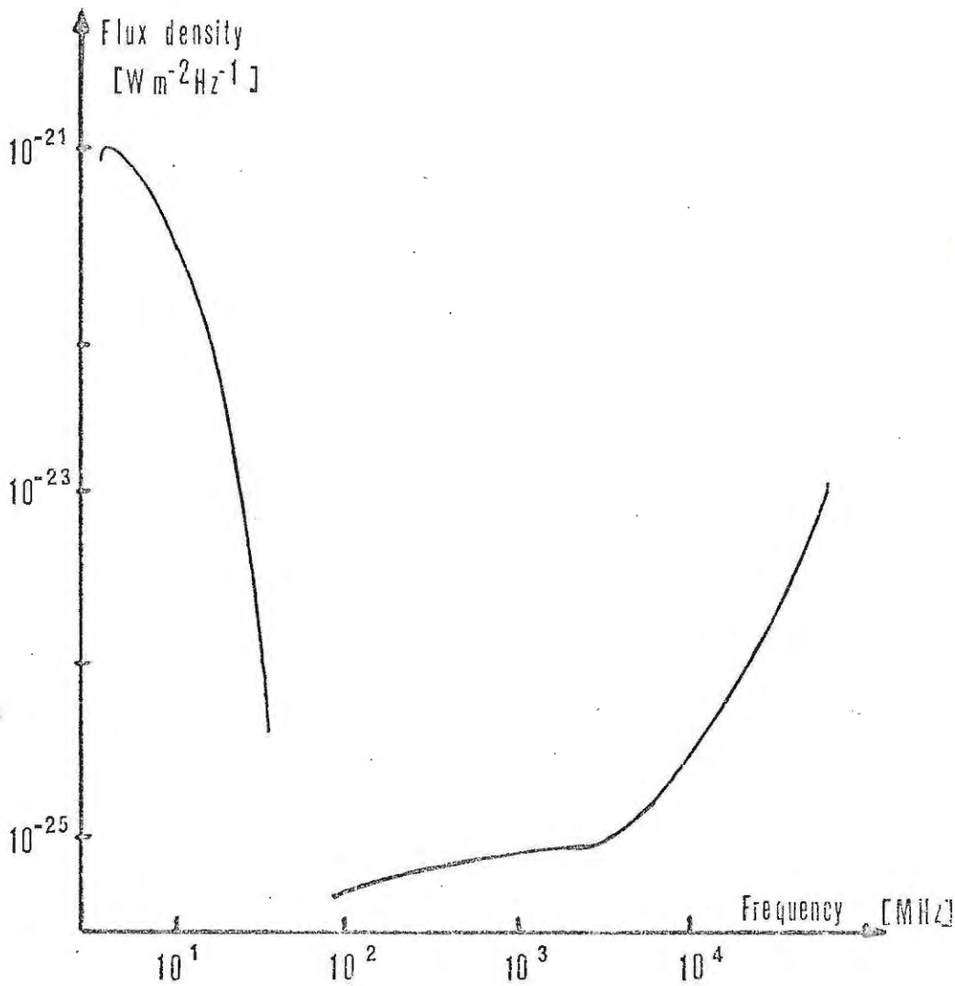

Figure 1: Average spectrum of Jupiter in the frequency range 3 to 10^5 MHz. The figure is adopted from Schmahl (1970).

In 1969 Dulk reported long-baseline interferometer measurements of Jupiter's decametric radiation at 34 MHz. His results are basically in agreement with several previous measurements (Brown et al, 1968 and Slee and Higgins, 1966), which are, however, all less accurate than the ones reported by Dulk. Dulk's results allow for two interpretations:

1. If the source of radiation were incoherent, its size would be less than 0".1 which corresponds to 400 km at Jupiter;

2. The upper limit of a coherent source would be 1" or 4 000 km at Jupiter.

The stability of the fringe pattern shows that in any case the source is highly stable to within 700 km at Jupiter on a time scale of at least 10 seconds.

The first interpretation would call for an extremely high brightness temperature ($T > 10^{17}K$). Coherent radiation would be possible with much smaller brightness temperatures. Dulk himself suggests an interpretation of these results in terms of a coherent source emitting near the feet of the field lines passing through Io. Without going into further details, we will use the following results, on which we will base our theoretical model:

a) The average power involved in a decametric burst is $\approx 10^{8}W$.

b) The source radiates coherently.

c) The source size is less than 1" or 4 000 km at Jupiter.

2.2 The Io Control

Before describing the Io effect, the nomenclature,

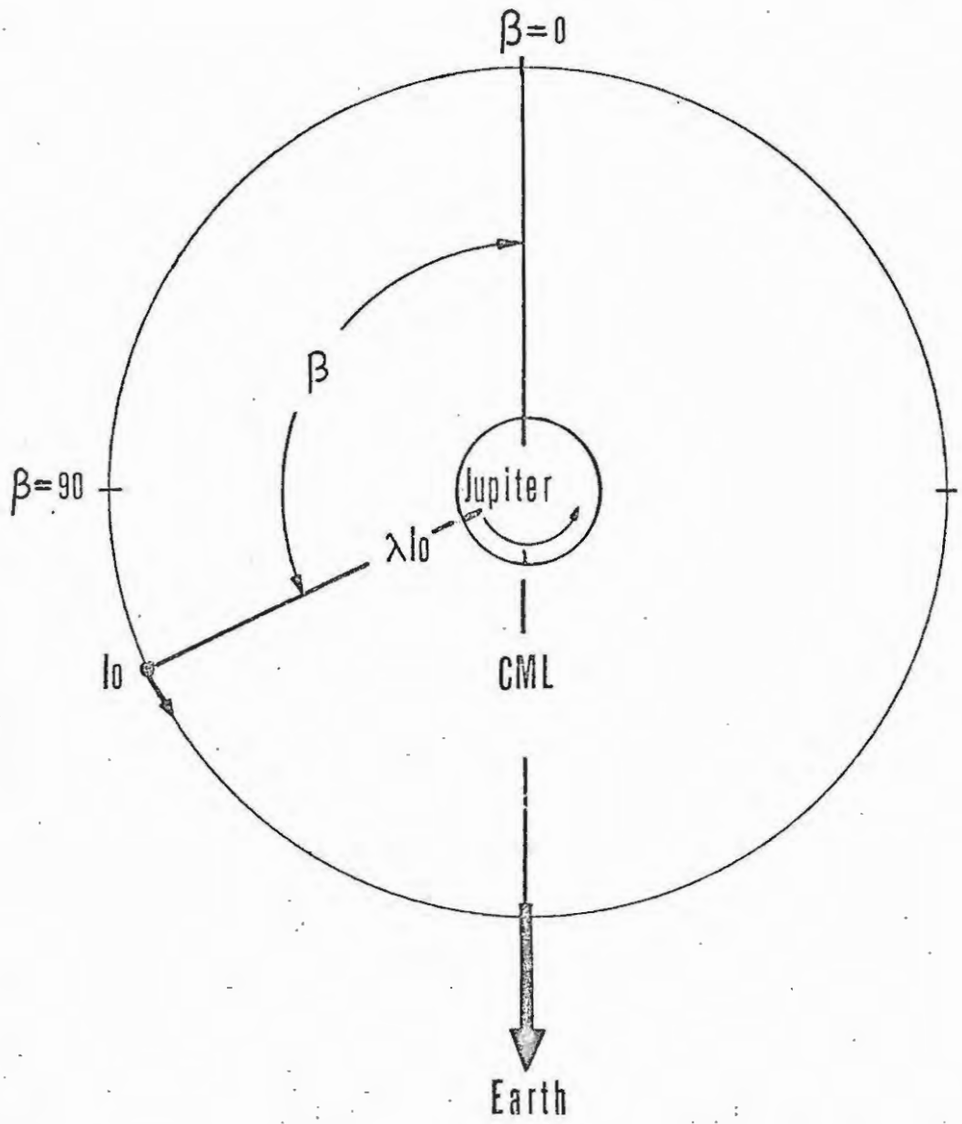

Figure 2: The Jupiter - Io - Earth geometry.

which will be used throughout this thesis, must be explained. Figure 2 shows the geometry of the Jupiter-Io-Earth system. The longitude of Jupiter, facing Earth, is called CML (Central meridian longitude). If not otherwise stated, the 1967 system for longitude specification will be used (Donivan and Carr, 1969). The position of Io relative to the Earth-Jupiter line is characterised by β. β = 0 means that Io is at superior geocentric conjunction. The Jupiter longitude below Io is called sub Io longitude (or: λ Io).

2.2.1 Sources

Histograms of the occurrence probability as a function of CML have been published by many observers. Figure 3 shows such a histogram. The various peaks are usually called "sources". In 1965 the following nomenclature was adopted by the Jupiter Observers' Conference at the Goddard Space Flight Center.

CML range	Designation
0 - 70	D
70 - 190	B
190 - 280	A
280 - 360	C

A histogram showing the occurrence probability as a function of β is shown in figure 4. It is clearly visible from this figure that the probability for receiving radiation is greatly enhanced when Io is within two well defined regions namely

$$80 \leq \beta \leq 120$$
$$220 \leq \beta \leq 260$$

In figure 5 the probability is plotted as a function of both CML and β for various frequencies. (Wilson et al, 1968). It is important to realize that there are 4

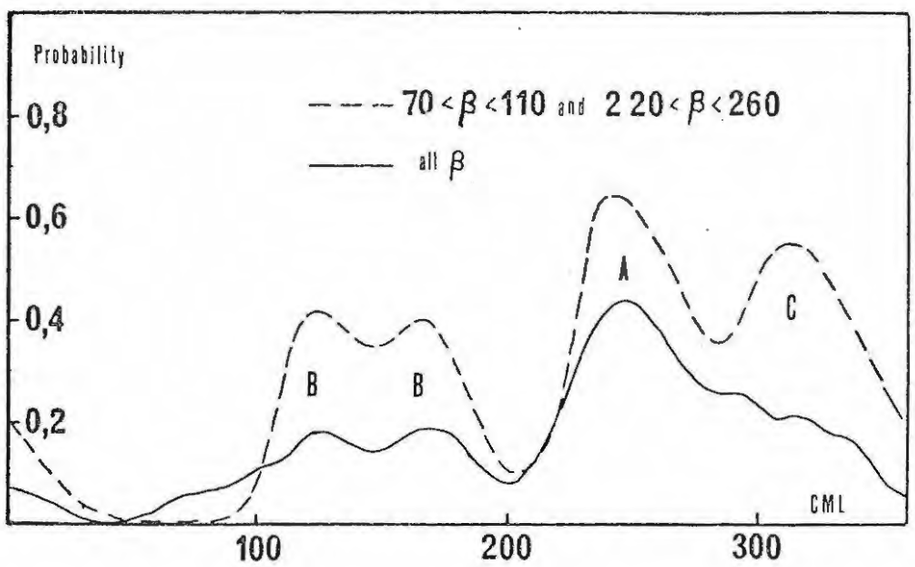

Figure 3: Receiving probability for Io and non-Io controlled radiation as a function of CML.

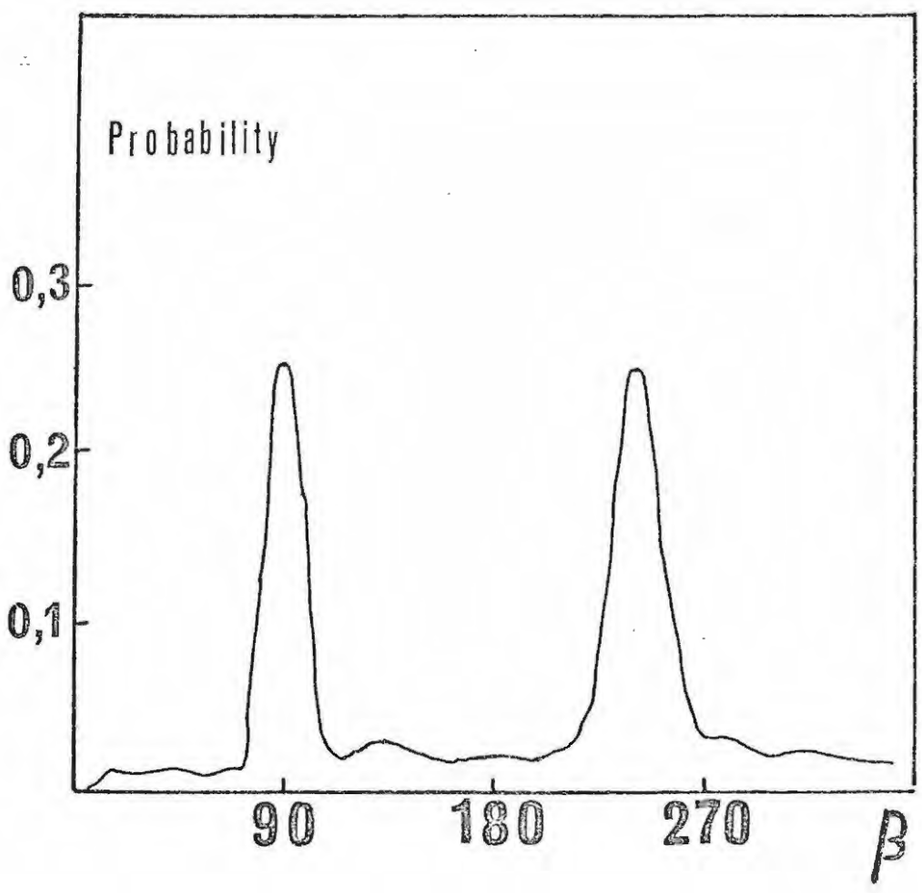

Figure 4: Receiving probability as a function of β (after Schmahl, 1970).

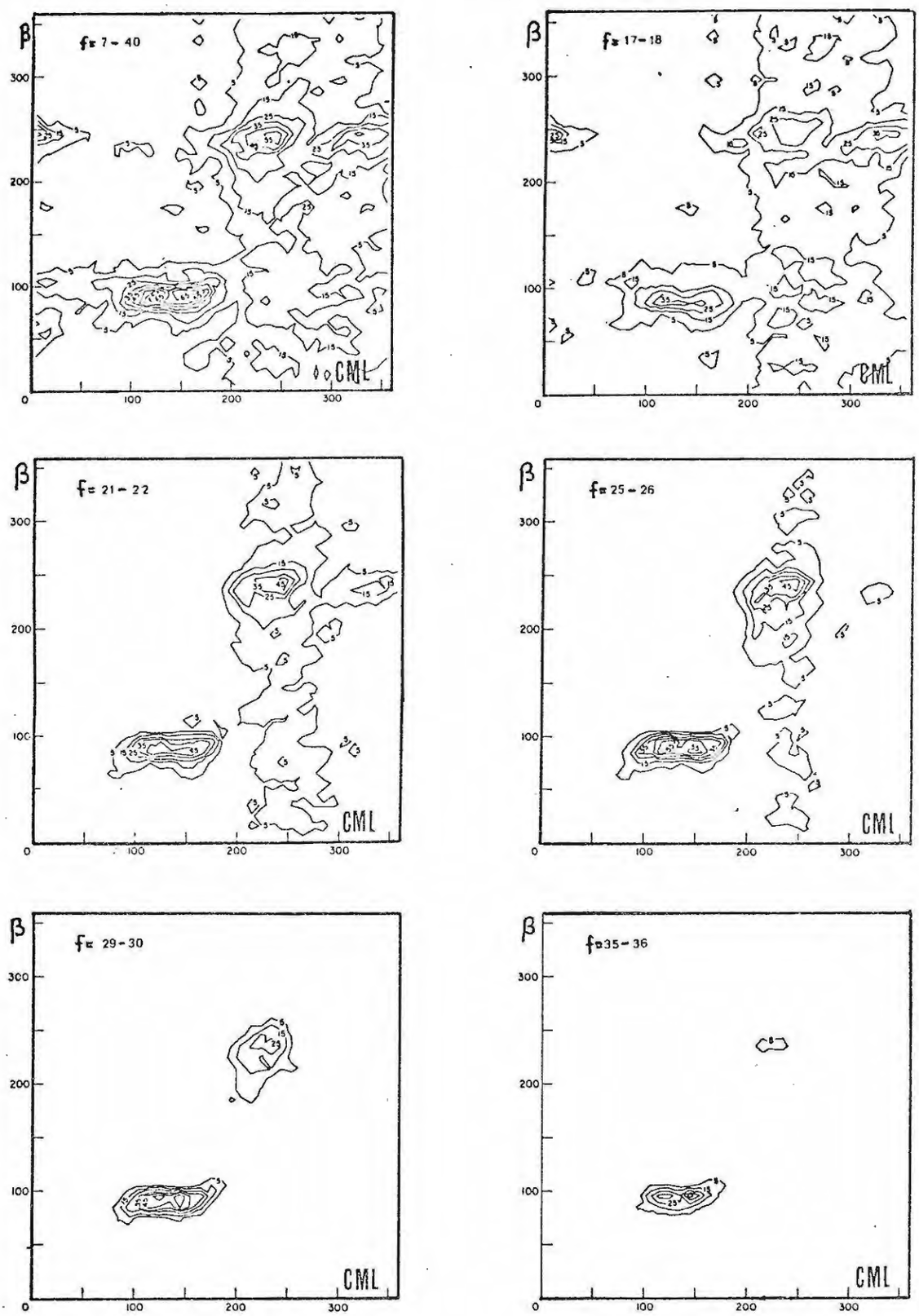

Figure 5: Probability of decametric radiation in the β-CML domain. (from: Wilson et al. 1968). Frequencies expressed in MHz.

Io-controlled sources.

CML	β	λ_{Io}	Designation
95	110	195	B_1
95	160	245	B_2
240	240	180	A
240	320	260	C

It is also evident that the Io-control is more pronounced for higher frequencies. A small drift of the CML of the A source towards larger CML with increasing frequency can also be seen.

The separation of the B source into two sources might seem artificial, as they are hardly separated and only noticeable as a drop in the probability curve. But since there is some theoretical reason for expecting two slightly separated sources the dip is taken as a real effect. It is remarkable that the λ_{Io} values for the 4 sources are symmetrical about $\lambda_{Io} = 220^{\circ}$.

The important results which any theoretical model must explain are therefore:

1. There are four Io-controlled sources which are placed symmetrically about 220° λ_{Io}.

2. The Io-control becomes more pronounced for high frequencies.

2.2.2 The Maximum Frequency Variation

Baart et al. (1971) have made an investigation into the maximum cut-off frequency of the decametric radiation as related to Io co-ordinates. They showed that the highest cut-off frequency ($f \simeq 40$ MHz) is observed only when Io is above 230° Jovian longitude. This thesis deals with the effect of Io on the decametric radiation. In order to investigate this important aspect of

maximum cut-off frequency variation, it was found necessary to make a distinction between Io-controlled radiation and that radiation over which Io has no control. Only with this distinction will a comparison between theoretical predictions and observations be relevant.

When considerating Io controlled radiation we will only consider radiation occurring when Io is within the regions 70° - 110° and 200° - 260° from SGC. All other radiation is classified as "non-Io controlled" radiation.

It must be noted that in using this procedure some "non-Io controlled" radiation has been classified with the Io-controlled radiation, especially in the region $70^{\circ} < \beta < 110^{\circ}$ and $200^{\circ} < \text{CML} < 360^{\circ}$. However, the probability of emission in this region is very much less than that in the vicinity of the Io-controlled "sources" and we would not expect radiation from this region to have a great effect on results when examining the effect of Io on the radiation.

Microfilm records of the Boulder High Altitude Observatory observations, which were kindly supplied to Rhodes University by Dr. Dulk, were analyzed as described previously by Baart et al. (1971). A computer program was used to sift through the frequency storm data, and count the number of times a particular frequency occurs within a particular five degree interval of Io λ III co-ordinates. This frequency count is printed out in a 40 x 72 matrix, whereby the Io λ III axis is divided up into 72 five degree intervals.

Putting in conditions so as to exclude all radiation which was classified as non-Io controlled, frequency count analyses were made for six apparitions from

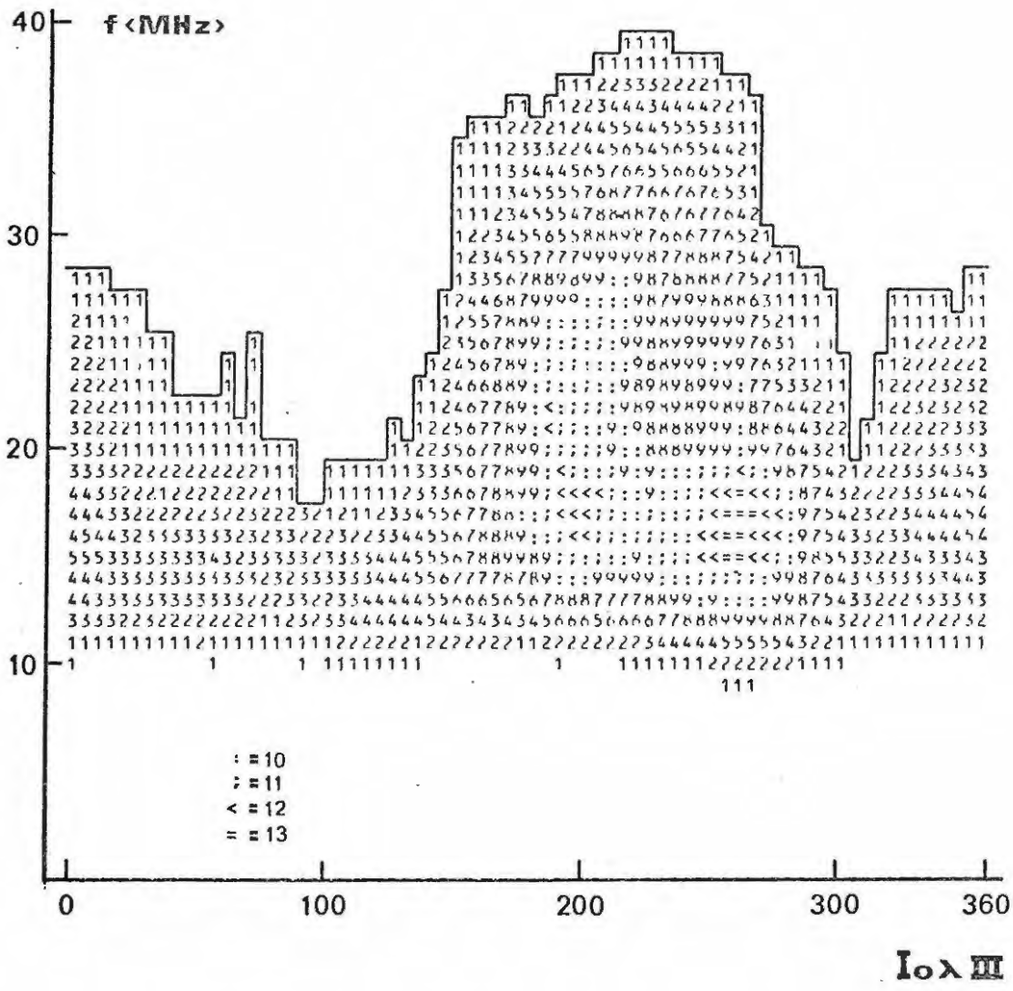

Figure 6: Frequency - sub Io longitude (Io λ III or λIo) matrix for the Io controlled radiation. The heavy line indicates the variation of f_M.

1961 - 1967. (Haschick, 1970). As the number of storms occurring during one apparition is rather small and therefore does not allow for a statistically significant analysis, the number of storms occurring within a particular 5 degree Io λ III interval at a particular frequency was added over all six apparitions (1961 - 1967). In order to get a picture of the average behaviour we divide the numbers in each segment of the 40 x 72 matrix by 5. This ratio is then rounded to the nearest integer, which is printed out in the final 40 x 72 matrix. Thus a number 1 in a particular segment of the final matrix represents at least 3 storms occurring in the particular Io λ III interval and at the particular frequency during the time 1961 - 1967. The result is shown in figure 6.

A similar procedure is followed for the non-Io controlled radiation. All radiation occurring when Io is within the intervals 70° - 110° and 200° - 260° away from SGC is excluded for the non-Io controlled radiation plot, which is shown in figure 7.

Figure 6 reveals a frequency peak occurring between Io λ III values of 215° - 235° with a maximum frequency of 39 MHz. Frequencies of greater than 39 MHz only occurred in one apparition. Figure 6 resembles the figures shown by Baart *et al*, except that the peak is more pronounced.

A secondary peak with a maximum frequency of 28 MHz occurs between values of Io λ III 325° to 20°.

Figure 7 shows that there is no obvious correlation between the maximum cut-off frequency of the non-Io controlled radiation and the Io III co-ordinates. This would tend to support the hope that we have separated

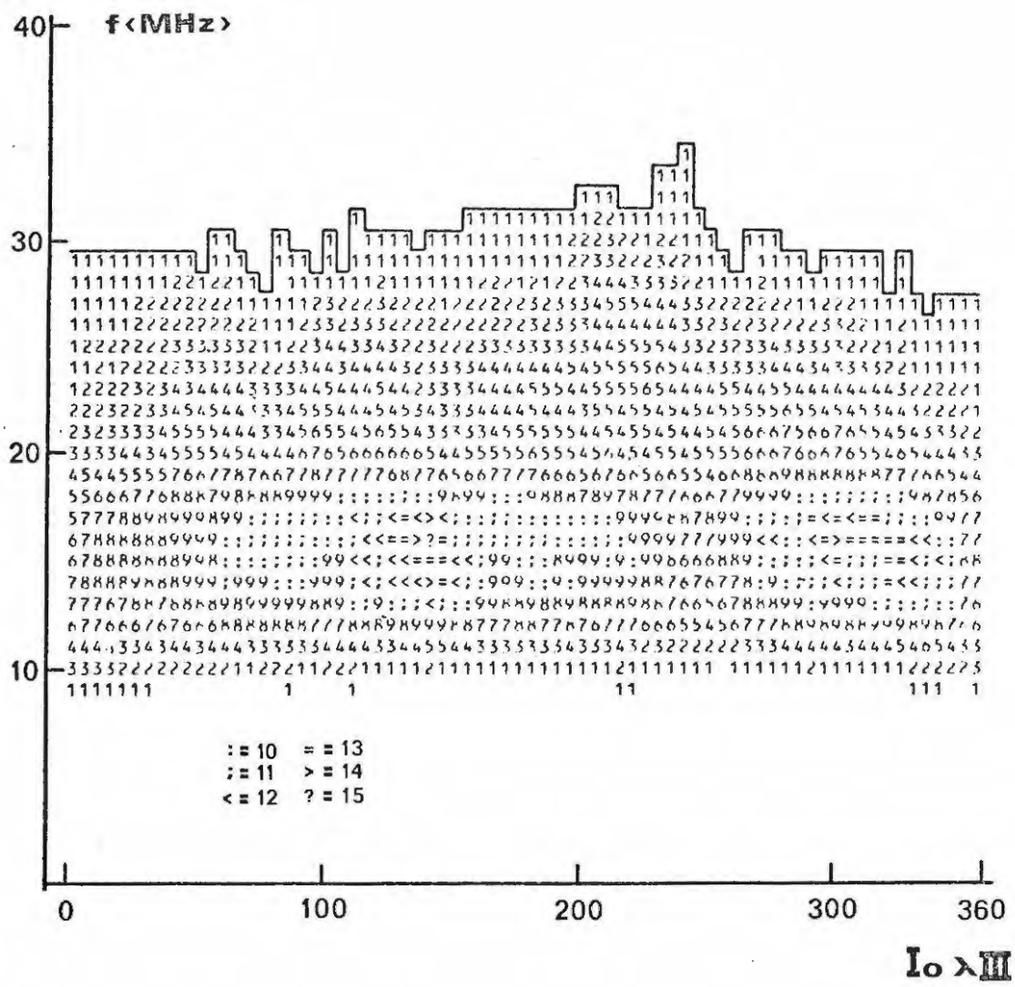

Figure 7: Frequency-sub Io longitude (Io λ III or λ Io) matrix for the non-Io-controlled radiation.

most of the Io related radiation from the non-Io controlled radiation. The drop off in cut-off frequency above 350° Io λ III, however, seems to indicate that some non-Io controlled radiation has been removed from this region and included with the Io controlled radiation. Thus a little less significance should be attached to the secondary peak in figure 6 occurring between 325° and 20° Io λ III.

The heavy lines in figures 6 and 7 indicate the variation of highest cut-off frequency, hereafter called f_M.

There are two theories predicting a highest cut-off frequency variation with Io λ III co-ordinates. Gledhill (1967) predicts two peaks of highest cut-off frequency at 230° and 150° Io λ III respectively. Whereas the peak at 230° is supported, the absence of a peak at 150° seems to be in direct contradiction to Gledhill's predictions.

Another theory, often referred to as the unipolar theory, dealing with the high frequency cut-off variation was published by Goldreich and Lynden-Bell (1969). A comparison of the results with the predictions made by the unipolar theory will be made below.

In this section we will relate the highest cut-off frequency variation to a variation of the height above Jupiter's surface at which the particular frequency (f_M) is emitted. All deductions made in this section are based on the following 3 assumptions.

i) The frequency of the radiation received on earth is the electron gyrofrequency at the point of emission.

ii) The Io controlled radiation is emitted close to Jupiter's surface along the magnetic flux tube passing through Io (IFT). The magnetic field of Jupiter is assumed to be that of a magnetic dipole.

iii) The foot of IFT leads Io by approximately 15^{o}, as has been suggested by several other authors (Marshall and Libby, 1967 and Carr and Culkis, 1970).

As the magnetic field is assumed to control the observed frequency, a change in frequency corresponds to a change in magnetic field strength at the point of emission. A change in the observed frequency could thus correspond to a change in the height above the surface of Jupiter from which the radiation is emitted. Assuming a dipole field one would expect a change in emission radius (i.e. height plus Jupiter radius), of approximately 20% for a frequency change of roughly 60%.
A change in the magnetic field strength and hence gyrofrequency due to the rotation of Jupiter would also cause a variation of f_M with Io λ III. Changes in the magnetic field strength at a fixed height above Jupiter could be caused by either a dipole displacement along or perpendicular to the rotational axis or a change in L value of Io's flux tube (IFT) and thus the co-latitude Θ due to a tilt of the magnetic dipole axis of Jupiter with respect to the rotational axis. These magnetic field "anomalies" (dipole displacement and tilt) are believed to exist. The variation of f_M with Io λ III could also be due to beaming of the radiation. This idea is incorporated in the unipolar model, the predictions of which will be examined below.

It is found that one cannot account for the variation in terms of "known" magnetic field "anomalies" alone, as deduced from observations of the decimetric radiation

from Jupiter. We thus conclude, considering the assumptions made, that the radiation is generated at different heights above the surface of Jupiter depending on Io λ III. The following parameters are used to describe the magnetic field anomalies :

1. δ is the displacement of the dipole axis in the equatorial plane.

2. λ_o is the longitude towards which the dipole is displaced by δ .

3. B_E is the (magnetic) equatorial field strength at longitude

4. S is the north-south displacement of the magnetic dipole centre.

5. α is the tilt of the magnetic dipole axis with respect to Jupiter's rotational axis.

6. λ_T is the longitude towards which the dipole axis is tilted in the northern hemisphere of Jupiter.

From figure (6) a smooth curve is drawn to represent the variation of f_M as a function of Io λ III co-ordinates. The height of emission (h) corresponding to f_M at a particular sub Io longitude is then calculated given a particular set of the 5 parameters described above. (See Appendix A).
This is repeated for a different Io λ III and h is then plotted as a function of Io λ III. For all sets which we have tried, the height variation is very similar. Figure 8 shows examples of these curves. The parameters used to deduce these curves are indicated on the figure. It is interesting to see, that the variation of height from which the highest cut-off frequency is emitted shows some degree of symmetry.

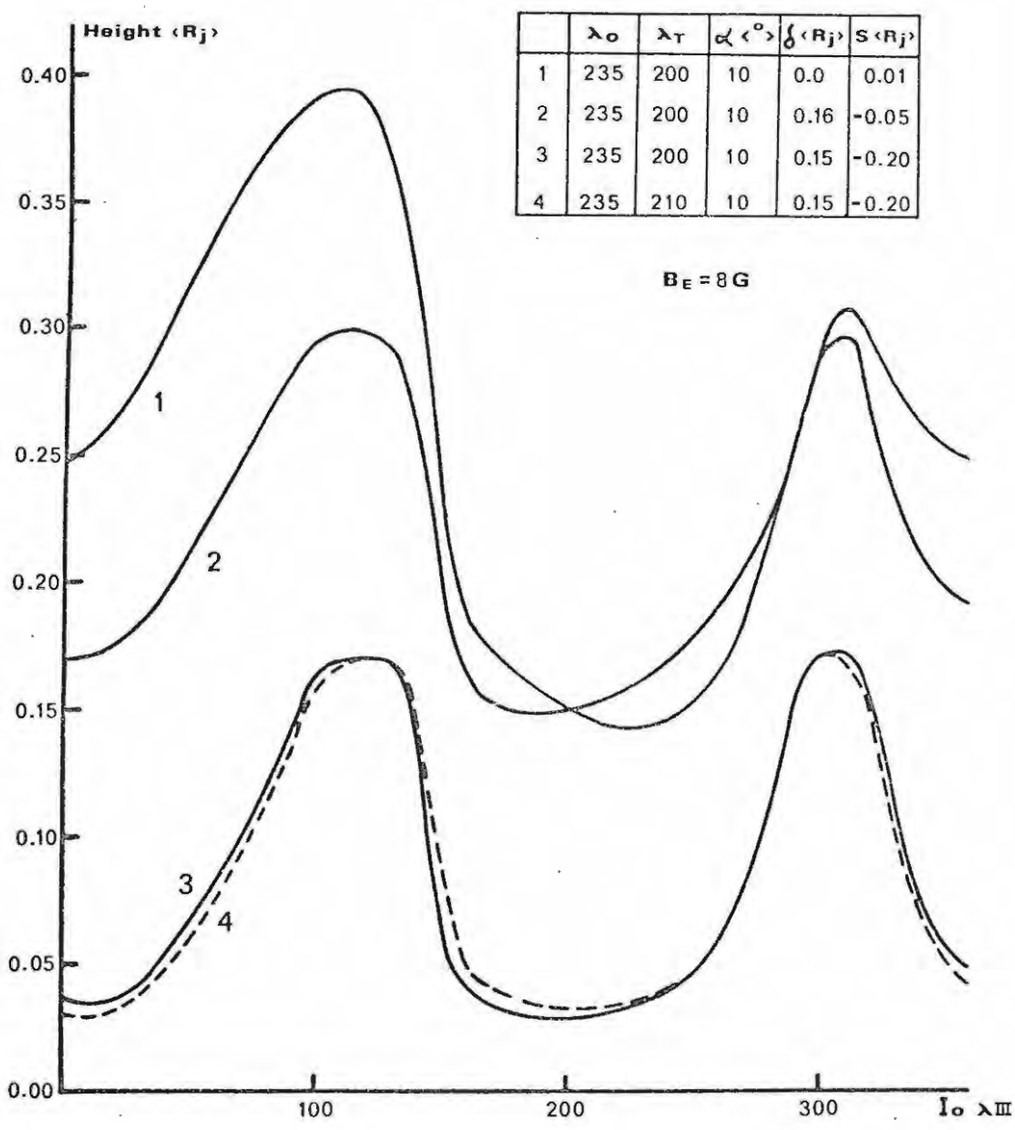

Figure 8: The variation of height above Jupiter's surface (in R_J) at which f_M (see figure 6) is emitted. See text for explanation of symbols. The radiation is generated in the northern hemisphere.

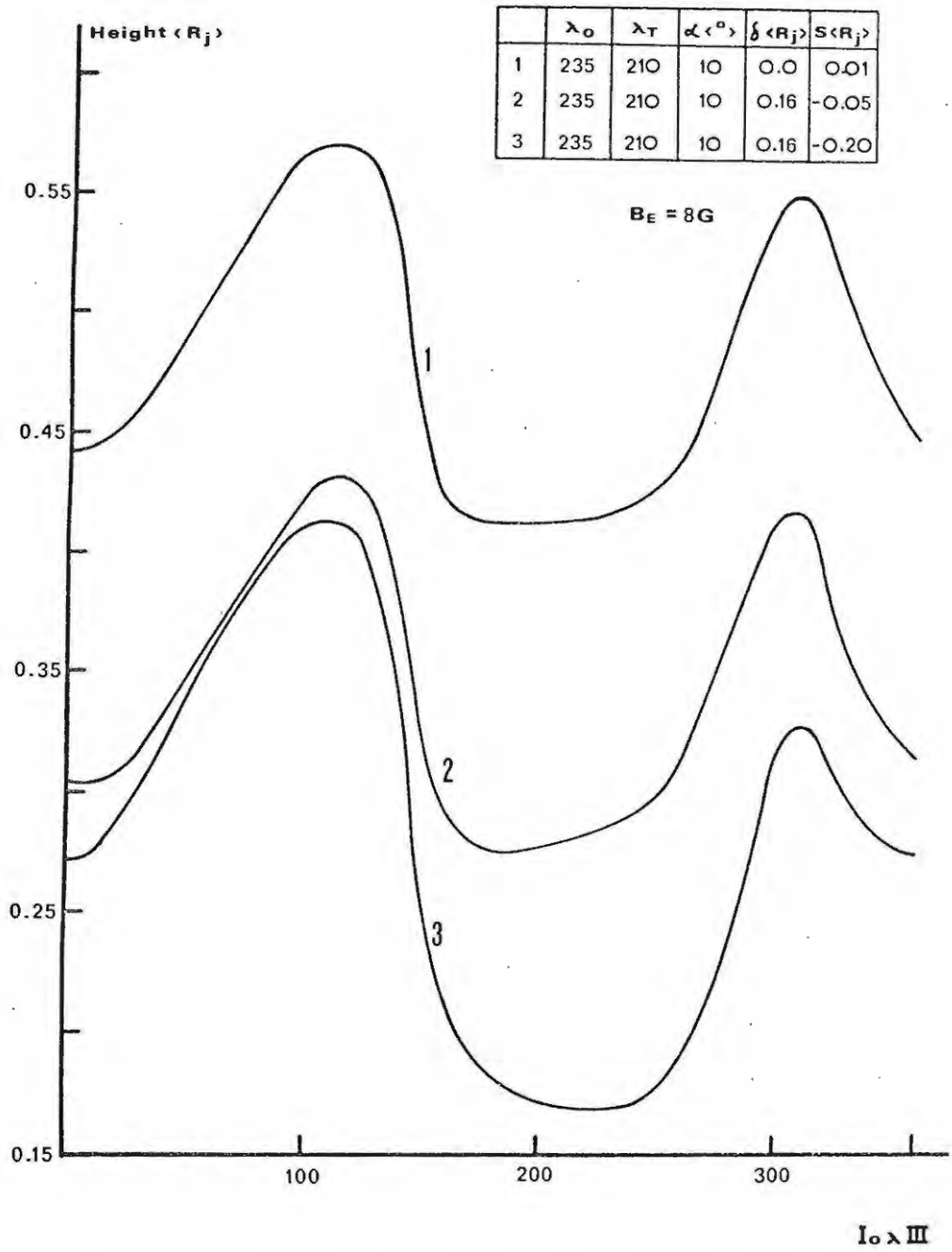

	λ_o	λ_T	$\alpha\langle^o\rangle$	$\delta\langle R_j\rangle$	$S\langle R_j\rangle$
1	235	210	10	0.0	0.01
2	235	210	10	0.16	-0.05
3	235	210	10	0.16	-0.20

Figure 9: Same as figure 8, except that the radiation is assumed to be generated in the southern hemisphere.

It must be noted that the curves shown in figure (8) were calculated on the assumption that the radiation is generated at the foot of IFT in Jupiter's northern hemisphere. Figure (9) shows the variation of h for the radiation being generated in the southern hemisphere. Both sets of curves show some degree of symmetry. The model of the Io controlled radiation developed in this thesis requires a symmetrical variation of h vs. λ Io (that is: the two height maxima and two minima should each have the same values and the maxima and the minima should be separated by about 180°). The curve which fits these requirements best is obtained for the following set of parameters.

$\delta = 0.15\ R_J$ (R_J = Jupiter's radius), $\lambda_o = 235^{\circ}$, $B_E = 10G$, $S = -0.2\ R_J$ (that is: the dipole centre is displaced southward with respect to the planet's centre) $\alpha = 10^{\circ}$ and $\lambda_T = 210^{\circ}$. The "best" curve is obtained if the radiation at f_M is assumed to be generated in the northern hemisphere of Jupiter. It is interesting that these values agree well with values deduced from completely different observations (Carr and Gulkis, 1970).

Goldreich and Lynden-Bell (1969) use the same three assumptions (i to iii) mentioned above as a basis for predicting a f_M variation with λ Io. According to Goldreich and Lynden-Bell the radiation is emitted into a conical sheet of opening angle $\gamma = 79^{\circ}$. The axis of the cone is parallel to the magnetic field at the position of emission. If the magnetic field makes an angle τ larger than 79° with the ecliptic the conical sheet will not intersect the ecliptic and no radiation will be received on earth. The northern end of Io's flux tube makes an angle $\tau = 53^{\circ}$ with the ecliptic. As Jupiter rotates, taking into account a 10° tilt of the

dipole axis, τ will vary between 43° and 63°. In order to explain the distinct sources, Goldreich and Lyden-Bell, assume that the conical sheet is not uniformly filled with radiation. For reception of radiation, the angle τ must be smaller than 46°. At high frequencies the radiation is emitted close to the planet where τ is large. Only when the dipole is very nearly pointing towards the foot of Io's flux tube will the high frequency radiation be received on earth. As Jupiter rotates the angle τ increases and the high frequency radiation will not be received on earth, whereas low frequency radiation can still be detected, as it is generated further away from the planet where τ is smaller.

The angle τ' between the magnetic field line and the magnetic equator plane is related to the colatitude Θ by the following relation:

$$(2.1) \quad \cos \tau' = \frac{3 \sin\Theta \cos\Theta}{(1+3\cos^2\Theta)^{1/2}}$$

The relation of the magnetic field to the angle Θ is

$$(2.2) \quad \frac{B}{B_E} = \left(\frac{R_J}{r}\right)^3 \left(1+3\cos^2\Theta\right)^{1/2} = \frac{f}{f_o}$$

where f_o is the frequency corresponding to the magnetic field B_E. With:

$$(2.3) \quad r = L R_J \sin^2\Theta$$

(2.2) becomes

$$(2.4) \quad \frac{f}{f_o} = \frac{1}{L^3} \frac{(1+3\cos^2\Theta)^{1/2}}{\sin^6\Theta}$$

From the variation of f/f_o (assuming f_o to be 40 MHz) with λ Io (figure 6) Θ as a function of λ Io can be calculated. Inserting this into formula (2.1)

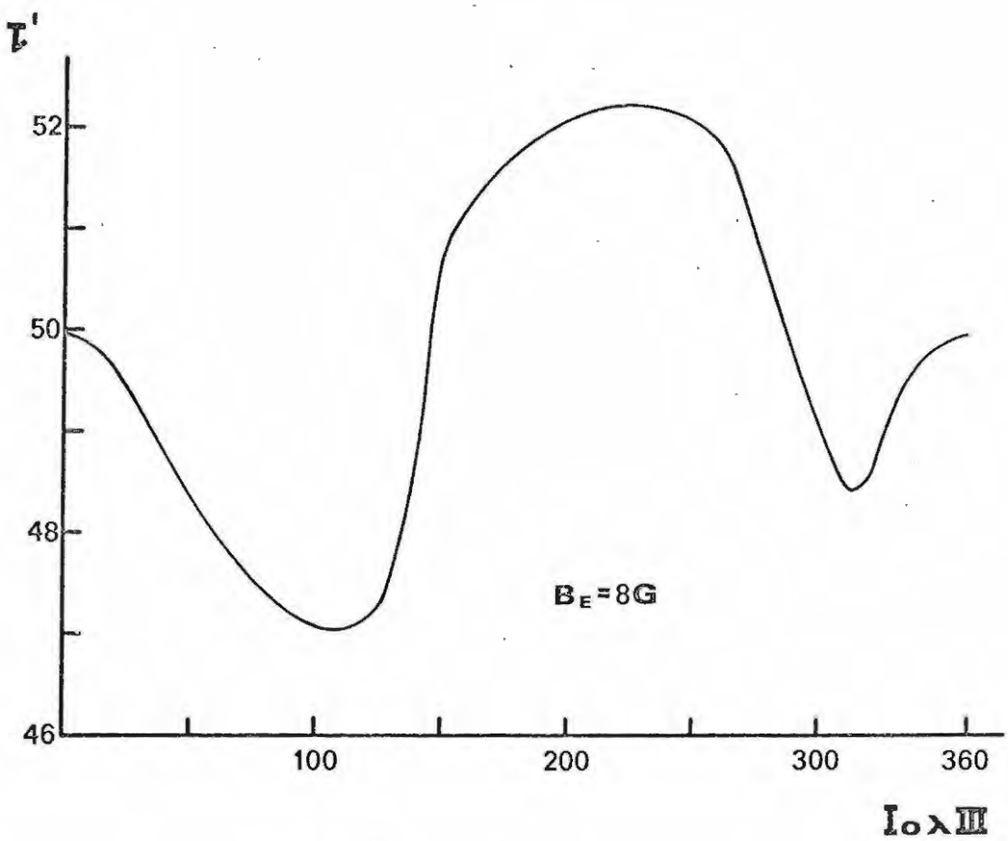

Figure 10: The variation of the angle τ' between the magnetic field line and the magnetic equator plane required to produce the variation of f_M displayed in figure 6.

the variation of τ' between the magnetic field line and the magnetic equator plane which corresponds to the observed variation of f_M can be determined. The result is shown in figure 10. The angle τ between the magnetic field and the Jovian equatorial plane is $\tau = \tau' - \alpha'$ where $\alpha' = \alpha \cos (Io\lambda III - \lambda_T)$ is the angle between the magnetic dipole axis and the rotational axis as measured in the meridional plane Io λ III. For radiation to be received, τ must be smaller than a critical value τ_c (46^o in Goldreich and Lynden-Bell's model). f_M should always be emitted at points along a field line where $\tau = \tau_c$. Thus the variation of α' due to Jupiter's rotation should be balanced by a variation of τ'. Figure 10 indicates a variation of τ' less than 6 degrees in magnitude. Increasing the value of f_o does not have any great effect on the relative variation of the angle τ'. Nor does inclusion of a dipole displacement alter the magnitude of the τ' variation considerably. The variation of τ' is always smaller than the variation of α' by 20^o.

If the angle τ did happen to have the modulating effect on the maximum frequency as predicated by the unipolar model we would expect a maximum frequency variation with an extremely sharply sloped peak occurring around 230^o Io λ III with the modulating effect extending right below 10 MHz. This type of frequency variation does not seem to have been observed.

A possible interpretation of the maximum frequency variation in terms of a change of τ' would require a dipole which is tilted by less than 3^o with respect to the rotational axis. It would then seem to be difficult to explain the sharp sources observed. Furthermore, a tilt of 10^o seems to be experimentally

established with great certainty by now.

The following results are considered to be important and the proposed model is an attempt to account for these

1. The maximum frequency reached by an Io controlled storm varies with sub Io longitude.

2. The variation corresponds to a change of source height above the planet's surface.

3. The radiation is generated close to the planet when Io is above 220° and 30°.

4. The radiation is generated furthest away from the planet when Io is either above 130° or 300°.

2.3 Polarization

It is found that most of the decametric radiation is highly polarized. The polarization seems to vary with frequency and source position. For details of polarization measurements and the results thereof the reader is referred to Green and Sherrill (1969), Sherrill (1965).

The following results are believed to be important for a theoretical discussion of the Io effect.

1. Most of the decametric radiation is elliptically polarized.

2. Low frequency decametric radiation shows both R.H. and L.H. polarization whereas high frequency radiation shows exclusively R.H. polarization.

2.4. Time Structure of the Storms

Jovian radio emission exhibits a time structure on different scales.

1. hours
2. minutes
3. seconds
4. milliseconds

2.4.1 The variation of the radiation on a time scale of hours is due to the geometry of the emission sources. The emission geometry changes from favourable to unfavourable on a time scale of hours (see section 2.2.1), as the rotation period of Jupiter is about 10 hours, and only certain ranges of CML are favourable for receiving radiation on earth.

2.4.2. The variation on a time scale of minutes is probably due to a change of ionospheric conditions in the vicinity of the earch.

2.4.3 The variation of the radiation over times of the order of seconds is most likely due to inter-planetary scintillations (Douglas and Smith, 1967).

2.4.4 The millisecond pulses or spitting (S) pulses are believed to be intrinsic properties of the emitting source at Jupiter, as there is a strong correlation of the spitting pulse activity with CML and λ Io.

Figure 11 (Hill, 1969) shows the probability of spitting pulses and normal bursts as a function of CML, while figure 12 (Rihiimaa, et al, 1969) shows the number of spitting pulses during the years 1963 - 1968 as a function of λ Io. There are 2 weakly defined peaks of S pulse activity at λ Io 245 and 260 which evidently coincide with the B_2 and C source. These figures show clearly that S pulses are Io related. The S - pulses

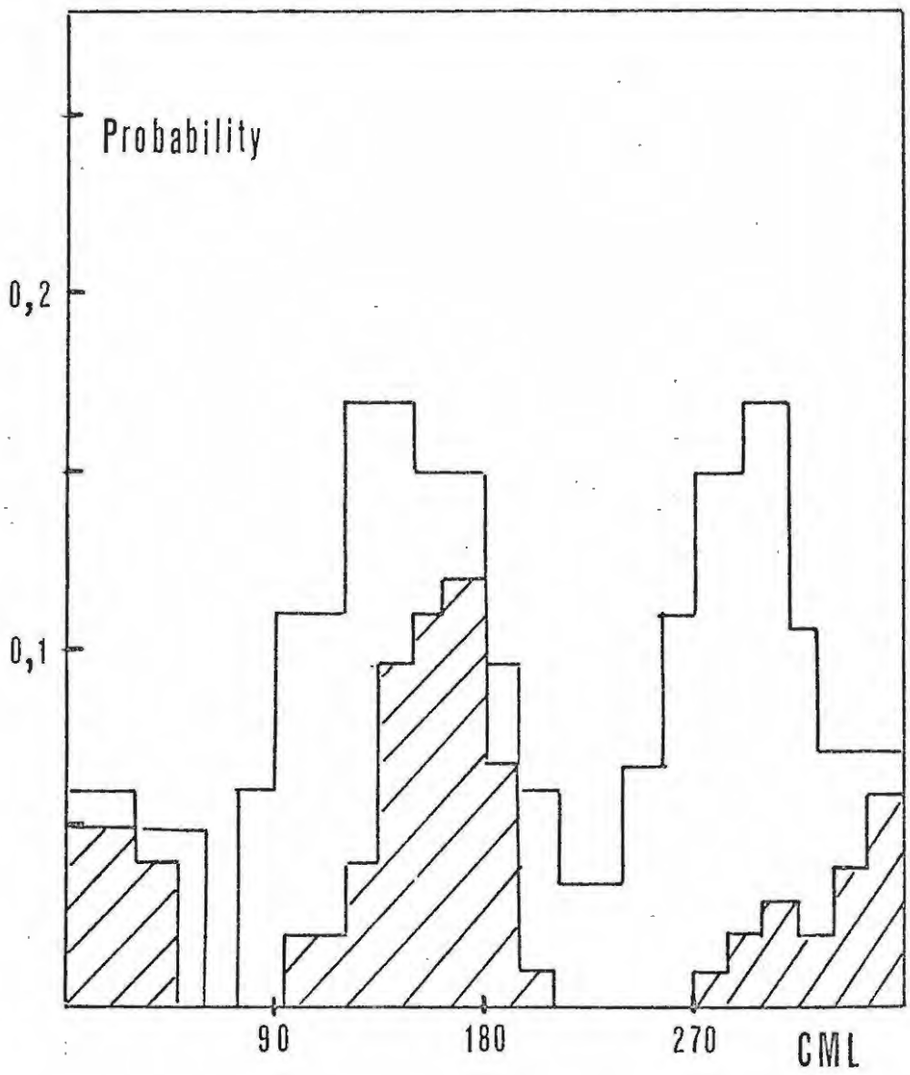

Figure 11: Receiving probability of S-pulses (shaded area) and normal pulses as a function of CML. Frequency range: 16-22 MHz (Hill, 1969).

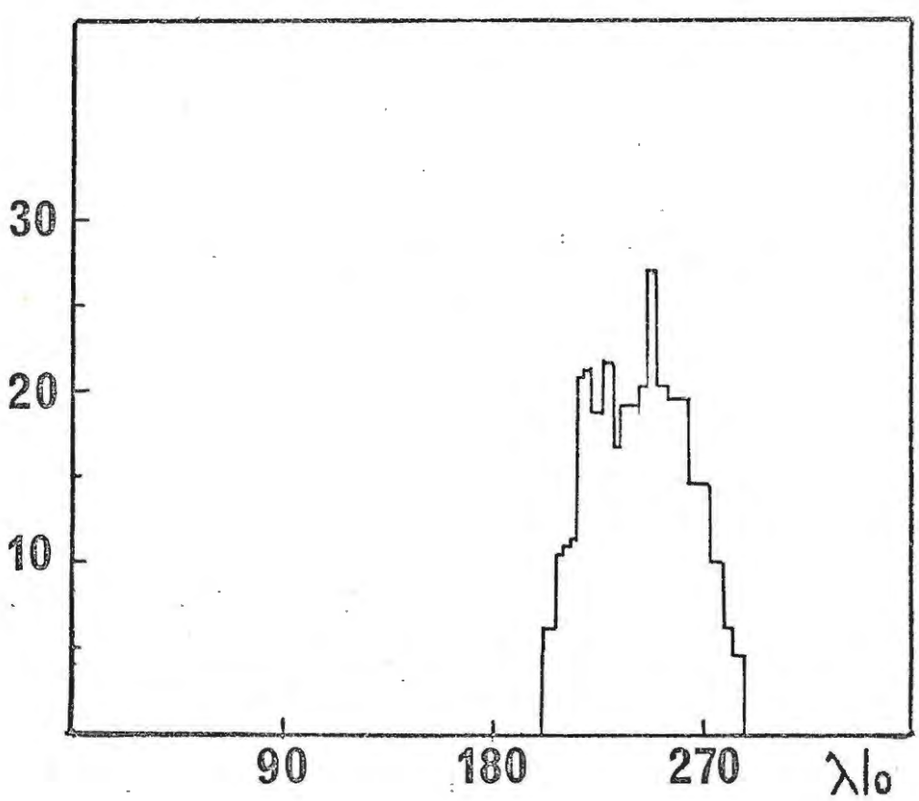

Figure 12: Number of S-burst events during 1967-1968. Frequency range: 21-23 MHz. (Riihimaa et al. 1970).

exhibit a rapid negative frequency drift,

$$\frac{df}{dt} \approx -20 \text{ MHzs}^{-1},$$

and a narrow bandwidth of about

$$\delta f = 50 - 100 \text{ kHz}.$$

The phenomenon of S pulses could point to some transient emission process. Ellis had predicted the negative frequency drift on the basis of his theory in 1965 before the actual discovery of the drift. The drift is supposed to be due to fast electrons spiralling along magnetic field lines away from the planet with a velocity parallel to the field lines of $v_{\parallel} \geq 0.1$ c. Although this prediction was beautifully confirmed by later observations, it is not without the somewhat artificial assumption of electron "blobs" of a certain dimension that the narrow bandwidth can be explained. The duration of the bursts is related to the mean collision time of the electrons. This explanation, however, still demands an irregular and intermittent appearance of electron blobs.

The important results of this section are then:

1. Only the long time scale (hours) and the millisecond time scale variation of the radiation are intrinsic properties of the Jovian radiation source.

2. The hourly variation is due to the radiation geometry.

3. S pulses appear to be strongly Io related and occur mainly in the B_2 and C source.

4. The S pulses are of narrow bandwidth and exhibit a negative frequency drift.

2.5 11 Year Cycle

There are two main aspects of the Jovian decametric radiation which seem to be related to an 11 year cycle.

2.5.1 The Variation of Occurrence Probability.

Gruber (1966) investigates the variation of occurrence probability on a time scale of years and he shows that correlation of probability with declination (that is the angle of declination at which the earth appears as seen from Jupiter) is better than that with the sunspot number. A clear cut decision as to whether the probability variation on an 11 year time scale is due to solar activity or declination, however, is not possible at the moment, because the radiation has only been observed for some 15 years, which does not even cover 2 sunspot cycles, and because the sunspot cycle (11.2 years) is very close to one Jupiter year (11.9 years).

2.5.2 The Variation of the Source A Position

In 1969 Donivan and Carr reported a sinusoidal variation of the source A position with time. The analysis was repeated using Boulder data, distinguishing, however, between the Io controlled and non Io controlled radiation.

The definition of the Io controlled A source is

$$220 < \beta \text{Io (A source)} < 260$$

Figure 13 shows the results.
It appears that the variation is much more pronounced for the non Io controlled than for the Io controlled source A. Figure 14 shows the variation for the non-Io controlled A source. Donivan and Carr explain the variation of source A position as due to the beaming of

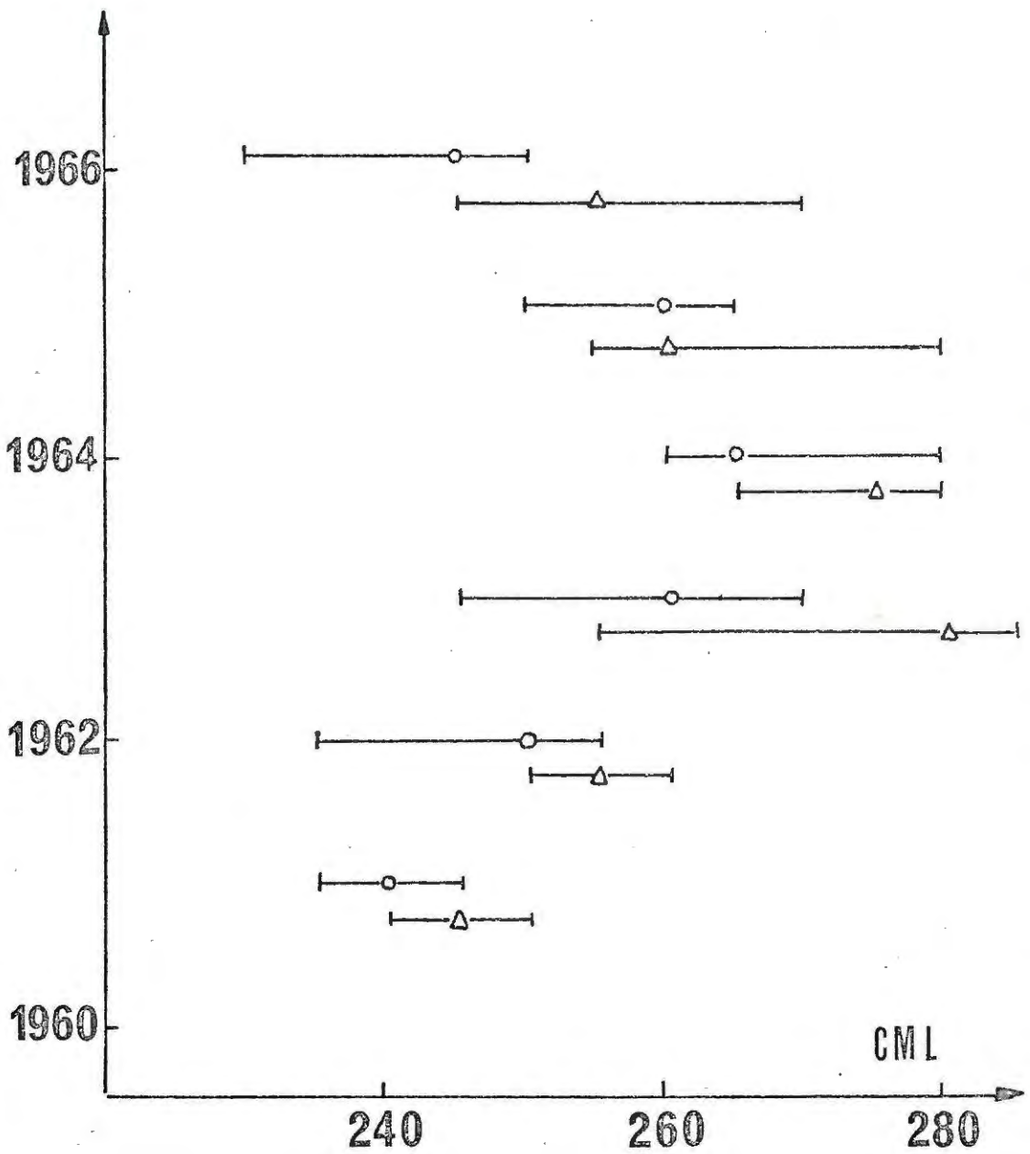

Figure 13: Variation of source A position of the Io-controlled radiation during the years 1961 to 1966. The error bars indicate the extent of the source over which the receiving probability remains nearly constant. O and Δ indicate the position of the probability maximum. Δ , all frequencies; O, f > 25 MHz.

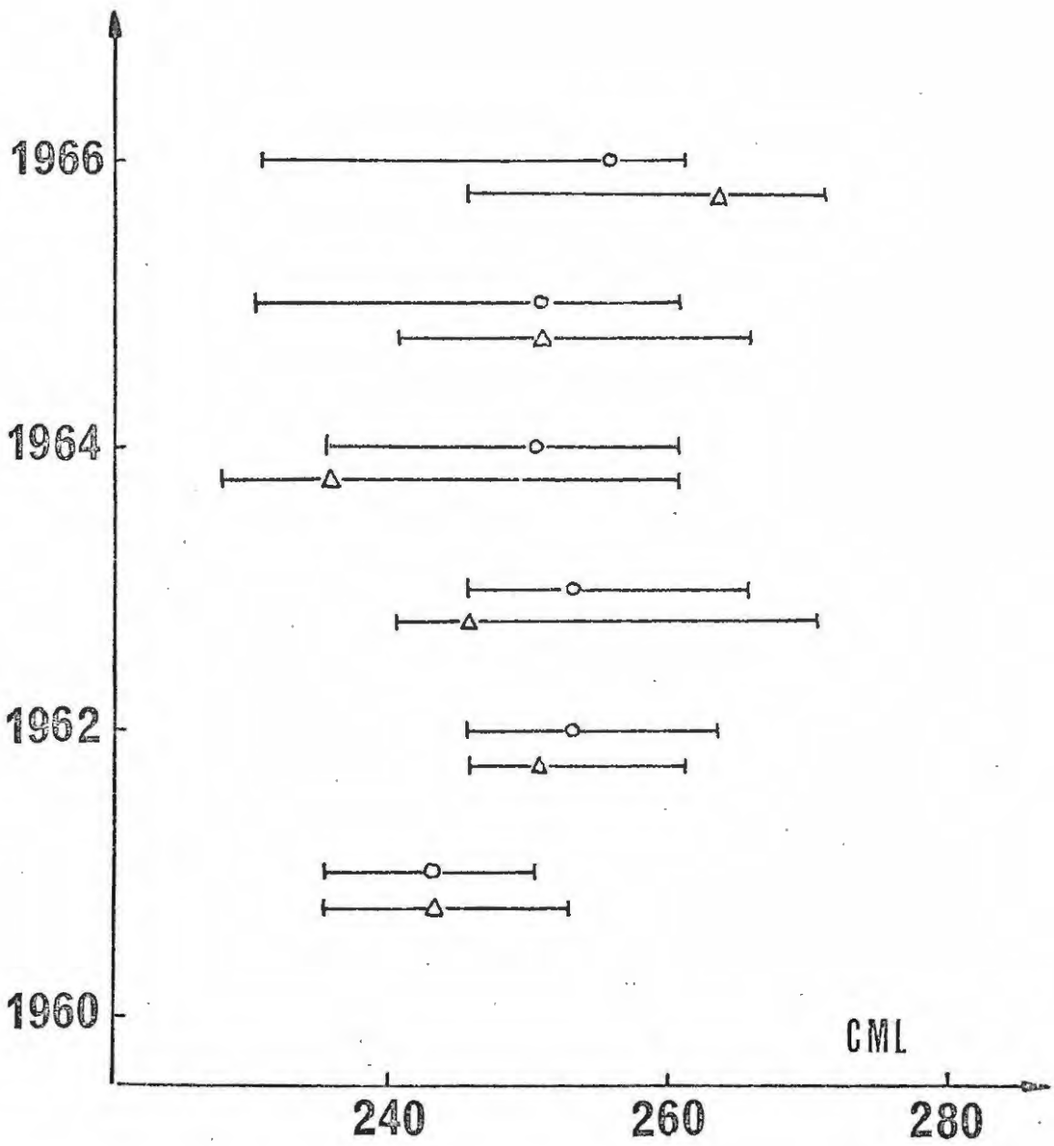

Figure 14: Variation of source A position of the non-Io-controlled radiation during the years 1961 to 1966. For explanation of error bars and the symbols o, Δ see figure 13.

the radiation into a conical sheet. In order to explain the large amplitude of the variation a great distortion of the magnetic field had to be assumed. The author (Goertz, 1971) has shown that a distinction between Io and non Io controlled radiation removes the need for a distorted magnetic field. He has also shown that figures 13 and 14 can be explained easily, if one assumes that the Io related radiation is generated in Jupiter's ionosphere along IFT whereas the non Io radiation is generated in the ionosphere at high latitudes.

3. Jupiter's Ionosphere and Magnetosphere

The determination of the plasma distribution in Jupiter's ionosphere and magnetosphere is of major importance for the explanation of the Jovian decameter radiation. Many authors have constructed various ionospheric models ranging from a very cold and thin (Warwick, 1967) to a hot and extended ionosphere (Piddington, 1967). The Io effect makes it necessary to know the plasma distribution in Jupiter's magnetosphere out to at least the radius of Io's orbit around Jupiter (this is about 6 R_J) in order to allow for a reasonable evaluation of Io's influence over part of the decameter radiation. Values suggested for the plasma density at Io's orbit vary from 10^{-1} particles/cm^3 (Warwick, 1967) to some 10^7 particles /cm^3 (Gledhill, 1967). The most thorough analysis of the plasma distribution in Jupiter's ionosphere was done by Gross and Rasool (1964). During the years following their article important new observations of Jupiter have been made. These observations together with the calculations of Hogan et al.(1969) (see their paper for reference of recent infrared (IR) and microwave measurements of Jupiter) suggest the following points which are of relevance to the estimation of the density of the Jovian ionosphere.

1. It appears that the atmospheric composition of Jupiter is similar to that of the sun. It seems likely that the H_2: He ratio is as large as 5.

2. The brightness temperature of Jupiter in the IR atmospheric window of Jupiter (1μ - 9μ) may be as high as 230 K. This temperature is likely to be characteristic of the temperature at the top of the dense cloud layer.

3. Gillet et al. (1969) interpret their IR

observations of Jupiter as indicating the existence of a temperature inversion in Jupiter's atmosphere. They suggest that the absorption of solar radiation in the 3020 cm^{-1} CH_4 band may be responsible for the formation of this temperature inversion. The calculations by Hogan et al. (1969) confirm this.

4. Hogan et al. (1969) suggest that the best fit of the IR and microwave brightness temperatures calculated by them with observations is obtained if the following conditions at the cloud top level are adopted. The atmospheric temperature (T_N) is 220 K. The amount of H_2 above this level is 150 km atm, that of He 20 km atm; for CH_4 it is o,15 km atm and for NH_3 it is o,o21 km atm. The H_2 pressure at cloud top level is 4 atm. They obtain thermal profiles by calculating the balance of energy at each atmospheric level. Their models differ from those by Trafton (1967) in that they include the opacity due to CH_4. The temperature T_N decreases to a value of about 110 K at 65 km above the cloud top level. The temperature inversion mentioned above occurs at this level. T_N increases to 150 K at about 150 km. Eventually the temperature increases up to at least 400 K at levels where photochemical processes occur. These have not been included in the calculation by Hogan et al. (1969). The effective temperature of the radiative losses to space corresponding to the boundary conditions at the cloud top level was calculated at 127 K, which is higher than the range 88 - 105 K estimated as the solar equilibrium effective temperature for the albedo measurements of Jupiter. Thus the presence of an internal heat source on Jupiter is indicated by these calculations.

The atmospheric density above the cloud tops decreases with an average scale height of about 20 km. This is

somewhat larger than the maximum value of Baum and Code (1953) of 12.5 km which was derived from occultation measurements. This experiment is, however, now considered as unprecise (McElroy, 1969, as quoted by Encrenaz et al, 1971).

Recent occultation measurements (unknown author in Science, 1971) show that the atmospheric scale height of Jupiter is most probably larger than the one given by Baum and Code.

Thus we see that calculations of the ionospheric ionization based on a cold atmosphere ($T \leq 100$ K) are probably not realistic. In the following we will adopt Hogan's results as the lower boundary conditions for the calculation of the ionization and variation of the temperatures of the neutral atoms and molecules, electrons and ions at heights larger than 200 km above the cloud top layer.

3.1 Jupiter's Ionosphere

The distribution of ionization in the Jovian ionosphere can be determined by solving simultaneously the momentum and chemical equations for electrons, ions and neutrals together with their respective heat transport equations. The equations and parameters used for this work are given in the Appendix B.

A similar set of equations was applied to the earth's ionosphere by Herman and Chandra (1969). The present problem is greatly simplified by the fact that at heights above 200 km the amount of CH_4 and NH_3 is very small compared with that of H_2 and He. Thus the contributions of CH_4 and NH_3 to the ionization is neglected in the calculations.

The set of differential equations of heat transfer was

solved by using a modified Runge-Kutta method employing Kutta-Simpson formulae. It is known that the integration of the heat transfer equations is difficult because of stability problems. This was overcome by adopting a variable integrating step method. I have integrated the equations by fixing the boundary conditions at the bottom of the ionosphere. Geisler and Bowhill (1965) solve a similar set of equations by integrating downwards from the topside ionosphere, varying the boundary conditions at some height above which the temperatures remain nearly constant (say 5 000 km or so) until stability at the lower boundary of the ionosphere is obtained. I have done the same and the results of this calculation are close to the ones obtained from the method described above except in the very low parts of the ionosphere where both methods are highly unstable because of relatively large temperature and density gradients. The results are shown in figures (15) and (16). A variation of He: H_2 ratio has very little effect on the electron density and temperature variation in the ionosphere. The effect of variation of atmospheric pressure at the cloud level is due to the variation of T_N with cloud level pressure.

It must be noted that the calculations were done only for the steady state. They are characteristic of maximum solar radiation (i.e. for the Jovian ionosphere at noon). Without further knowledge about the composition of the Jovian atmosphere calculation of the variation of the ionization with time does not seem to be justified.

It can be seen from figure 16, that the maximum density of the Jovian ionosphere is about 6×10^6 electron cm^{-3}. This is somewhat larger than the value calculated by Gross and Rasool (1964). It agrees,

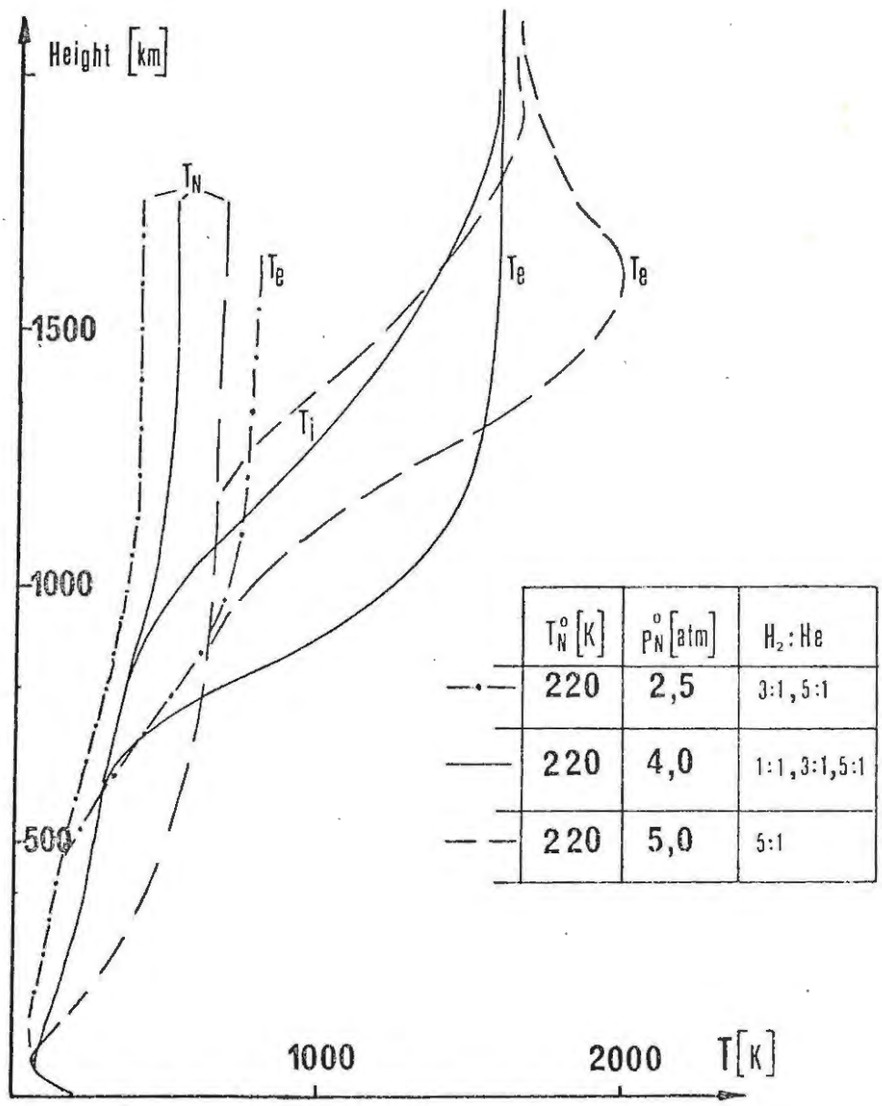

Figure 15: Variation of neutral (T_N), electron (T_e) and ion - temperature (T_i) with height above Jupiter's cloud top level. T_N^o is the neutral temperature at cloud top level and P_N^o is the neutral gas pressure there.

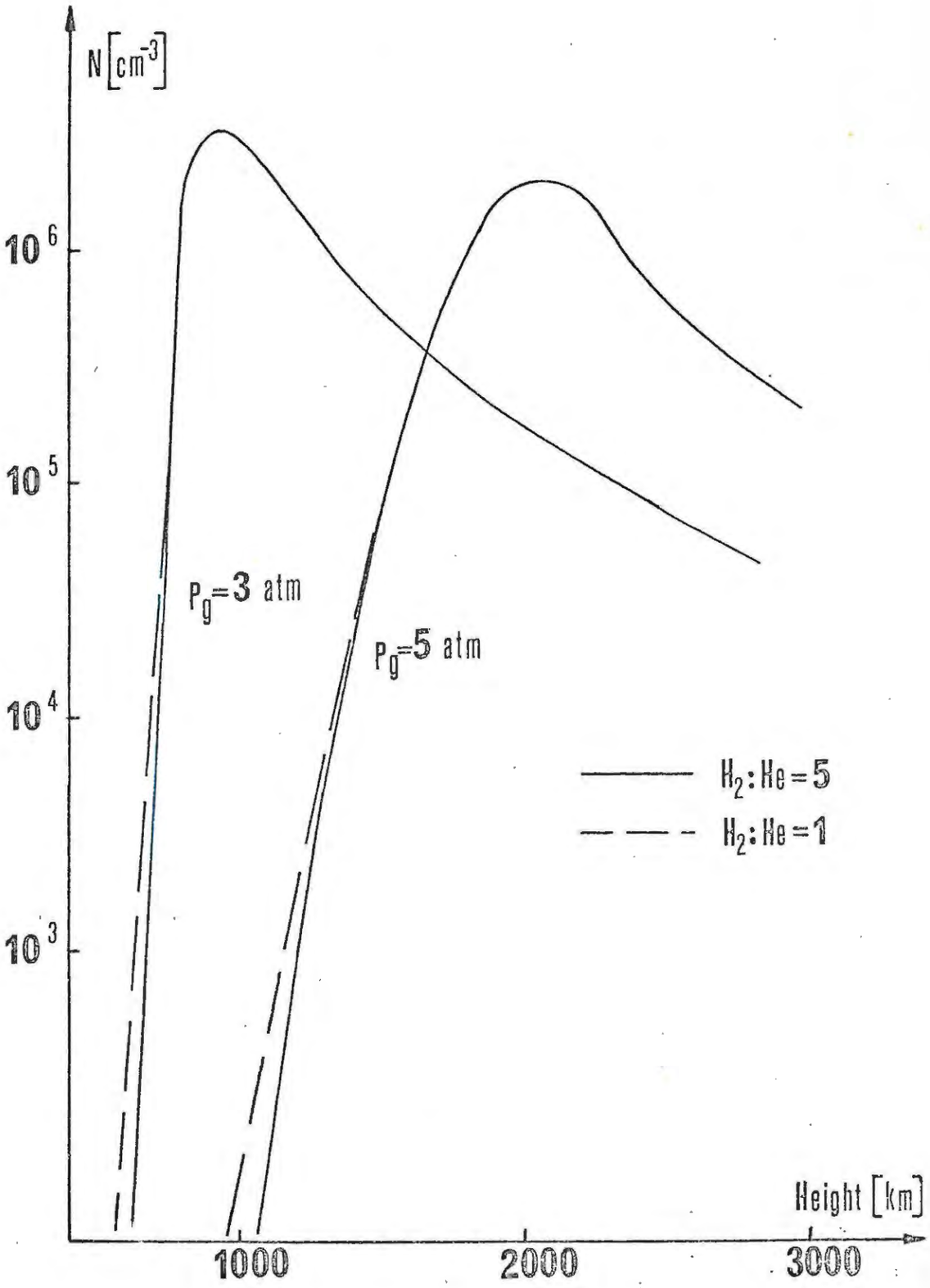

Figure 16: Variation of ionospheric plasma density with height above Jupiter's cloud top level.

however, well with the value for the maximum electron density estimated by Warwick (1970).

The plasma distribution in the topside ionosphere is mainly determined by diffusion. For a static ionosphere in diffusive equilibrium the density decreases exponentially with the plasma scale height $H_p = \frac{2kT_p}{m_i g}$ where $T_p = \frac{1}{2}(T_e + T_i)$, and m_i is the average ionic mass. In the Jovian ionosphere the main ionic component in the topside ionosphere is H^+. There is thus no upward diffusion flux of H^+ like the polar wind or polar breeze in the terrestrial ionosphere, which is due to the acceleration of the minor ionic constituent in the upwardly directed electric field created by the separation of the heavy and light ions and electrons. In the following I will show that nevertheless the Jovian ionosphere cannot be strictly static. It has been suggested by several authors (Gledhill, 1967, Melrose, 1967, and Piddington, 1967) that, if the magnetosphere is corotating with Jupiter, the combined action of the gravitation and centrifugal force will lead to an outward force along a magnetic line of force beyond some distance from the planet.
This force can be expressed as the gradient of a potential V (Gledhill, 1967).

$$(3.1)\quad V = V_0 + g_0 R_J (1 - R_J/r) - \tfrac{1}{2}\Omega^2 (r^2 \sin^2\Theta - R_J^2 \sin^2\Theta_i)$$

where g_0 is the gravitational acceleration at the surface of the planet, R_J Jupiter's radius, Ω the angular velocity of Jupiter, and Θ is the colatitude.

The variation of V along IFT is shown in figure 17.

If the plasma is controlled by collisions, i.e. if the plasma velocity distribution is Maxwellian, this will

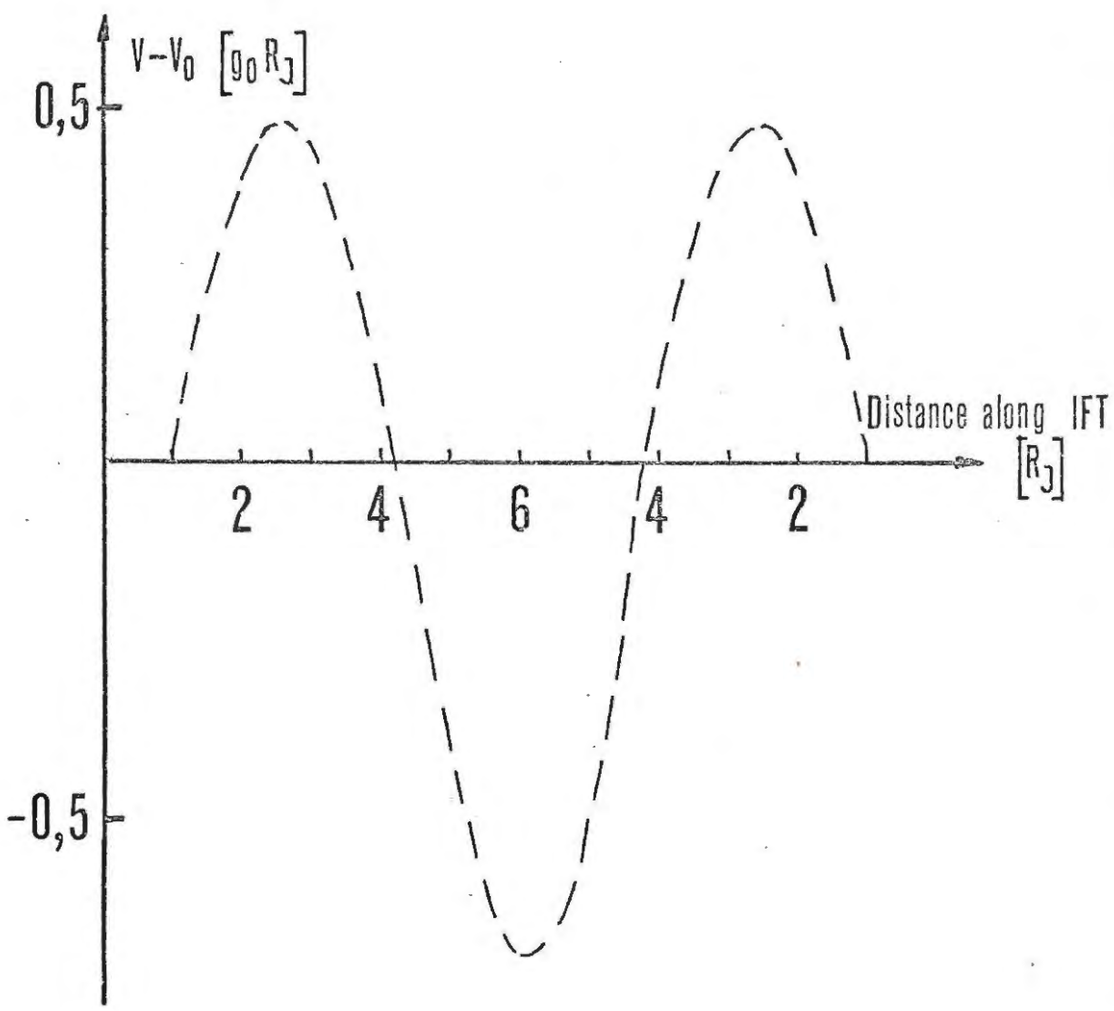

Figure 17: Variation of potential along IFT.

lead to a density variation along a line of force with a minimum at the position where the potential along a field line has a maximum. The density will reach a maximum value in the equatorial plane. The plasma density in the equatorial plane will increase with distance (r) from the planet. Melrose (1967) suggests that this cannot be a reasonable magnetospheric model and that the plasma distribution in the magnetosphere should not be calculated on the assumption of a Maxwellian plasma. Indeed the mean free path of the H^+ ions ($\lambda_{H^+} = v_{th}^4 \, (3 \times 10^{-12})/N \, \ln\Lambda$ where $\Lambda = 1.24 \times 10^4 T^{3/2}/N^{\frac{1}{2}}$) is larger than the plasma scale height if the density drops below a value of $\simeq 10^4$ particles cm^{-3}. In the ionosphere shown in figure 16, the plasma density will decrease below 10^4 particles cm^{-3} at a distance of about $1.3 R_J$ from the planet's centre. At this point the hydrodynamic approximation breaks down and the plasma density must be calculated by methods similar to those given by Johnson (1961) for a collisionless neutral atmosphere. The escape flux, that is the flux of plasma having gained sufficient energy by collisions to overcome the gravitational attraction, can be calculated using a corrected Jeans formula as given by Marubashi (1970).

$$(3.2) \quad \phi = A N \iint_{\substack{v_\parallel > 0 \\ v^2 = v_\parallel^2 + v_\perp^2 > v_{esc}^2}} v_\parallel f(v_\parallel, v_\perp) \, 2\pi v_\perp \, dv_\parallel \, dv_\perp \; ; \; v_{esc}^2 = \frac{2}{m} V(r_0)$$

$$(3.3) \quad f(v_\parallel, v_\perp) = \left(\frac{m}{2\pi kT}\right)^{3/2} \exp\left(-[m/2kT]\{v_\perp^2 + (v_\parallel - v_0)^2\}\right)$$

where $v_\parallel$ stands for the particle velocity component parallel to the magnetic field line and $v_\perp$ is the component perpendicular to the magnetic field. v_0 is an upward diffusion velocity, which can be determined by the following method: Below I will show that the excape flux is actually lost from the ionosphere because

of trapping in the outer parts of the magnetosphere, i.e. very little of the flux escaping from one hemisphere will contribute to the ionization in the other hemisphere. There is thus a loss of particles (from both the northern and southern hemispheres) which must be replenished by an upward diffusion of plasma in the ionosphere. Hence the ionosphere will not be static but will have an upward flow, the velocity (v_o) of which at the level where the hydrodynamic approximation breaks down can be determined by equating the escaping flux to $F = N_o A_o v_o$, where N_o is the plasma density at that level and A_o an area. Thus the ballistic loss of particles given by (3.2) is equated to the upward diffusion flux $A_o N_o v_o$ at that level ($r = r_o$). At the height where $N_o = 10^4$ particles cm^{-3} $F = N_o A_o v_o$ gives $v_o \simeq 10^4$ cm s^{-1} which is much less than the thermal speed of the protons at that level ($T_i = 1500$ K). The loss $A_o N_o v_o$ over an area $A_o = 1 cm^2$ is thus 10^8 particles per second. The total production rate of ion-electron pairs below that level by solar UV radiation is $\int_{r=o}^{r_o} Q(r)A(r)dr$ where $Q(r)$ is the local production rate of ion-electron pairs (see Appendix B), $A(r)$ is the area of the flux tube and r is the distance from the top of the cloud level along the flux tube. r_o is the value of r at the level where $N = 10^4$ cm^{-3}; i.e. where collisions become negligible. The upper estimate of $\int_{r=o}^{r_o} Q(r)A(r)dr$ can be obtained by noting that Q decreases with r at about the same rate as the neutral atmosphere density. Thus $\int_{r=o}^{r_o} Q(r)A(r)dr = Q_M \bar{A} H_N \simeq 5 \bar{A} \times 10^9$ particles s^{-1}. ($Q_M = 3 \times 10^2$ cm^{-3} s^{-1}, $H_N \simeq 160$ km at the level where $Q = Q_M$). Thus the escape flux amounts to less than 2% of the total production rate ($\bar{A} \simeq A_o$).

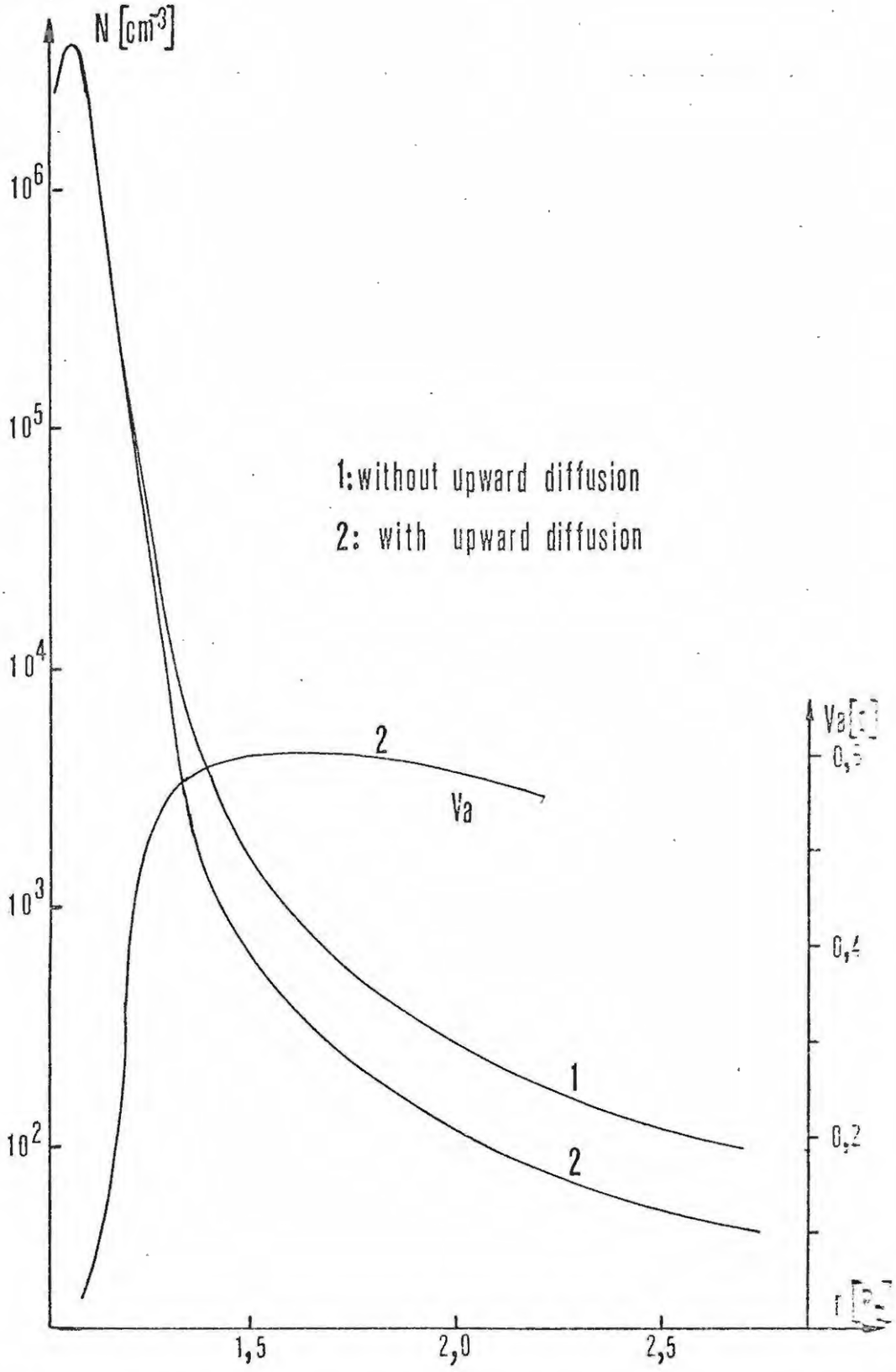

Figure 18: Plasma density and Alfvén velocity along IFT.

The inclusion of the diffusion flux will, however, decrease the density below the value which one would obtain for a static ionosphere for $r \leq 1.3\ R_J$. The density will decrease more steeply for the nonstatic ionosphere. The distribution of plasma along a magnetic field line passing through Io ($L = 5.9$) is shown in figure 18. This figure includes the upward diffusion flux.

In the following we will see that Alfvén waves propagating along the field lines are of major importance in the model of the Io effect presented in this work. I have therefore indicated the variation of Alfvén speed $V_A = B/(\varsigma \mu_o)^{\frac{1}{2}}$ along IFT assuming a field $B_E = 8$ G. ς is the plasma density and μ_o is the permeability of free space. It is obvious that the Alfvén speed changes rapidly in the region 1.05 - 1.20 R_J and is nearly constant for larger distances.

3.2 Jupiter's Magnetosphere

The treatment, described in the last section, is adequate only for the ionosphere itself, where Jupiter's rapid rotation has only a small influence on the plasma distribution. Ellis (1965) pointed out that, if the magnetosphere corotates with the planet, beyond about three Jupiter radii the net acceleration on a corotating particle is directed away from the planet. Also the rotational kinetic energy density exceeds the thermal energy density at some distance. One would expect the rotational kinetic energy to be the dominant term in any magnetosphere.

The centrifugal acceleration is included in the model magnetospheres of Angerami and Thomas (1964), Gledhill (1967), Piddington (1967) and Melrose (1967).

Assuming a Maxwellian velocity distribution, the plasma density increases with distance in the region where the centrifugal force exceeds the gravitational force. Clearly a density which increases above all limits at large distances is unrealistic. One must therefore look for physical conditions which limit the density in such a way that it decreases with distance in some regular manner. The following physical conditions have been suggested to be effective in limiting the density.

1. Gledhill (1967) assumes that the maximum plasma density able to corotate with Jupiter is determined by the ability of the magnetic field to exert enough force on the plasma to provide the required centripetal acceleration for corotation. He estimates the maximum number density of plasma in the equatorial plane by equating the magnetic and rotational kinetic energy densities, which leads to

$$(3.4) \quad N_{MAX} = \frac{B_E^2}{\mu_0 m \Omega^2 R_J^2 L^8}$$

Thus the density decreases as $N \propto 1/r^8$ (where $r = R_J L$) in the equatorial plane.

2. Piddington (1967) calculates the maximum density by assuming, that the force exerted on the plasma by the magnetic field just cancels the centrifugal force. The force is a $\vec{j} \times \vec{B}$ force, as in a curved field, electrons and ions execute drift motions perpendicular to both the field and the radius of curvature. The current density is given by

$$(3.5) \quad j = \frac{N m r^4 R_J}{2 B_E \mu_0}$$

He then makes an order of magnitude estimate for stability by requiring that the magnetic field gradient

due to the current j must be less than the gradient of the dipole field. This leads to

$$(3.6) \qquad N \leq \frac{3 B_E^2}{\mu_o m \Omega^2 R_J^2 L^8}$$

This is very similar to Gledhill's condition. The plasma density also drops as $N \propto 1/r^8$.

3. Melrose (1967) requires the magnetosphere to be stable against interchange motion. If the density falls off too fast then the interchange motion of flux tubes will tend to decrease the density gradient by replacing inner, denser flux tubes by outer, less dense flux tubes. The condition for this not to happen, can be written, as Melrose has shown (assuming constant pressure in the magnetosphere)

$$(3.7) \qquad -\frac{1}{N}\frac{dN}{dr'} \leq \frac{\beta^2 \gamma a^{-1} (\gamma - 1)}{r'\left(b r'^2 - \frac{1}{r'} + \beta\gamma/a\right)}$$

β is 1 plus the exponent in the radial dependence of the magnetic induction. For a dipole field β is 4. γ is the ratio of specific heats.

$a = R_J/H_p$ where H_p is the plasma scale height.

$$b = \frac{\Omega^2 R_J}{g_o} = 8.6 \times 10^{-2}$$

r' is the radius normalized to R_J

$r' = r/R_J$

At the point r' = 2.3, where $br'^2 - 1/r' = 0$, the gravitational force just balances the centrifugal force. At this point the density cannot fall off faster than

$$(3.8) \qquad N \propto r^{-(\beta)} = r^{-4}$$

For r' > 10 the density should, according to equation (3.7), be nearly constant. Melrose (1967) calculates the density along any given field line and finds

assuming a collionless plasma:

$$(3.9)\quad N = N_m \left[(1 - \operatorname{erf} x_1) \exp x_1^2 - \left(1 - \frac{B}{B_m}\right)^{1/2} (1 - \operatorname{erf} x_2) \exp x_2^2 \right]$$

where $$x_1^2 = \frac{m_i}{2kT} \left(V(r_m) - V(r) \right) = \frac{a}{2} \frac{V(r_m) - V(r)}{g R_J}$$

$$x_2^2 = \left(1 - \frac{B}{B_m}\right) x_1^2$$

V is the potential energy per unit mass (see formula (3.1)).

At $r_m = \left(\frac{3}{2} \; b \sin^2 \Theta_i\right)^{-\frac{1}{4}}$

V has a maximum. The plasma density at this point is N_m, B_m is the magnetic induction and V_m the potential energy density. For $r > 2\, r_m$ one can take the asymptotic form of (3.9) and write

$$(3.10)\quad N \approx \frac{N_m}{B_m} \left(\frac{2}{a b \pi} \right)^{1/2} B r^{-1} \propto r^{-\beta}$$

For the field lines passing through Io ($r' \simeq 6$), the density in a collionless plasma model should fall off faster than allowed by this interchange instability condition. Thus there must be some plasma trapped in the outer region between the potential maxima in the northern and southern hemisphere, in order to make the whole magnetosphere stable against interchange motion. A similar conclusion is reached by Gledhill (1967), although on different grounds. The question, however, is: by what physical mechanism can plasma be supplied to the outer regions of the magnetosphere?

Brice (1968) suggests that unthermalized photoelectrons released high in the ionosphere cause a flux of electrons which can fill the centrifugally dominated region. He finds that the minimum density in the magnetosphere due to these photoelectrons alone will be $0{,}1\ \mathrm{cm}^{-3}$ at a few R_J with an increase to $N \approx 10\ \mathrm{cm}^{-3}$ at $r > 10\ R_J$. Piddington (1967) has suggested that

heating of the ionosphere plasma may supply large electron fluxes which will fill up the outer parts of the magnetosphere. In the following section, the possibility of filling the outer regions of the magnetosphere with plasma by a two stream instability process will be investigated.

Beyond r_m the net force (centrifugal plus gravitational) accelerates particles outwards. The resulting electron velocity distribution will be double-humped. The particles will flow along the field lines with a velocity $u = (2\ (V_m - V))^{\frac{1}{2}}$. There are two streams penetrating each other, one flowing from the northern to the southern hemisphere and the other flowing in the opposite direction. Such a distribution is unstable against the two stream instability. The conditions for this instability to set in will be investigated in the following. Basically the instability leads to a flow of energy from the streaming motion of the particles into electric fields. Electron bunches will be formed which will move with a smaller velocity than u along the field line.
Their velocity is thus not sufficient to allow them to move over the potential barrier set up by the combination of centrifugal and gravitational forces. These electrons will consequently be trapped in the outer region of the magnetosphere and increase the density above that given by a collisionless model. Collisions within these bunches will lead to fast thermalization. One would expect the plasma in the magnetosphere to consist of two components:

a) Two plasma streams streaming with a velocity u and

b) a thermalized plasma trapped between the

potential barriers in the outer regions of the magnetosphere. This plasma might not be uniformly distributed but rather be made up of irregularly occurring "blobs".

3.3 The Two Stream Instability

It is known that the possibility of instability or growth of waves is associated with plasma streams. (For a definition of instability see Clemmow and Dougherty (1969)). There are various instabilities possible in the case of two plasma streams penetrating each other. For a number of plasma parameters a wave (longitudinal or transverse) may have a speed appreciably less than the speed of light in vacuum. It may then be possible that the charged particles in the stream move with a speed close to that of the wave. As a consequence of this they are under the influence of a nearly constant electric field. Under some circumstances the particles may steadily convert their macroscopic streaming energy to the field energy of the wave. In this case the waves are amplified or, in other words, the waves are unstable. If the field energy of the wave accelerates the particles, the wave is damped. A different possiblity of wave amplification may be due to the following process: the wave field accelerates the particles away from some region and they are returned to the region with a different density by the macroscopic streaming motion. If this bunching of the particles is phased appropriately the wave may be amplified. The first process is analogous to a travelling wave amplifier whereas the second process is analogous to that of an oscillator.

The analysis of instabilities is conveniently done by linearizing Maxwell's equations and looking for harmonic solutions in time and space. This method only allows for a prediction of an instability but not for a description of the increase of the wave amplitude in time or space. This can only be done by nonlinear analysis. Here we will adopt the following argument. If the plasma beam system in the Jovian magnetosphere allows for an instability the (linear) growth rate of which is large enough, then the plasma beams will lose energy in such a way that the whole system is driven towards a stable situation. We are interested to find instabilities which feed on the macroscopic streaming energy $\frac{1}{2} \varsigma U^2$ of the plasma beam. For $U = 0$, the plasma is Maxwellian and stable. If U is initially larger than a critical velocity U_c instabilities will start. The instability will reduce the streaming velocity to a value less than U_c. In the limiting steady state case the plasma beam will have a velocity U_c, because if $U > U_c$ the instability will decrease U to $U \lesssim U_c$. If U decreases below U_c the agent responsible for the initial streaming motion will accelerate the particles to larger values of U until at U_c the instability sets in again.

There are two streams in the Jovian magnetosphere, each of which is neutral and of the same density. There may also be plasma at rest with respect to the magnetic field (this, of course, means at rest with respect to Jupiter if the plasma corotates with Jupiter). Each stream will make a contribution to the conductivity σ_{ij} and the conductivity of the whole system is simply obtained by the addition of the contributions from each component of the whole magnetospheric plasma system.

The perturbation is assumed to vary as $e^{i(\omega t - kx)}$ where x is the direction of the magnetic field $\vec{B} = (B,0,0)$. The velocities of the streams are $\vec{U}_1 = (U,0,0)$ $\vec{U}_2 = (-U,0,0)$. ($U \ll c$). The density of each stream is N and the density of the stationary plasma is N_o. The pressure force per unit volume in the non-relativistic form is given by $-\gamma KT \operatorname{grad} n$, where γ is the specific heat ratio, and n is the excess number density of particles over the equilibrium value N. The linearized current density is then given as (neglecting the motion of the heavy ions)

$$(3.11) \qquad \vec{j} = -eN\vec{v} - e\vec{U}n$$

the charge continuity equation is:

$$(3.12) \qquad \operatorname{div}\vec{j} = e\frac{\partial n}{\partial t}$$

The components of the current density are then:

$$(3.13) \qquad \begin{aligned} j_x &= -eN\frac{\omega}{\omega - kU}v_x \\ j_y &= -eN\, v_y \\ j_z &= -eN\, v_z \end{aligned}$$

The non-relativistic equation of motion of the electrons can be written as

$$(3.14) \quad \frac{D}{Dt}(\vec{U}+\vec{v}) = \frac{\partial}{\partial t}(\vec{U}+\vec{v}) + (\vec{U}+\vec{v})\nabla\cdot(\vec{U}+\vec{v}) = -\frac{e}{m}\left[\vec{E} + (\vec{U}+\vec{v})\times\vec{B}\right] - a^2 \operatorname{grad} n$$

where $a^2 = KT/m$ is a velocity of sound. The Fourier transform of this equation gives for the perturbation of the stream (U,0,0)

$$(3.15) \qquad \begin{aligned} v_x &= i\frac{e}{m}\frac{\omega - kU}{(\omega - kU)^2 - a^2k^2}E_x \\ v_y &= i\frac{e}{m\omega}\left[E_y + i\frac{\Omega}{(\omega - Uk)}E_z\right]A^{-1} \\ v_z &= i\frac{e}{m\omega}\left[E_z - i\frac{\Omega}{(\omega - Uk)}E_z\right]A^{-1} \end{aligned}$$

where $\Omega = eB_o/m$ and $A = ((\omega - Uk)^2 - \Omega^2)/(\omega - Uk)^2$

with equations (3.13) and (3.15) one obtains

$$(3.16)\quad j_x = -i\omega\varepsilon_0 \frac{\omega_p^2}{\omega^2} \frac{1}{(1-\frac{k}{\omega}u)^2 - a^2k^2/\omega^2} E_x$$

$$j_y = -i\omega\varepsilon_0 \frac{\omega_p^2}{\omega^2} \left[E_y + i\frac{\Omega}{(\omega-uk)} E_z\right] A^{-1}$$

$$j_z = -i\omega\varepsilon_0 \frac{\omega_p^2}{\omega^2} \left[E_z - i\frac{\Omega}{(\omega-uk)} E_y\right] A^{-1}$$

where $\omega_p^2 = Ne^2/\varepsilon_0 m$ is the square of the plasma frequency times 2π.

The conductivity tensor is thus

$$(3.17)\quad \sigma = \begin{pmatrix} \sigma_{11} & 0 & 0 \\ 0 & \sigma_{22} & \sigma_{23} \\ 0 & \sigma_{32} & \sigma_{33} \end{pmatrix}$$

where:

$$(3.18)\quad \sigma_{11} = -i\omega\varepsilon_0 \frac{\omega_p^2}{\omega^2} \frac{1}{(1-\frac{k}{\omega}u)^2 - a^2k^2/\omega^2}$$

$$\sigma_{22} = -i\omega\varepsilon_0 \frac{\omega_p^2}{\omega^2} A^{-1} = \sigma_{33}$$

$$\sigma_{23} = -i\omega\varepsilon_0 \frac{\omega_p^2}{\omega^2} \left\{\frac{i\Omega}{\omega-ku}\right\} A^{-1} = -\sigma_{32}$$

Including the stream $(-U,0,0)$ with the same plasma density (i.e. $\omega_{p_1} = \omega_{p_2}$) and the stationary background plasma with a plasma frequency ω_{p_0} gives:

$$(3.19)\quad \sigma_{11} = -i\omega\varepsilon_0 \left\{\frac{\omega_p^2}{\omega^2}\left(\frac{1}{(1-\frac{k}{\omega}u)^2 - a^2k^2/\omega^2} + \frac{1}{(1+\frac{k}{\omega}u)^2 - a^2k^2/\omega^2}\right) - \frac{\omega_{p_0}^2}{\omega^2} \frac{1}{1 - a_0^2k^2/\omega^2}\right.$$

$$\sigma_{22} \simeq \sigma_{33} = -i\omega\varepsilon_0 \left\{\frac{\omega_p^2}{\omega^2}\left(A_+^{-1} + A_-^{-1}\right) + \omega_{p_0}^2 \frac{1}{\omega^2-\Omega^2}\right\}$$

$$\sigma_{23} = -\sigma_{32} = -i\omega\varepsilon_0 \left\{\frac{\omega_p^2}{\omega^2}\left(\frac{A_+^{-1}}{\omega-ku} - \frac{A_-^{-1}}{\omega+ku}\right) i\Omega + \omega_{p_0}^2 \frac{i\Omega}{\omega(\omega^2-\Omega^2)}\right.$$

where $A_+ = A$ and $A_- = ((\omega + ku)^2 - \Omega^2)/(\omega + ku)^2$

The equivalent dielectric tensor $\underline{K}_{ij} = \delta_{ij} - i\frac{\sigma_{ij}}{\omega\varepsilon_0}$ is easily derived from these equations

(3.20)
$$\underline{K} = \begin{pmatrix} K_{11} & 0 & 0 \\ 0 & K_{22} & K_{23} \\ 0 & K_{32} & K_{33} \end{pmatrix}$$

where

(3.21)
$$K_{11} = 1 - \left[\omega_p^2 \left\{ \frac{1}{(\omega - kU)^2 - a^2k^2} + \frac{1}{(\omega + kU)^2 - a^2k^2} \right\} + \frac{\omega_{po}^2}{\omega^2 - a_o k^2} \right] = 1 - B$$

$$K_{22} = 1 - \left[\omega_p^2 \left\{ \frac{A_+^{-1} + A_-^{-1}}{\omega^2} \right\} + \frac{\omega_{po}^2}{\omega^2 - \Omega^2} = K_{33} = \right] 1 - C$$

$$K_{23} = i\Omega \left[\frac{\omega_p^2}{\omega^2} \left\{ \frac{A_+^{-1}}{\omega - kU} + \frac{A_-^{-1}}{\omega + kU} \right\} + \frac{\omega_{po}^2}{\omega(\omega^2 - \Omega^2)} \right] = -K_{32} = iD$$

From Maxwell's equations

(3.23)
$$\nabla \times \vec{E} = -i\omega\mu_o \vec{H}$$
$$\nabla \times \vec{H} = i\omega\varepsilon_o \underline{K} \vec{E}$$

we get by elimination of $\vec{H}$

(3.24)
$$-\mu^2 \hat{k} \times (\hat{k} \times \vec{E}) = \underline{K} \vec{E}$$

where $\hat{k}$ is a unit vector along the direction of wave propagation ($\vec{k} = k\,\hat{k}$) and μ is the refractive index $\mu = ck/\omega$. For waves propagating along the x-axis one obtains $\vec{k} = (k_x, 0, 0)$

(3.25)
$$\mu^2 (0, E_y, E_z) = \underline{K} \vec{E}$$

The solution of this equation yields the secular determinant

(3.26)
$$\begin{vmatrix} K_{11} & 0 & 0 \\ 0 & K_{22} - \mu^2 & K_{23} \\ 0 & K_{32} & K_{33} - \mu_2 \end{vmatrix} = 0$$

The dispersion equations for the characteristic waves are then given either by

(3.27) $$K_{\parallel} = 1 - B = 0$$

or by

(3.28) $$(K_{22} - \mu^2)(K_{33} - \mu^2) = K_{23} K_{32}$$

The wave described by (3.27) is a purely longitudinal wave as can be seen from (3.25). For the plasma system with two beams and a stationary background plasma (3.27) is written as

(3.29) $$1 = \frac{\omega_{p_1}^2}{(\omega - kU_1)^2 - a_1^2 k^2} + \frac{\omega_{p_2}^2}{(\omega - kU_2)^2 - a_2^2 k^2} - \frac{\omega_{p_0}^2}{\omega^2 - a_0^2 k^2}$$

where the indices 1, 2, 0 refer to beam 1, beam 2 and the stationary background plasma respectively.
In the case of the Jovian magnetosphere we have (as above) $\omega_{p1} = \omega_{p2} = \omega_p$, $U_1 = -U_2 = U$, $a_1 = a_2 = a$.
Then the dispersion equation reads:

(3.30) $$1 = \omega_p^2 \left(\frac{1}{(\omega - kU)^2 - a^2 k^2} + \frac{1}{(\omega + kU)^2 - a^2 k^2} \right) + \frac{\omega_{p_0}^2}{\omega^2 - a_0^2 k^2}$$

The analysis of this equation with respect to possible instabilities is conveniently done if we rewrite it by introducing $W = \omega/k$ (the phase velocity of the wave under consideration)

(3.31) $$G(W) = \omega_p^2 \left(\frac{1}{(W-U)^2 - a^2} + \frac{1}{(W+U)^2 - a^2} \right) + \frac{\omega_{p_0}^2}{W^2 - a_0^2} = k^2$$

Suppose first that $a \ll U$ then figure (19) shows $G(W)$ as a function of U. Clearly for $a_0 < U$ there is always a pair of conjugate complex values for ω for all real values of k for which k^2 is less than a minimum value. These correspond to an instability. According to the criteria for instabilities given by Glemmow and Dougherty (1969) this instability is a non-convected instability. This case corresponds to a cold beam and a cold stationary plasma. Figure (20) shows

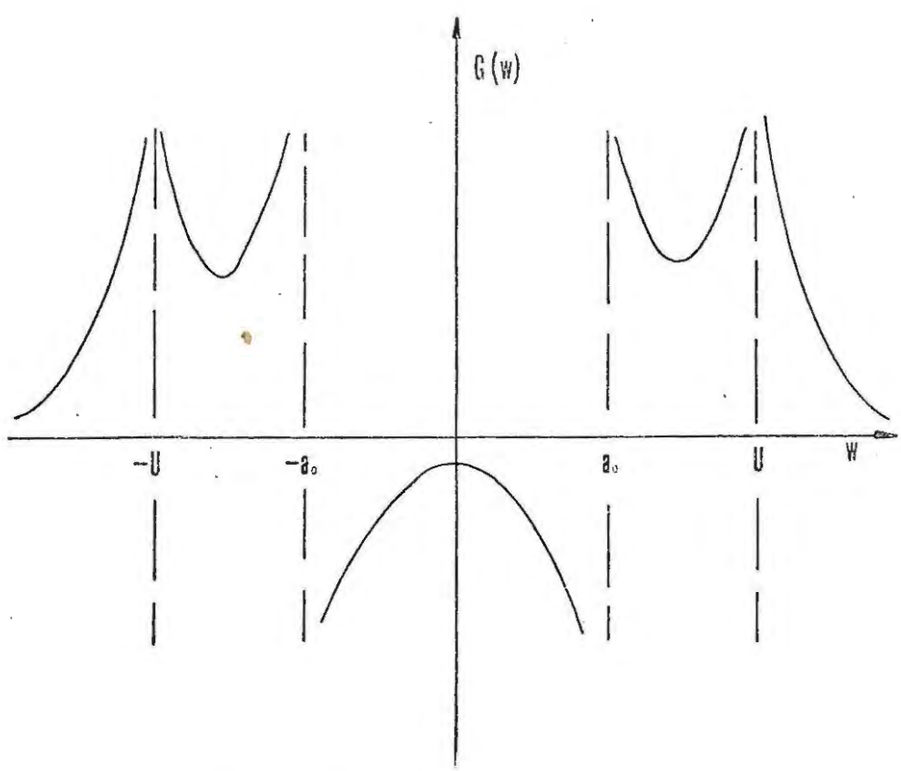

Figure 19: G (W) as a function of W for the case: $a_o < U$, $a \approx 0$.

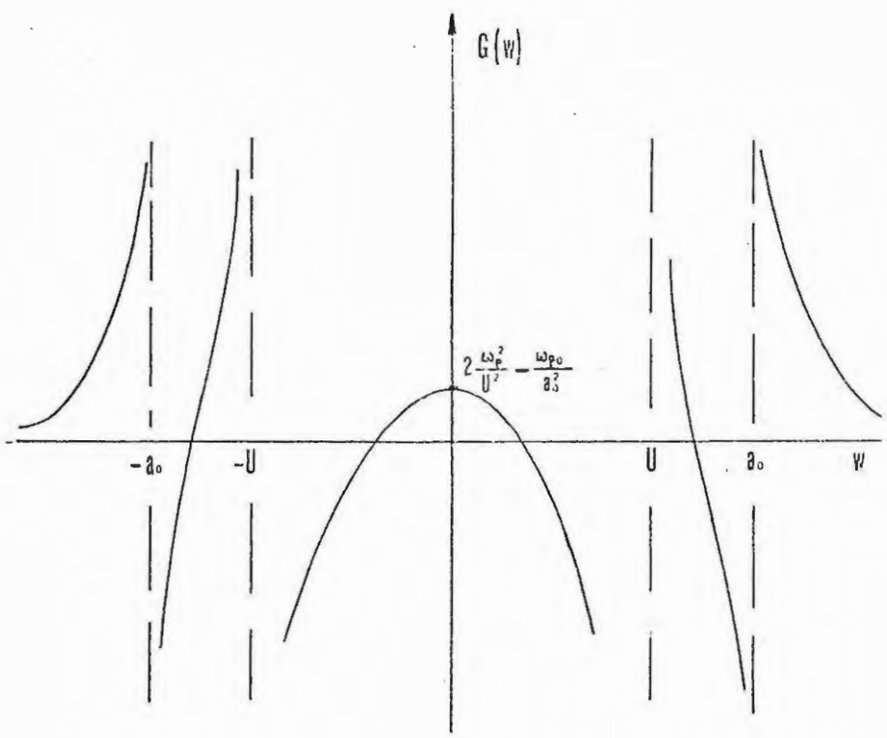

Figure 20: G (W) for hot background plasma, $a_o > U$, but cold streaming plasma, $a \approx 0$.

that for $a_o > U$ the instability is prevented if the background plasma density becomes larger than the density of the plasma in the beams (exactly : $\omega_{po} > \sqrt{2}\,\frac{a_o}{U}\,\omega_p$).

This case corresponds to a cold beam but a hot background plasma (a refers to a velocity of sound in the beam and a_o refers to the same quantity in the stationary background plasma).

Along IFT the velocity U is given by

$$(3.32)\quad \frac{U^2}{2} = \left(V_m - V\right) = -g_o R_J^2\left(\frac{1}{r'_m} - \frac{1}{r'}\right) - \frac{1}{2}\Omega^2\left(r_m^2 \sin^2\Theta_m - r^2\sin^2\Theta\right)$$

The index m again stands for the potential maximum. The maximum value of U accurs for $\sin\Theta = 1$. For IFT $r'_m \simeq 2{,}6$. Thus

$$(3.33)\quad U^2 = 2 g_o R_J\left[\frac{1}{5{,}9} - \frac{1}{2{,}6} - 2{,}3\times10^{-2}\left(\frac{(2{,}6)^3}{5{,}9} - (5{,}9)^2\right)\right] = 0{,}95\, g_o R_J$$

The velocity U is calculated from this as 50 km/s. Thus in this case the electron temperature of the stationary plasma in the magnetosphere should be less than 100 K, for the instability to be active. This is very unlikely, if the ionosphere (where $T_e \gtrsim 1\,000$ K) is the only source of magnetospheric plasma. If the plasma beams have finite temperature whereas the background plasma is cold, the condition for instability is $U > a$ as can be seen from figures (21a) and (21b). If both the plasma and the background plasma have a finite temperature the conditions for instability is again $U > a$ /see figure (22)/. From this discussion we conclude that the electrons in the beams propagating through the Jovian magnetosphere will not excite longitudinal waves. The treatment above has, however, completely neglected the perturbation of the ion motions. Longitudinal waves can also be excited by

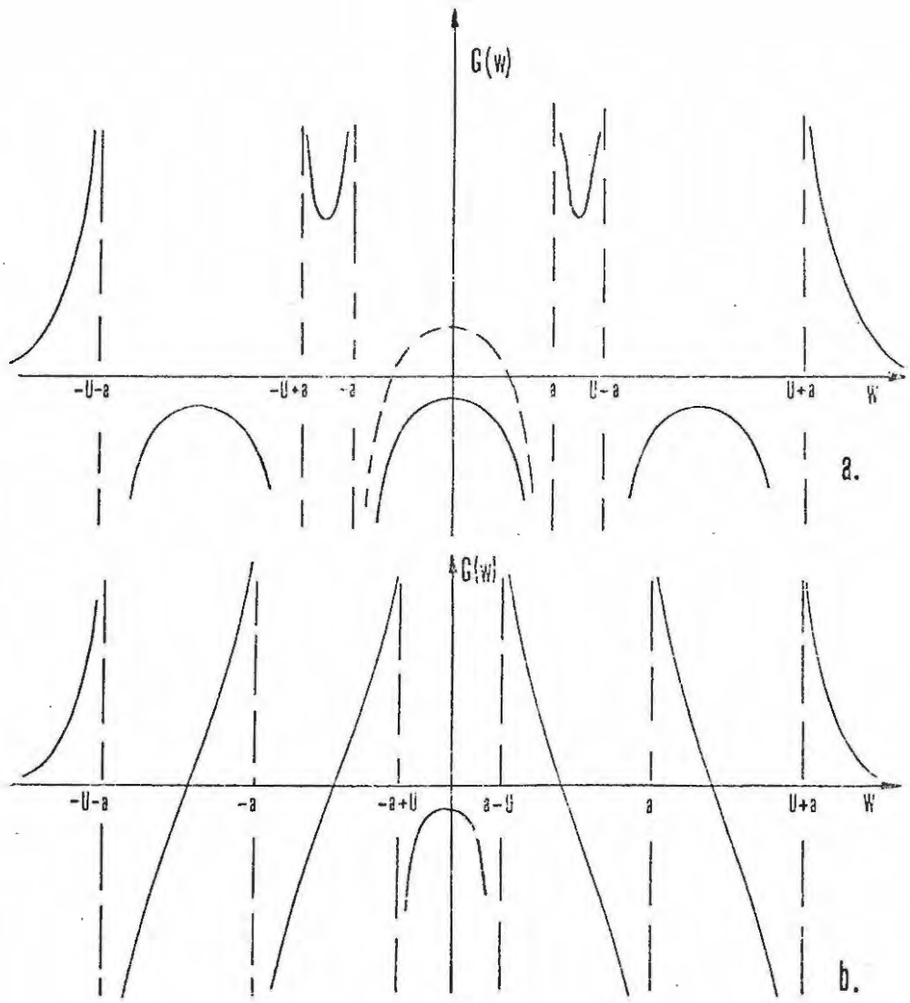

Figure 21: a) G (W) for a_o << U and a < U, i.e. cold background and beam plasma.

b) G (W) for a_o << U but a > U, i.e. cold background but hot beam plasma.

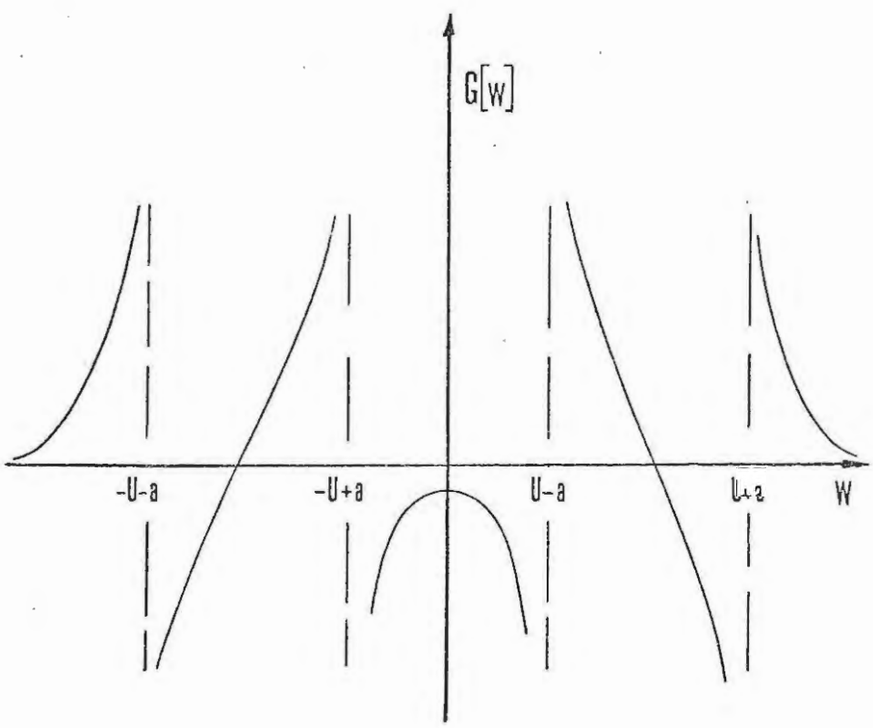

Figure 22: G (W) for equal temperature of the background and beam plasma, $a = a_o$. a) $a < U$ b) $a > U$.

the ions in the two streams which flow with the same average velocity as the electrons (the velocity U is related to the change in potential energy per unit mass which is, of course, independent of the particle's mass). A treatment exactly like the one above must be applied to the ion motion.

The dispersion relation (3.31) is then

$$(3.34)\quad \Phi(W) = \omega_{pe}^2\left(\frac{1}{(W-U)^2-a^2} + \frac{1}{(W+U)^2-a^2}\right) + \frac{\omega_{pe0}^2}{W^2-a_0^2}$$
$$+ \omega_{pi}^2\left(\frac{1}{(W-U)^2-b^2} + \frac{1}{(W+U)^2-b^2}\right) + \frac{\omega_{pi0}^2}{W^2-b_0^2}$$
$$= G_e(W) - G_i(W)$$

where $\omega_{pi}^2 = Ne^2/\varepsilon_0 m_i \quad b^2 = \gamma KT/m_i$

The subscript i refers to ions and the index e to electrons. Figure (23) shows a plot of $\Phi(W)$ versus W. It is seen that the ion contribution $G_i(W)$ allows for an instability.

In this case the condition for the instability to set in is $U > b$, at IFT the ion temperature must be larger than 4 000 K to prevent the instability. T_i will most likely be less than 4 000 K in the beam and in the stationary plasma and the ions will excite the longitudinal waves.

The initial growth rate ($\omega_{po} < \omega_p$) is a maximum at $k = \frac{1}{2}\sqrt{3}\,\omega_{p_i}/U$ and has the value $e^{\omega_{pi}t/2}$. At Io's orbit the plasma streams have a density of $N = 10\ cm^{-3}$ and $U = 50$ km/s. The e-folding time of the instability is $\tau_e \approx 5 \times 10^{-4}$ [s] and $k = 7.3 \times 10^{-1}$ [m^{-1}]. This instability will grow rapidly in its initial stage until either non-linear effects limit the further growth or the background plasma becomes dense enough to prevent the instability.

The condition for instability $U > b$ can be

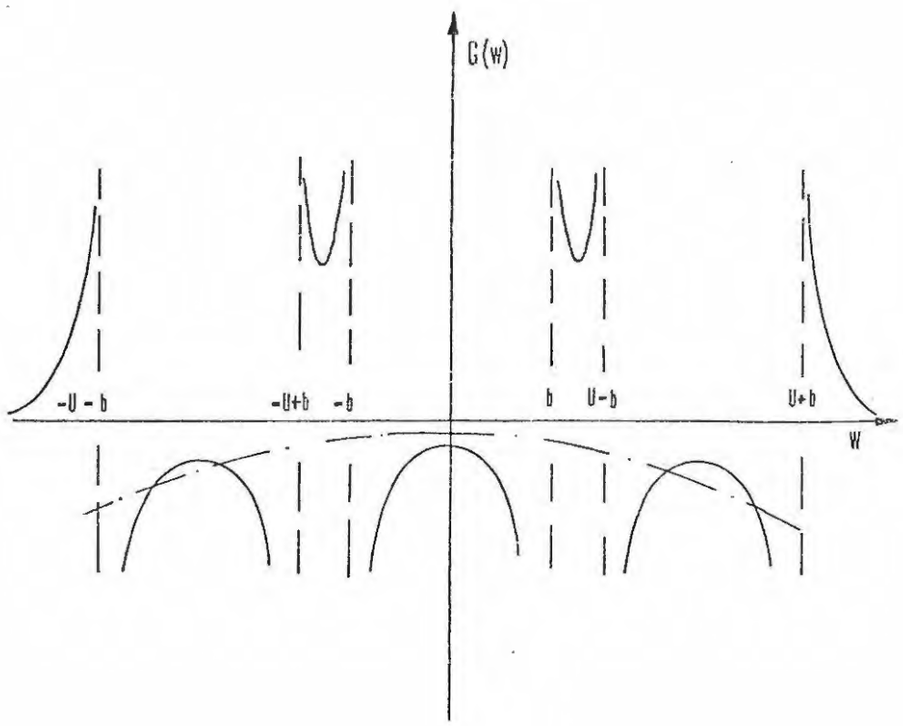

Figure 23: G (W) including the contribution of the ions in the station background plasma:
G_i (W) ——— G_e (W) —·—·—

written as (taking U in the equatorial plane, i.e. at $\sin\Theta = 1$, from (3.33) and

$$-2g_0 R_J^2\left(\frac{1}{r_m}-\frac{1}{L}\right)-\Omega^2\left(r_m^2\sin^2\Theta_m - R_J^2L^2\right) > \frac{\gamma KT}{m_i}$$

or

$$\left(\frac{R_J}{r_m}-\frac{R_J}{L}-\frac{1}{2}b\left(\frac{r_m^2}{R_J^2}\sin^2\Theta_m - L^2\right)\right) > \frac{\gamma KT}{m_i g_0}\frac{1}{2R_J}$$

now $r = R_J L \sin^2\Theta$ along a magnetic field line

$$(3.35)\quad \left(\frac{R_J}{r_m}-\frac{R_J}{L}-\frac{1}{2}b\left[\frac{r_m^3}{R_J^3 L}-L^2\right]\right) > \gamma\frac{H}{2R_J}$$

where $b = \Omega^2/g_0 R_J = 4.6 \times 10^{-2}$ for Jupiter

and $H = KT/m_i g_0$ is the scale height of the positive ions. Taking $T \simeq 1\,500$ K as in the ionosphere the RHS of (3.35) is $3{,}6\,\gamma \times 10^{-3}$. For $\gamma = 3$ (1 dimensional particle motion) one obtains the condition for instability:

$$(3.36)\quad \left(\frac{R_J}{r_m}-\frac{R_J}{L}-2{,}3\times10^{-2}\left[\frac{r_m^3}{LR_J^3}-L^2\right]\right) > 1{,}1\times10^{-2}$$

Figure (24) is a plot of the LHS of (3.36) as a function of L it is seen that only for $L \geq 3$ will the condition for instability ($U > b$) be fulfilled. i.e. only that plasma which moves along field lines with L values larger than 3 will have a sufficiently high streaming velocity to trigger the instability.

The dispersion equation (3.28) describes a transverse wave. With the notations (3.22) equation (3.28) can be rewritten as:

$$(3.37)\quad (1-\mu^2-C)^2 = D^2$$

$$(3.38)\quad \mu^2 = 1-\frac{\omega_p^2}{\omega^2}\left(A_+^{-1}+A_-^{-1}\right)-\frac{\omega_{p_0}^2}{(\omega^2-\Omega^2)}\pm\frac{\Omega\omega_p^2}{\omega^2}\left(\frac{A_+^{-1}}{\omega-kU}+\frac{A_-^{-1}}{\omega+kU}\right)$$

$$\pm\frac{\Omega}{\omega}\frac{\omega_{p_0}^2}{\omega^2-\Omega^2}$$

$$= 1-\frac{\omega_p^2}{\omega^2}\left(\frac{\omega-Uk}{(\omega-Uk)\pm\Omega}+\frac{\omega+Uk}{(\omega+Uk)\pm\Omega}\right)-\omega_{p_0}^2\frac{1}{\omega(\omega\pm\Omega)} = \frac{c^2k^2}{\omega^2}$$

or

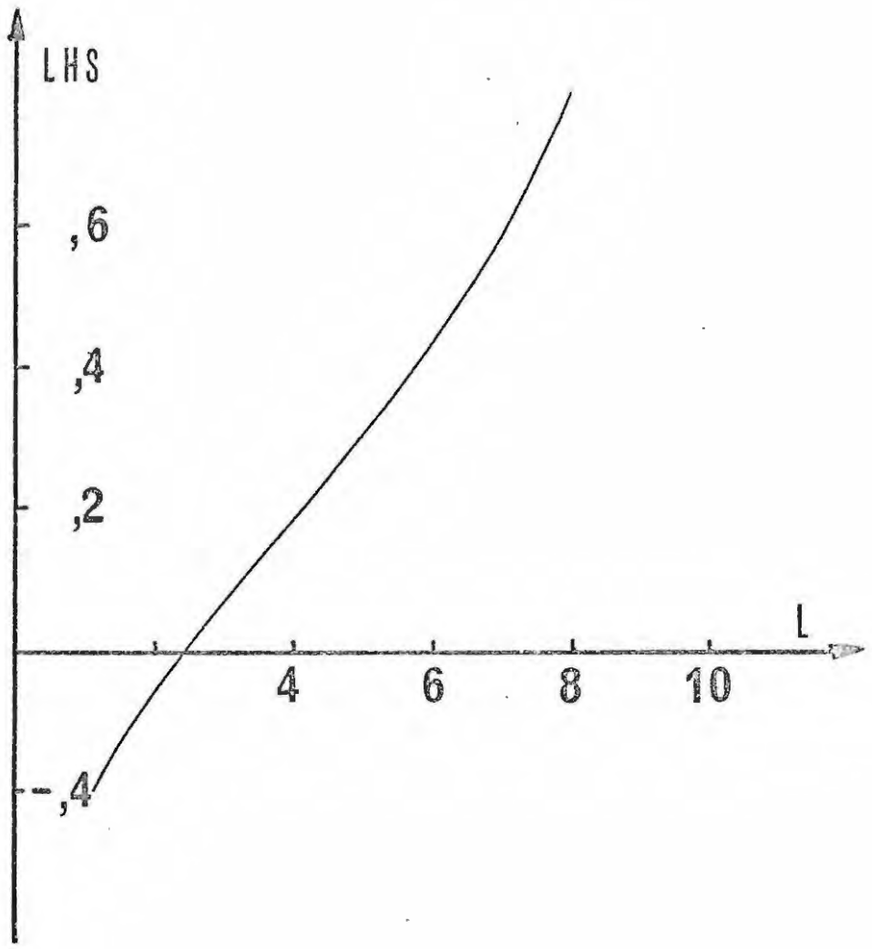

Figure 24: LHS of equation (3.36).

$$(3.39)\qquad c^2k^2 = \omega^2 - \omega_{po}^2\frac{\omega}{\omega\pm\Omega} - \omega_p^2\left(\frac{\omega-Uk}{\omega-Uk\pm\Omega} + \frac{\omega+Uk}{\omega+Uk\pm\Omega}\right)$$

This can be written in a general form

$$(3.40)\qquad c^2k^2 = \omega^2 - \omega_{po}^2\frac{\omega}{\omega-\Omega} - \omega_p^2\left(\frac{\omega-Uk}{\omega-Uk-\Omega} + \frac{\omega+Uk}{\omega+Uk-\Omega}\right)$$

In this expression (3.40) ω and k may both be positive or negative. If the electric field vector rotates clockwise when the observer looks in the positive x-direction(i.e. in the direction of B_o) ω is positive. The phase velocity of the wave is ω/k. The wave propagates in the direction of B_o if $\omega/k > 0$ and opposite to B_o when $\omega/k < 0$. Including the perturbation of the ions in the stationary plasma (as $U \gg V_i$ we may neglect the effect of the ions in the beams) yields the following dispersion equation:

$$(3.41)\qquad \Phi(\omega) = c^2k^2 - \omega^2 + \omega_{po}^2\left\{\frac{\omega}{\omega\pm\Omega_e} - \frac{\alpha\omega}{\omega\mp\Omega_i}\right\} + \omega_p^2\,G(\omega) = 0$$

where

$$\alpha = m_e/m_i \ll 1 \qquad \Omega_e = \frac{eB_o}{m_e} \qquad \Omega_i = \frac{eB_o}{m_i}$$

$$G(\omega) = \frac{\omega-Uk}{\omega-Uk\pm\Omega_e} + \frac{\omega+Uk}{\omega+Uk\pm\Omega_e}$$

Figure (25a) is a plot of $G(\omega)$ for a fixed positive value of k. It is seen that there are four resonance frequencies $\tilde{\omega}$

$$\tilde{\omega}_1 = Uk + \Omega_e$$
$$\tilde{\omega}_2 = Uk - \Omega_e$$
$$\tilde{\omega}_3 = -Uk + \Omega_e$$
$$\tilde{\omega}_4 = -Uk - \Omega_e$$

In first order nonresonant waves ($\omega \neq \tilde{\omega}$) cannot be excited by the beams (see Neufeld and Wright, 1963). We will therefore only consider resonant waves, i.e. those waves which have the frequencies $\pm\Omega_e$ in the frame of either of the beams. The frequency of these waves in the frame of the background plasma is $\omega = \tilde{\omega} + \delta$ where the real part of δ is much smaller than $\tilde{\omega}$. If δ

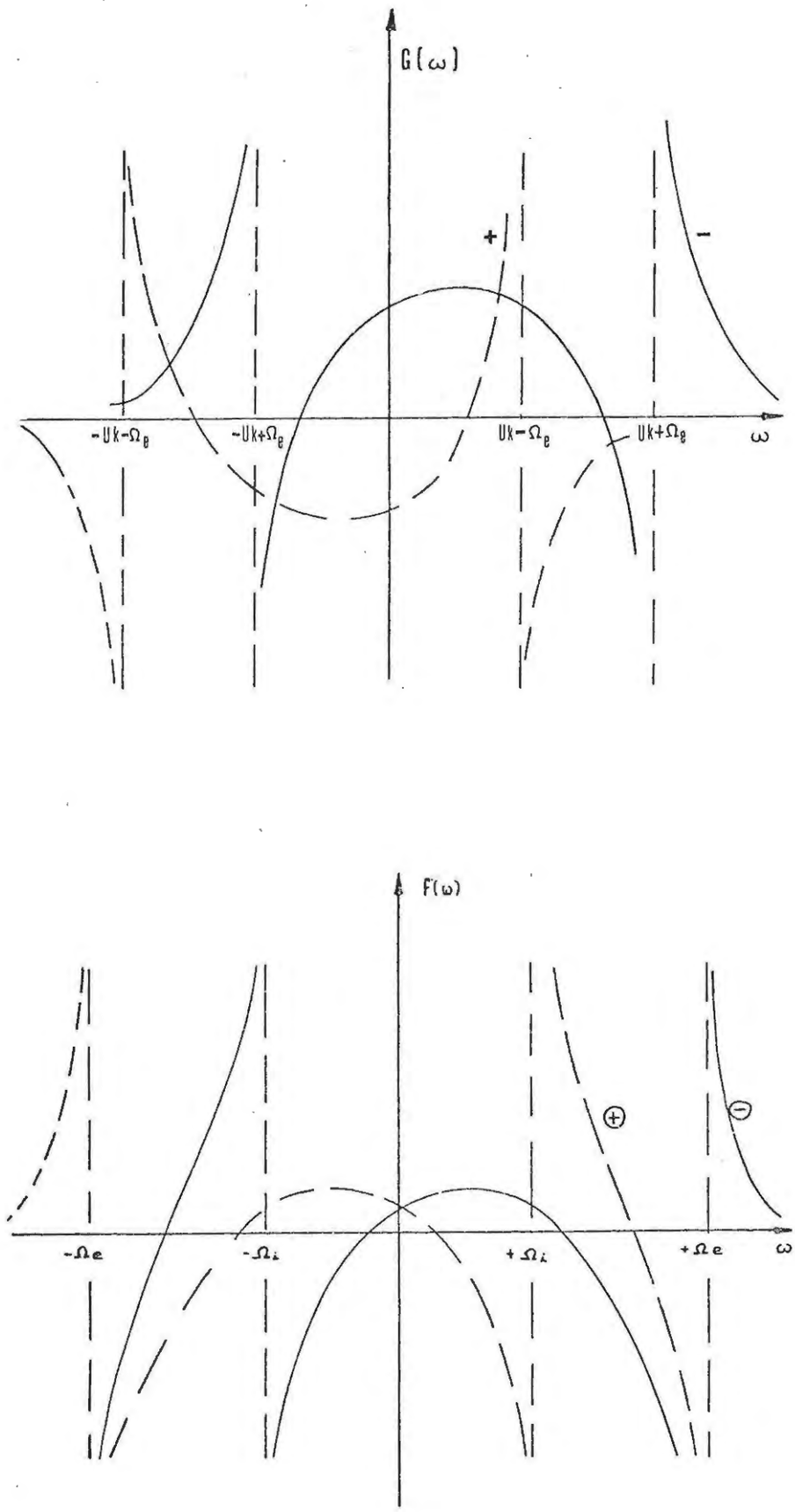

Figure 25: a) G (ω) as a function of ω
b) F (ω) as a function of ω .

is complex, then $\mathrm{Im}\,\delta$, if positive, represents the growth rate of the excited waves.

The dispersion relation (3.41) can be split into two parts, the first one $F(\omega)$ describing the effect of the stationary plasma whereas the second $G(\omega)$ describes the effect of the two plasma beams

$$(3.42) \qquad \Phi(\omega) = F(\omega) + G(\omega) = 0$$

where:

$$(3.43) \qquad F(\omega) = c^2k^2 - \omega^2 + \omega_{p_0}^2 \left(\frac{\omega}{\omega - \Omega_i} + \alpha \frac{\omega}{\omega + \Omega_i} \right)$$

where, again, ω can be positive or negative

$$(3.44) \qquad G(\omega) = \omega_p^2 \left(\frac{\omega - uk}{\omega - \tilde{\omega}_{1/2}} + \frac{\omega - uk}{\omega - \tilde{\omega}_{3/4}} \right)$$

where $\tilde{\omega}_{i/k}$ are the resonance frequencies $\tilde{\omega}_i$ or $\tilde{\omega}_k$ respectively.

In the neighbourhood of $\tilde{\omega}_i (i=1,2)$, $F(\omega)$ can be approximated by a Taylor series

$$(3.45) \qquad F(\omega = \tilde{\omega}_i + \delta) = F(\tilde{\omega}_i) + \delta \frac{\partial F}{\partial \omega} (\omega = \tilde{\omega}_i)$$

Now:

$$(3.46) \qquad G(\omega) = \omega_p^2 \left(1 + \frac{\Omega_e}{\omega - \tilde{\omega}_{1/2}} + 1 + \frac{\Omega_e}{\omega - \tilde{\omega}_{3/4}} \right)$$

Thus at $\omega = \tilde{\omega}_i + \delta$ the dispersion relation $\phi(\omega) = 0$ reads:

$$(3.47) \qquad \phi(\omega = \tilde{\omega}_i + \delta) = F(\tilde{\omega}_i) + \delta \frac{\partial F}{\partial \omega} (\tilde{\omega}_i) + 2\omega_p^2 + \omega_p^2 \frac{\Omega_e}{\delta} + \frac{\Omega_e \omega_p^2}{\Delta\tilde{\omega} + \delta} = 0$$

where $\Delta\tilde{\omega} = \tilde{\omega}_i - \tilde{\omega}_k = 2ku$

For small δ for which (3.47) holds this can be re-written as:

$$(3.48) \qquad \delta^2 \frac{\partial F}{\partial \omega} (\tilde{\omega}_i) + \delta F(\tilde{\omega}_i) + \Omega_e \omega_p^2 = 0$$

which gives for δ

$$(3.49) \qquad \delta = \frac{-F(\tilde{\omega}_i) \pm \sqrt{(F(\tilde{\omega}_i))^2 - 4 \frac{\partial F}{\partial \omega}(\tilde{\omega}_i)\, \Omega_e \omega_p^2}}{2 \frac{\partial F}{\partial \omega}(\tilde{\omega}_i)}$$

Thus the conclution for instability is immediately written as:

$$(3.50) \qquad \frac{\partial F}{\partial \omega}(\tilde{\omega}_i) > 0 \qquad \left| \frac{(F(\tilde{\omega}_i))^2}{\frac{\partial F}{\partial \omega}(\tilde{\omega}_i)} \right| < 4 \Omega_e \omega_p^2$$

Figure (25b) shows a plot of $F(\omega)$ as a function of ω. It can be seen that the condition $\frac{\partial F}{\partial \omega}(\tilde{\omega}_i) > 0$ is only fulfilled for $\tilde{\omega} < 0$ and only when $-\Omega_i < \tilde{\omega}_i < 0$ (for i = 1, 2). Thus the electron beam moving along Bo, for which $\tilde{\omega}_{1,2}$ are the resonant frequencies, can only excite transverse waves travelling opposite to the field ($\tilde{\omega} < 0$). This conclusion was also arrived at by Bailey (1950) and Neufeld and Wright (1963), who have first investigated dispersion relations of the type (3.41) by the method used above. For the other electron beam the condition for instability is $\frac{\partial F}{\partial \omega}(\tilde{\omega}_i) < 0$ and $\tilde{\omega}_i$ (i = 3, 4) must then be between 0 and $+\Omega_i$. The second condition of (3.50) limits the range of frequencies ($\omega = \tilde{\omega}$) still further. If ω_p^2 is very small, this condition can, however, always be fulfilled when $F(\omega = \tilde{\omega}) = 0$.

We can now write down the conditions for U under which the instability will be present. Since

$$-\Omega_i < kU - \Omega_e < 0 \qquad \text{it follows that}$$

$$+\Omega_e - \Omega_i < kU < \Omega_e$$

Let us write for the frequency at which instability is present $\omega = -\Omega_i + \beta$. Then, neglecting the electron term in $F(\omega)$

$$F(\omega) = c^2k^2 + \Omega_i^2 + 2\Omega_i\beta + \beta^2 + \alpha\omega_{p_0}^2 \frac{\Omega_i}{\beta}$$

$$\frac{\partial F}{\partial \omega} = \frac{\Omega_i}{\beta^2}(\alpha\omega_{p_0}^2) + 2\Omega_i - 2\beta$$

From (3.50)

$$\left|\beta(c^2k^2 - \omega^2) - \alpha\omega_{p_0}^2\Omega_i\right| < \left|\Omega_i(\omega_{p_0}^2\alpha - 2\omega\beta^2)\right|^{1/2} 2\omega_p\sqrt{\Omega_e}$$

for $\beta = 0$, i.e. $\omega = -\Omega_e$

$$\alpha\omega_{p_0}^2\Omega_i < 2\omega_p\omega_{p_0}\sqrt{\alpha\Omega_e\Omega_i} = 2\omega_p\omega_{p_0}\Omega_i$$

and hence

$$(3.51) \qquad \omega_{p_0} < \frac{2}{\alpha}\omega_p$$

Thus this instability will be present, as long as the density of the background plasma is small enough. On the other hand for $\beta = \Omega_i$, i.e. $\omega = 0$, the condition for instability is written as

$$(3.52) \qquad U > c\Omega_e\left(\omega_{p_0}(2\omega_p - \alpha\omega_{p_0})\right)^{-1/2}$$

which at Io's orbit where $\Omega_e \approx 8.8 \times 10^5$ sec^{-1} (this figure is based on an equatorial field strength $B_E = 8$ G), $\omega_p = 1.8 \times 10^4$ s^{-1} and $\omega_{p_0} \leq 5.7 \times 10^5$ s^{-1} (as will be shown in the next section) reduces to

$$U > 6 \times 10^{-2}\, C \simeq 18\,000 \text{ km/s}$$

Thus the instability will be present only near $\omega = -\Omega_i$, where the growth rate is, however, very small because

$$\lim_{\omega \to -\Omega_i} \frac{\partial F}{\partial \omega} = \infty \ .$$

The growth rate of transverse waves excited by the electron beams is certainly much smaller than that for longitudinal waves excited by the protons. We will not calculate the exact values of the growth rate for the transverse waves excited by the protons.

The analysis of the transverse wave instability produced by the protons in the beams is very similar to the one given above. Again the growth rate is

smaller than that for the longitudinal waves excited by the protons. A detailed investigation of one plasma beam penetrating a stationary plasma under the condition $\omega_p \ll \omega_{po}$ can be found in the articles by Neufeld and Wright (1963) and Bailey (1950). The reason for including the discussion of this transverse wave instability was to show that not only the protons in the beam will feed their energy into waves but also the electrons, although at a much smaller rate.

From the discussion above we conlude that the plasma streams travelling along the magnetic field lines through the Jovian magnetosphere will excite both longitudinal waves (due to the protons travelling with a speed greater than their thermal speed) and transverse waves. Since the energy contained in these waves is derived from the macroscopic streaming energy, growth of waves means loss of streaming energy and hence decrease of U. The e - folding time of the longitudinal waves is less than a second. The growth of the transverse waves is much slower. I will, therefore, only consider the longitudinal waves in the following.

From (3.36) it can be deduced that the longitudinal wave instability will only be present on field lines for which $L > 3$. For $L < 3$ the plasma distribution should be similar to the one described by Melrose (1967), which was based on the assumption of negligible collision effects in the magnetosphere.

For $L > 3$, however, the distribution will differ considerably from that given by Melrose. The instabilities, described above, will lead (mainly) to a loss of ion energy parallel to the magnetic field. The ions will not be able to get over the potential barrier any more and hence must accumulate in the outer

parts of the magnetosphere. The electrons are only subject to the transverse wave instability which has a much smaller growth rate. The loss of electron energy will not be as fast as that of the ions. They will retain a sufficient energy to overcome the potential barrier. The accumulation of positive particles in the outer parts of the magnetosphere will build up an electric field. This field will speed up the electrons which move towards the equatorial plane and decrease the velocity of the ions moving in the same direction. The acceleration of electrons however, will be much larger than that of the massive ions. The streaming velocity of the electrons hence will increase above U given by (3.32). The electric field will prevent the electrons from passing over the potential barrier. The exact treatment of the magnetosphere including this electric field is too complicated to be worked out in detail here. It requires the nonlinear treatment of instabilities; i.e. the exact behaviour of the energy loss from the particles to the waves. It seems likely, however, that the electrons will eventually acquire the same energy as the protons i.e. $U_e = (\alpha)^{-\frac{1}{2}} U_i$. If this happens, the electrons will also excite longitudinal waves as described above. The final result will be a trapping of the plasma in the outer parts of the magnetosphere. The trapped plasma particles will collide with each other (even though the collision frequency is small) and after some time the plasma will be approximately thermalized (by this I mean: its velocity distribution will be very nearly Maxwellian). The temperature of this plasma will be of the order of $T_p = \frac{1}{2}(T_e + T_i) \simeq m_i U^2/32K$ (equating the streaming energy of the protons to the thermal energy of the plasma). Assuming $T_e = T_i = T$, one obtains a particle

temperature T at Io's orbit of about 2 000 K.

The plasma density in the magnetosphere will be limited by recombination. In an equilibrium state the loss due to recombination must be balanced by the flux supplied by the ionosphere. The recombination loss per unit volume is given by $L = \alpha_{13} N_e^2$ where α_{13} is defined in Appendix B. Thus in a volume element A(s) ds, s is a length along the field line, the recombination rate is $\alpha_{13} N_e^2 A(s)\, ds$. The total recombination rate in the entire flux tube is $\int_0^{s_m} \alpha_{13} N_e^2 A(s)\, ds$ where s = o is taken in the equatorial plane and s_m is the distance between the equatorial plane and the ionosphere along a field line. This loss rate must be balanced by the flux $F = N_o V_o A_o$. We thus get:

$$(3.53) \qquad N_o V_o = \int_0^{s_m} \alpha_{13} N_e^2 \left(\frac{A(s)}{A_o}\right) ds$$

where A_o is the area of the flux tube at the level from which the flux originates. If we assume that the bulk of the plasma is thermalised the variation of N_e in the magnetosphere is given by Gledhill (1967).

$$(3.54) \qquad N_e = N_{eo} \exp\left(-B' s^2/2kT\right)$$

where T is the particle temperature and N_{eo} is the maximum plasma density along a particular field line with an L value L. The thermalised plasma will form a sort of discus.

$$(3.55) \qquad B' = m_i \left(\frac{g_o}{R_J L^3} - 3\frac{\Omega^2}{2}\right)$$

S is measured along the field line with s = o at the magnetic equatorial plane.

Thus we get the maximum plasma density N_{eo} at Io's orbit (L = 5.9).

$$(3.56) \qquad N_{eo}^2 = N_o V_o A_o / \alpha_{13} \int_0^{s_m} e^{-\frac{B}{2KT} s^2} A(s)\, ds$$

If the variation of A(s) is neglected we get, taking an average A(s) = A out of the integral

$$(3.57) \qquad N_{eo}^2 = N_o V_o \frac{A_e}{\bar{A}} \frac{1}{\alpha_{13} \left(\frac{KT}{B'}\right)^{1/2} \pi}$$

For Io's flux tube $N_o V_o = 10^{12}$ (particles m^{-2} s^{-1}), which gives $N_{eo} = 5 \times 10^3$ particles/cm^3. If the magnetic dipole is displaced along the rotational axis of Jupiter from the centre of the planet the plane of maximum density will not coincide with the equatorial plane but with the magnetic equatorial plane ($\sin \Theta = 1$). If the dipole is also tilted the plane of maximum plasma density will be somewhere between the equatorial and magnetic equator plane. Gledhill (1967) has made a detailed investigation of this case. His results are used to calculate the variation of plasma density along Io's orbit for various magnetic dipole displacement parameters as shown in figure (26a). Figure (26b) shows the variation of the Alfvén velocity along Io's orbit. This figure is based on $B_E = 10$ G (for definition of B_E see section 2.2.2)

3.4 The Plasma Distribution in the Magnetosphere

The density of plasma in the magnetosphere is determined by the balance between the flux of plasma supplied by the ionosphere and recombination. The recombination process will become important only if the plasma remains in the magnetosphere long enough, that is, longer than the time constant for density changes due to recombination. The recombination in the low density magnetosphere is an extremely slow process. If no electron-ion pairs were formed, the density N_e would

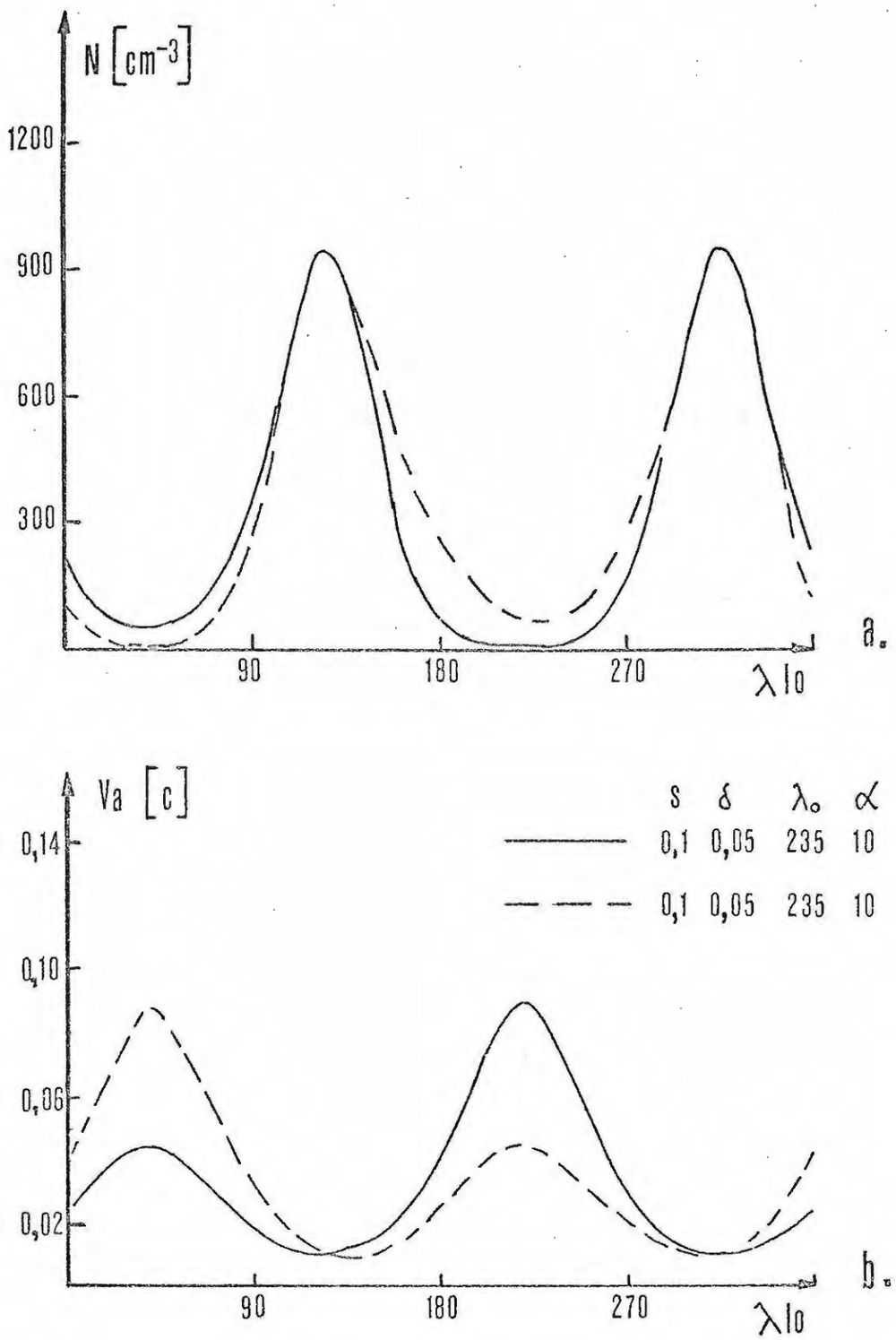

Figure 26: a) Plasma density along Io's orbit.
b) Alfvén velocity along Io's orbit.
See text for explanation of symbols.

decrease as $\frac{dN_e}{dt} = -\alpha_{13} N_e^2$. The time for the density to decrease by a factor of 2 is then $t = \alpha_{13}^{-1} N_o$ which for $N_o \simeq 10^3$ particles cm^{-3} gives $t = 2 \times 10^8$ seconds. The characteristic time for variation of the plasma distribution is the electron ion collision rate $\tau_c \simeq 0{,}02\, T^{3/2}$. For $T = 2 \times 10^3$ K this gives several hours. Collisions of the particles in the beam should therefore be entirely negligible. (As we have assumed all the way). Thus the presence of the two stream instability as described in the last section is essential for the trapping of a considerable plasma density in the outer parts of the magnetosphere. It was shown in the last section that trapping of plasma will become important along field lines which have L values larger than 3. The maximum plasma density in the equatorial plane can then be calculated with formula (3.57). For $L > 8$ (3.57) can be approximated by

$$(3.58) \quad N_{eo}^2 = N_o V_o A_o / \bar{A} \beta (T/B')^{1/2}$$

where $\beta = \pi \alpha_{13} K^{1/2}$ is a constant.

$\bar{A}$ is inversely proportional to the magnetic field strength $B \propto 1/r^3$, T is proportional to U^2 (see above discussion) and B' is proportional to L^{-3}. In the equatorial plane $U \propto L^2$, thus $T/B' \propto L^5$ and the density N_{eo} varies as $N_{eo} \propto (N_o V_o)^{\frac{1}{2}}\ L^{-2.75}$.

For $L > 8$ the flux of plasma supplied by the ionosphere is nearly constant, as the escape velocity $V^2_{esc} \propto V_{max}$ (the height of the potential barrier) is constant. (V_{max} - V ionosphere $= \frac{1}{2} m_i g_o R_J$).

Thus one would expect the equatorial plasma density N_{eo} to decrease as $r^{-2.75}$ for $r > 8\ R_J$. For $L < 8$ the density decrease will be faster. Calculating N_{eo} for different field lines indicates a decrease of equatorial plasma density at Io's orbit $N_{eo}\ (r) \propto r^{-3}$ and

$N_{eo}(r) \propto r^{-4}$ at $L = 4$. Taking Melrose's calculations to be valid for field lines with $L < 3$ we finally arrive at an equatorial plasma distribution as shown in figure (27). The density decrease in the equatorial plane indicated by (3.58) is faster than the decrease allowed by the condition Melrose (1967) has derived. He argues that only those magnetospheres will be stable, for which by interchanging two magnetic flux tubes at r and $r + \delta r$, the energy for a flux tube $E = \left(\frac{\gamma}{\gamma-1} P + \rho V(r)\right) V'$ increases. V' is the volume of a flux tube assumed to vary as r^{β}. For large distances from the planet the potential $V(r)$ can be approximated by $V(r) \simeq -\frac{1}{2} R_J^2 \Omega^2 r^{12}$.

Then $$\frac{\delta E}{E} = \frac{\delta V'}{V'} + \frac{\frac{\gamma}{\gamma-1}\delta p + V(r)\delta\rho + \rho\,\delta V(r)}{\frac{\gamma}{\gamma-1} P + \rho V(r)} = \beta\frac{\delta r}{r} + \frac{\delta N}{N} + \frac{NK\delta T_p + \rho\delta V(r)}{\frac{\gamma}{\gamma-1} P + \rho V(r)}$$

It was argued above that $T_p \simeq m V(r)/\gamma K$ for large r.

Hence $NK\delta T_p = \rho/\gamma\ \delta V(r)$ and

$$\frac{\delta E}{E} = \beta\frac{\delta r}{r} + \frac{\delta N}{N} + \frac{(\gamma+1/\gamma^2)\,\delta V(r)}{V(r)} = \left(\beta + 2\,\frac{\gamma+1}{\gamma^2}\right)\frac{\delta r}{r} + \frac{\delta N}{N}$$

It can be seen that in this case, where the plasma temperature of the magnetospheric plasma is allowed to vary as a function of r, the magnetosphere is stable if the density does not decrease faster than

$$N \propto r^{-\left(\beta + 2\,\frac{\gamma+1}{\gamma^2}\right)}$$

Hence the magnetosphere described above should be stable against the interchange motion.

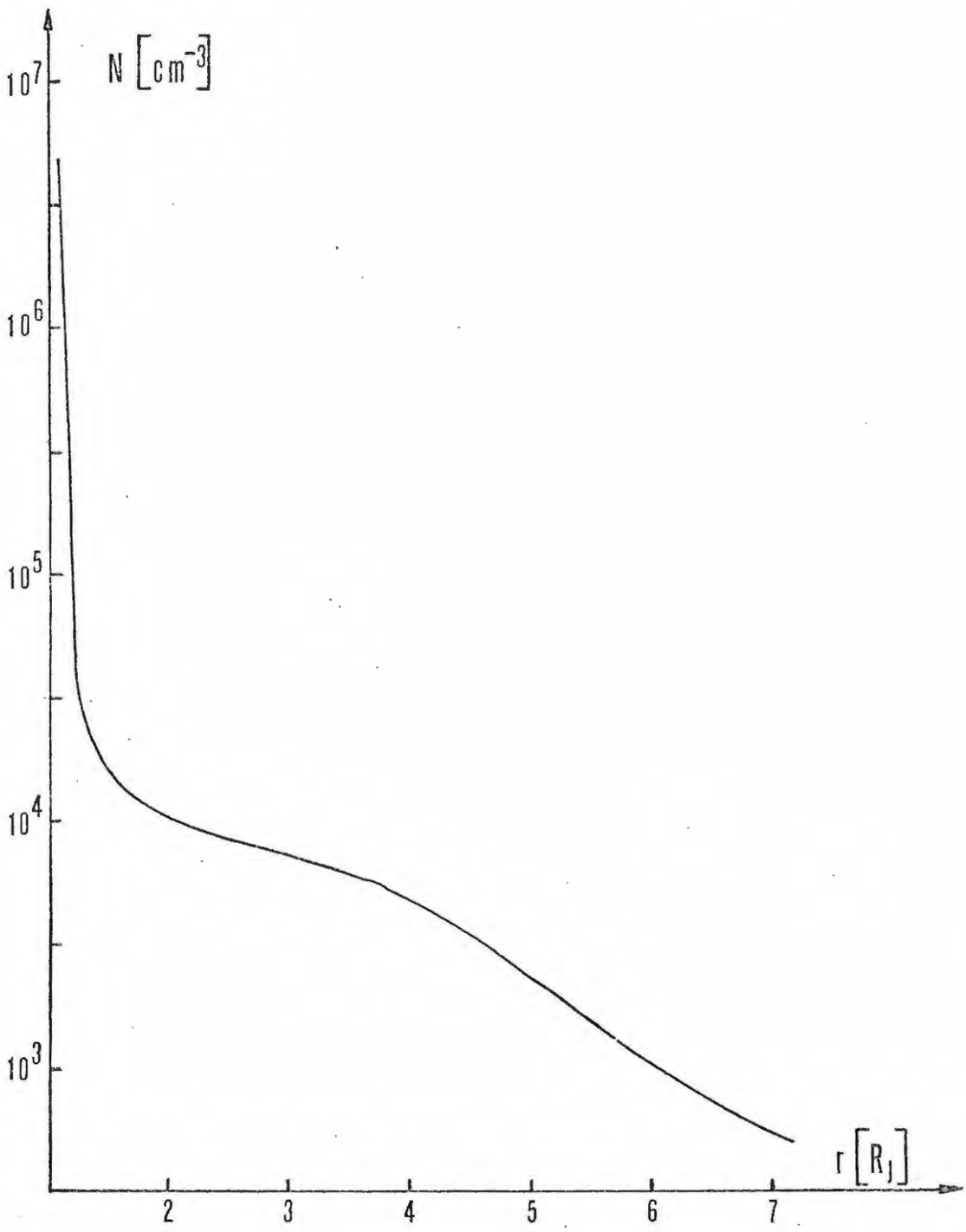

Figure 27: Equatorial plasma density variation as a function of distance r from the centre of the planet.

4. Io's Interaction with the Magnetosphere

4.1 Review of Existing Theories

A number of authors have considered Io's interaction with its plasma environment. The majority of their theories regard Io as a good conductor.

Warwick (1967, 1970) assumes that the induced emf due to the motion of Io through Jupiter's magnetic field drives currents in closed loops inside the satellite. These currents distort the external field which then cleaves around Io: the distortions are propagated away in the form of large-amplitude Alfvén waves. Schmahl (1970) expands Warwick's ideas and considers Io's movement through the magnetic field, which varies along Io's orbit. (This variation is due to the tilt of Jupiter's magnetic dipole and its displacement from the centre of the planet.) The motion of Io through this magnetic field causes Io to have a sizeable magnetic dipole moment, the magnitude and direction of which are related to Io's core conductivity and the amplitude of variation of magnetic field as seen by Io. Io will then act as a source of dipole radiation of Alfvén waves. The power of these waves is of the order of 10^{10}W. Both authors assume that the Alfvén waves propagate along the magnetic field lines connecting Io with the ionosphere. Warwick (1967) mentions the possibility of steepening of the Alfvén waves fronts and the development of instabilities in the steep wave fronts leading to the emission of strong electromagnetic radiation in the decameter band. No detailed attempt was made to account for the major characteristics of the decametric radiation in terms of these models.

Goldreich and Lynden-Bell (1969) regard the flux tube passing through Io as frozen into the satellite. In contrast to Warwick's theory they require currents to flow out of Io, along field lines into the ionosphere, across the field lines in the ionosphere and back towards Io. The satellite thus acts as a unipolar generator whereas the ionosphere can be thought of as a motor. The current is carried by high energy electrons which are accelerated at Io. The flow of these high energy electrons through the ionospheric plasma can lead to an instability. Goldreich and Lynden-Bell then argue in favour of coherent cyclotron radiation as the radiation mechanism. It has been pointed out before (see section 2.2.2) that some aspects of the decametric radiation cannot easily be explained by this model.

The above theories regard the interaction of Io with the magnetosphere as of the induction type. Carr and Gulkis (1970), in their excellent review article, describe other types of interaction. These will not be described here for two reasons. None of these theories has been worked out in great detail; and the theory of Io's interaction with the magnetosphere described below only incorporates some of the elements of the three models mentioned above.

4.2 Deformation of the External Magnetic Field

Let us consider the conductor of Io moving through a region of uniform magnetic field. Suppose, firstly, that no plasma surrounds the satellite. Then, in a frame of reference moving with Io, there will be an electrostatic field $\vec{E}_L$ given by $\vec{E}_L = \vec{V}_s \times \vec{B}_o$, where $\vec{V}_s$ is the velocity of the satellite as measured in the frame

reference in which the current sources of the magnetic field are stationary; that is, in a frame of reference corotating with Jupiter. In the frame of reference moving with the satellite, Io appears to be immersed in the practically homogenous electric field $\vec{E}_L$. We then have the simple problem of a conducting sphere immersed in a uniform electric field: charges accumulate on the surface of Io, cancelling in the field $\vec{E}_L$ inside the satellite exactly and outside superimposing an electrostatic dipole field onto the field E_L, giving a total electric field E_M outside Io (as measured in Io's frame), such that (see Jefimenko (1966) p. 154)

$$\vec{E}_M = \vec{E}_L + |E_L| 2 \frac{R_{Io}^3}{r^3} \cos\Theta \hat{r} + |E_L| \frac{R_{Io}^3}{r^3} \sin\Theta \hat{\Theta} \qquad (4.1)$$

$$\vec{E}_{int} = 0$$

where Θ is the polar angle and $\hat{r}$ and $\hat{\Theta}$ are unit vectors. The field E is shown in figure (28). Because there is no electric field in Io (as measured in Io's frame), there can be no steady ohmic currents in the satellite.

I assume that Io has been immersed in Jupiter's magnetic field for long enough to ensure that any eddy currents which would act to keep the magnetic field out of the satellite have long since died out. The external magnetic field, which was assumed uniform along Io's orbit, permeates Io.

Suppose now that the satellite has a conductivity σ_{Io} and the medium (assumed to corotate with Jupiter) outside the satellite has the conductivity σ_M. This problem has been studied by several authors (see Jefimenko (1966) p. 426). It can be shown that the electric potentials in the satellite (φ_{Io}) and in the medium (φ_M) are given by:

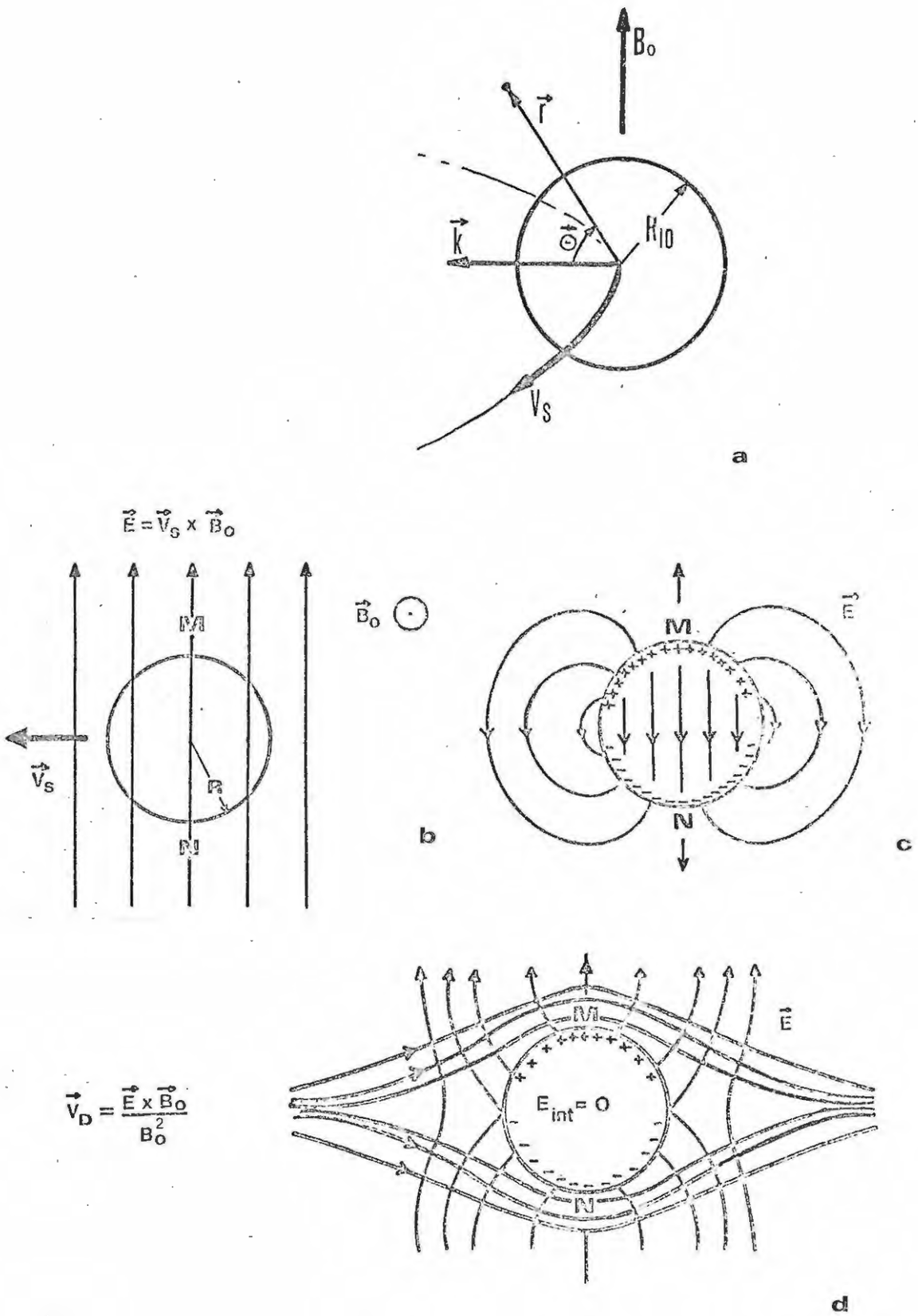

Figure 28: Io's interaction with the magnetosphere. The satellite is assumed to be a perfect conductor. See text for explanation.

a) The geometry of the problem.
b) The Lorentz field as seen from Io's frame.
c) The dipole field.
d) Superposition of Lorentz and dipole field.

$$(4.2)\quad \varphi_{Io} = \frac{\sigma_{Io}}{\sigma_{Io}+2\sigma_M} V_s B_o r\cos\Theta$$

$$\varphi_M = \frac{\sigma_{Io}}{\sigma_{Io}+2\sigma_M} V_s B_o \frac{R_{Io}^3}{r^2}\cos\Theta$$

Thus the electric field inside the satellite is (in Io's frame)

$$(4.3)\quad \vec{E}_{int} = -\nabla\varphi_{Io} + \vec{V}_s \times \vec{B}_o = -\frac{\sigma_{Io}}{\sigma_{Io}+2\sigma_M} V_s B_o \hat{k} + V_s B_o \hat{k}$$

and the field outside the satellite is (in Io's frame)

$$(4.4)\quad \vec{E}_M = -\nabla\varphi_M + \vec{V}_s \times \vec{B}_o = \frac{2\sigma_{Io}}{\sigma_{Io}+2\sigma_M} V_s B_o \frac{R_{Io}^3}{r^3}\cos\Theta\,\hat{r}$$

$$+ \frac{\sigma_{Io}}{\sigma_{Io}+2\sigma_M} V_s B_o \frac{R_{Io}^3}{r^3}\sin\Theta\,\hat{\Theta} + V_s B_o \hat{k}$$

It is seen that (4.3) and (4.4) reduce to (4.1) if $\sigma_M = 0$.

Although the treatment given neglects the anisotropy of the surrounding medium it shows a number of important effects. If Io were surrounded by plasma but no current were allowed to flow in the plasma ($\sigma_M = 0$) the electric field outside Io would cause an $\vec{E} \times \vec{B}/B^2$ drift of the plasma around Io. For $r \gg R_{Io}$ the drift velocity will be $\vec{V}_D = -\vec{V}_s$. The flow field of the plasma for this case is shown schematically in figure (28d). In this case the plasma would move around Io smoothly and continue to corotate with Jupiter.

The solution is, however, quite unrealistic. The plasma environment of Io will certainly allow charges to leak out of or into Io. We then have a current density

$$(4.5)\quad \vec{j}_{Io} = \sigma_{Io}\vec{E}_{int}$$

passing through the conductor, superimposing its

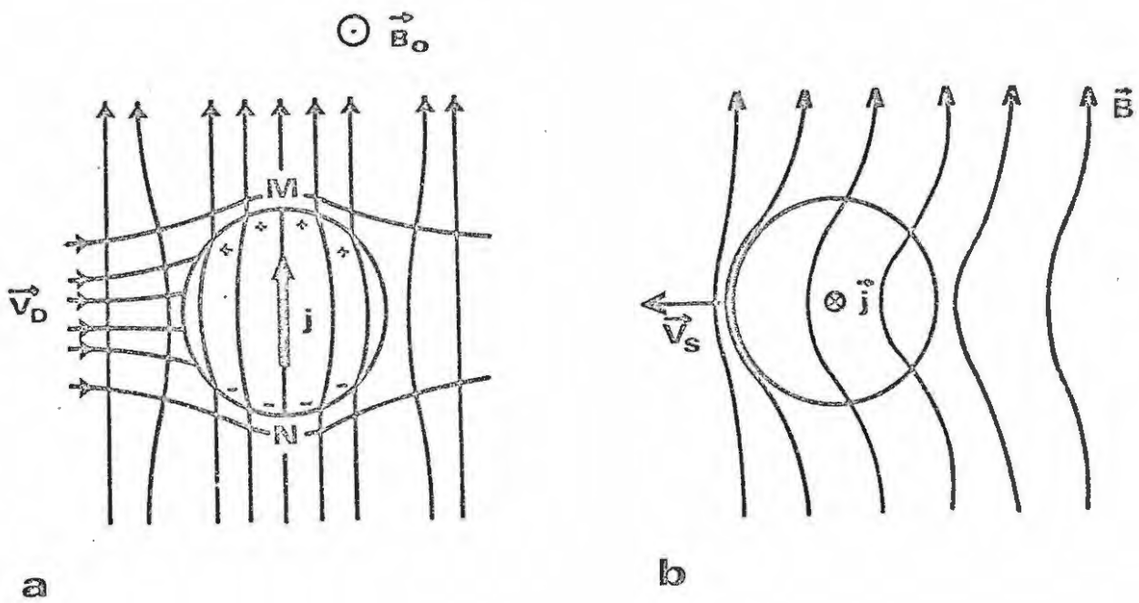

Figure 29: Io's interaction with the magnetosphere when Io is not a perfect conductor.

a) The electric field and stream lines ($\vec{V}_D$)

b) The distortion of the magnetic field.

magnetic field on the underlying field (see figure 29b). The field in front of Io will be enhanced while that to the rear is reduced. It can be seen from (4.3) that this effect will be important only if the conductivity of the surrounding medium is larger than Io's conductivity. If $\sigma_M \gg \sigma_{Io}$ we can write

$$\vec{j}_{Io} \simeq \sigma_{Io} V_s B_o \hat{k} \tag{4.6}$$

and the magnetic field due to this current (neglecting end effects, that is: treating Io as an infinite cylinder of area πR_{Io}^2)

$$\vec{H} = \begin{cases} \dfrac{\sigma_{Io} V_s B_o}{2} \dfrac{R_{Io}^2}{r} & r \geq R_{Io} \\ \dfrac{\sigma_{Io} V_s B_o}{2} r & r \leq R_{Io} \end{cases} \tag{4.7}$$

If however, $\sigma_M \ll \sigma_{Io}$ we have

$$\vec{j}_{Io} \simeq 0 \quad , \quad \vec{H} \simeq 0 \tag{4.8}$$

Thus we see that it is essential for Io's conductivity to be smaller than that of the surrounding medium to cause a large distortion of the external magnetic field.

In contrast to the ideas of Goldreich and Lynden-Bell (1969) I do not require a specific topology of magnetospheric current flow fixed to Io. I envisage the following process. The charge density ()() on the surface of Io is given by

$$\chi = D_{n,outside} - D_{n,inside} = \varepsilon_o \{ E_{n,outside} - \varepsilon E_{n,inside} \} \tag{4.9}$$

for a conducting sphere, where the index n stands for the component normal to the surface. With (4.3) and (4.4) we see that:

$$\chi \propto \cos\Theta \tag{4.10}$$

Thus the maximum surface charge density occurs in the vicinity of M and N in figures (28-30). The charges leaving the satellite from these regions will move onto and from magnetic field lines which have at most a fleeting contact with the satellite. This is because there is no mechanism to tie the magnetic field line to Io's sides M and N and the charges leaving the satellite will be blown away immediately by the $\vec{E} \times \vec{B}/B^2$ drift. Io is not in contact with a magnetic field line, along which the current might flow, long enough "feel" the d.c. resistance across the ionosphere. Io deposits its charge not onto one but onto many magnetic field lines. The current density through Io is determined chiefly by its own conductivity and that of its immediate surroundings.

Comparing (4.1) and (4.4) we see that the electric field outside Io is reduced if σ_M is not zero and charges are allowed to leak away. The plasma drift $\vec{E} \times \vec{B}/B^2$ will be reduced and the plasma will now impinge onto the satellite. If no current were allowed to flow out of Io (this is equivalent to setting $\sigma_M = 0$) there could nevertheless be currents in the plasma due to the field $\vec{E}_M$(4.1). These currents (which are, however, not connected to Io, i.e. they flow only in the plasma but not through Io) would cause the magnetic field lines to cleave around the satellite. Or, in other words, the magnetic field due to the currents in

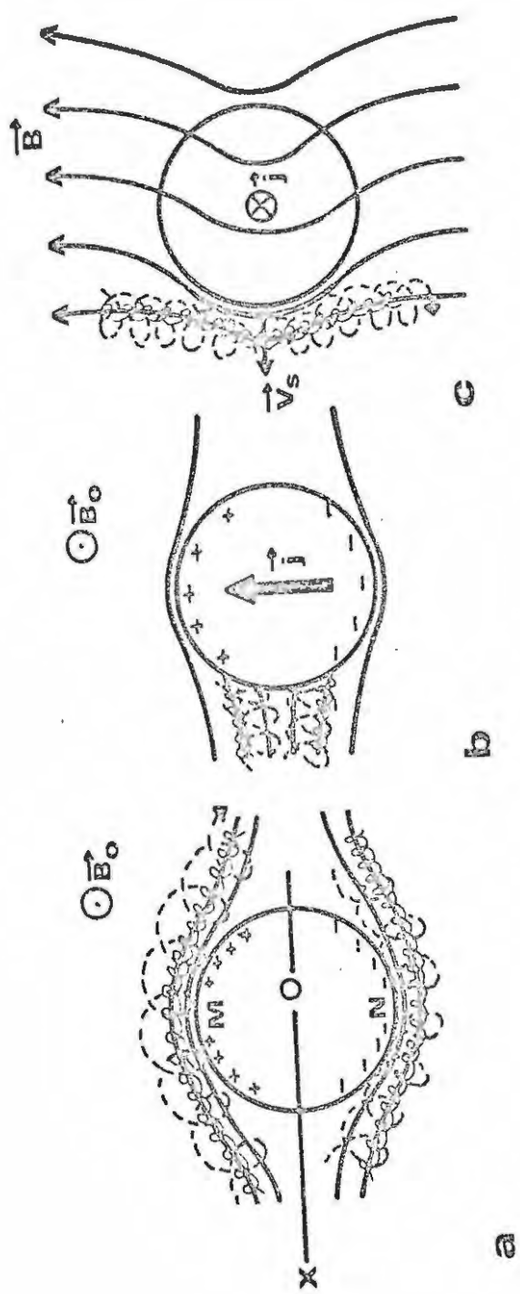

Figure 30: The motion of electrons (~~~) and protons (~~~) in the plasma impinging onto Io, when

a) Io is a perfect conductor and
b) Io is not a perfect conductor.
c) Side view for the case when Io is not a perfect conductor.

the plasma strengthens the field at the sides M and N of Io and weakens it along the line OX (figure 30). If the currents in the plasma are connected to currents in Io, i.e. if there is an electrical connection between Io and the surrounding plasma, the field $\vec{E}$ and hence the currents in the plasma are reduced (compare 4.1 and 4.4) and the magnetic field lines will no longer cleave around the satellite but impinge on Io. The plasma pressure increases in the front of Io much as in the hydrodynamic case. Because the plasma density at Io's orbit is low ($P = NKT \ll B^2/2\mu_o$, the magnetic pressure) the plasma, unaided by the $\vec{E} \times \vec{B}/B^2$ drift will not be able to move perpendicular to the magnetic field lines at Io. There is, however, no magnetic force along the field ($\vec{j} \times \vec{B} \cdot \vec{B} = 0$) to inhibit the flow of plasma along the magnetic flux tube. This flow is, of course, driven by the plasma pressure P.

Figure (30) is meant to illustrate the above discussion.

It should also be noted that the above treatment does not require electrons to be released from Io by photoionization. The contact between Io and the plasma in a particular flux tube is so short that only small deviations from charge neutrality will appear in the plasma near Io. Any excess charge in the plasma near M and N moving with Io relative to Jupiter will be blown away by a $\vec{V} \times \vec{B}$ force.

It can be seen from (4.7) that if $\sigma_{Io} > 10^{-5}\ \Omega^{-1}\ m^{-1}$ the currents through Io will generate a magnetic field the magnitude of which at Io's surface is larger than B_o (the Jovian magnetic field at Io's orbit). The conductivity of the Earth's upper mantle is $5 \times 10^{-3}\ \Omega^{-1}\ m^{-1}$ (Bullard, 1967) and Ness et al. (1969)

give $10^{-5}\ \Omega^{-1}\ m^{-1}$ as an upper limit of the Moon's conductivity. I will assume that Io's conductivity is indeed larger than $10^{-5}\ \Omega^{-1}\ m^{-1}$. In this case the magnetic field topology in Io's vicinity is shown in figure (34) and (35). At A there is a region of zero field at which the limiting field lines are perpendicular to each other.

4.3 The Generation of Alfvén Waves

In the last section I have shown how the magnetic field lines immediately in front of Io are trapped by the satellite. If they cannot easily diffuse through Io mhd waves will be generated in the following way. Consider the movement of Io through the magnetosphere now as seen in a frame of reference which rotates with Jupiter, i.e. in which the plasma far from Io is at rest whereas Io is moving. When the plasma impinges an Io it will be accelerated by the satellite. As seen from Jupiter this will appear as a motion of the plasma perpendicular to B_o. There is a $\nabla \times \vec{V}$ as can be seen by integrating $\int \vec{V} \cdot d\vec{\ell}$ around the contour ABCDA in figure (31). In a perfectly conducting plasma ($\vec{E} + \vec{v} \times \vec{B} = 0$) this will imply a curl of electric field $\vec{E}$ as can be seen by integrating $\vec{E}$ around the contour ABEFA. By Faraday's law ($\frac{\partial B}{\partial t} = -\nabla \times \vec{E}$) there will be an increase of B_y. If B_y was initially zero, B_y will at a later time point in a direction opposite to that of v_y. B_y and v_y are in antiphase for $\chi > 0$. For $\chi < 0$ B_y and v_y will be in phase. This is exactly the process which leads to the generation of Alfvén waves (see Kraus, 1969). It can be shown from basic magnetohydrodynamic relations that

$$(4.11) \qquad \frac{\partial B_y}{\partial t} = B_o \frac{\partial v_y}{\partial x}$$

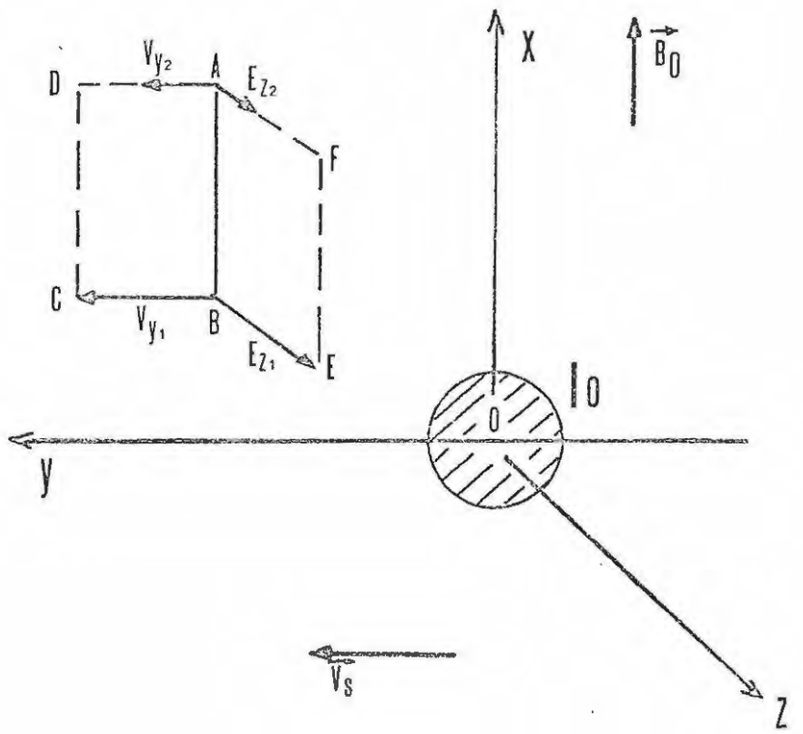

Figure 31: The generation of $\nabla \times \vec{E}$ in Io's vicinity.

$$(4.12)\quad \rho \frac{\partial v_y}{\partial t} = \frac{1}{\mu_0 \mu} B_0 \frac{\partial B_y}{\partial x} = \frac{B_0}{\mu_0} \frac{\partial B_y}{\partial x} \quad \text{for } \mu = 1$$

Thus we get a wave equation:

$$(4.13a)\quad \frac{\partial^2 B_y}{\partial x^2} - \frac{1}{V_A^2} \frac{\partial^2 B_y}{\partial t^2} = 0 \quad \text{with } V_A^2 = B_0^2/\mu_0 \rho$$

$$(4.13b)\quad \frac{\partial^2 v_y}{\partial x^2} - \frac{1}{V_A^2} \frac{\partial^2 v_y}{\partial t^2} = 0$$

Assuming a plane wave solution we can write the Fourier transform of (4.11) as

$$(4.13)\quad \omega B_y^0 = \mp B_0 V_S k \qquad \omega/k = V_A$$

where v_s is the amplitude of the v_y wave and B^0_y the amplitude of the B_y wave. We thus get:

$$(4.14)\quad B_y^0 = \mp \left(\frac{V_S}{V_A}\right) B_0 \quad (- \text{ for } x > 0, \quad \text{for } x < 0)$$

The Alfvén disturbance propagates away from Io along the magnetic field lines in both the positive and negative x- direction. The velocity gradient will be annihilated by the induction drag between adjacent regions of the plasma as indicated in figure (32a). Figure (32a) shows the condition for a momentary displacement of the plasma region ABCD and subsequent deceleration of the region. In the case of Io the plasma region ABCD cannot penetrate the satellite and is forced to move by Io with a contrast velocity v_s as seen from Jupiter. It was shown above that the plasma cannot go around Io smoothly if Io has a nonzero conductivity and currents are allowed to flow through Io. Thus the Alfvén waves generated by Io will be more of the type shown in figure (32b) where v_y (x = 0) = constant = v_s and also B_y (x = 0) = const. = B^0_y. Alfvén waves are often compared with waves on a stretched

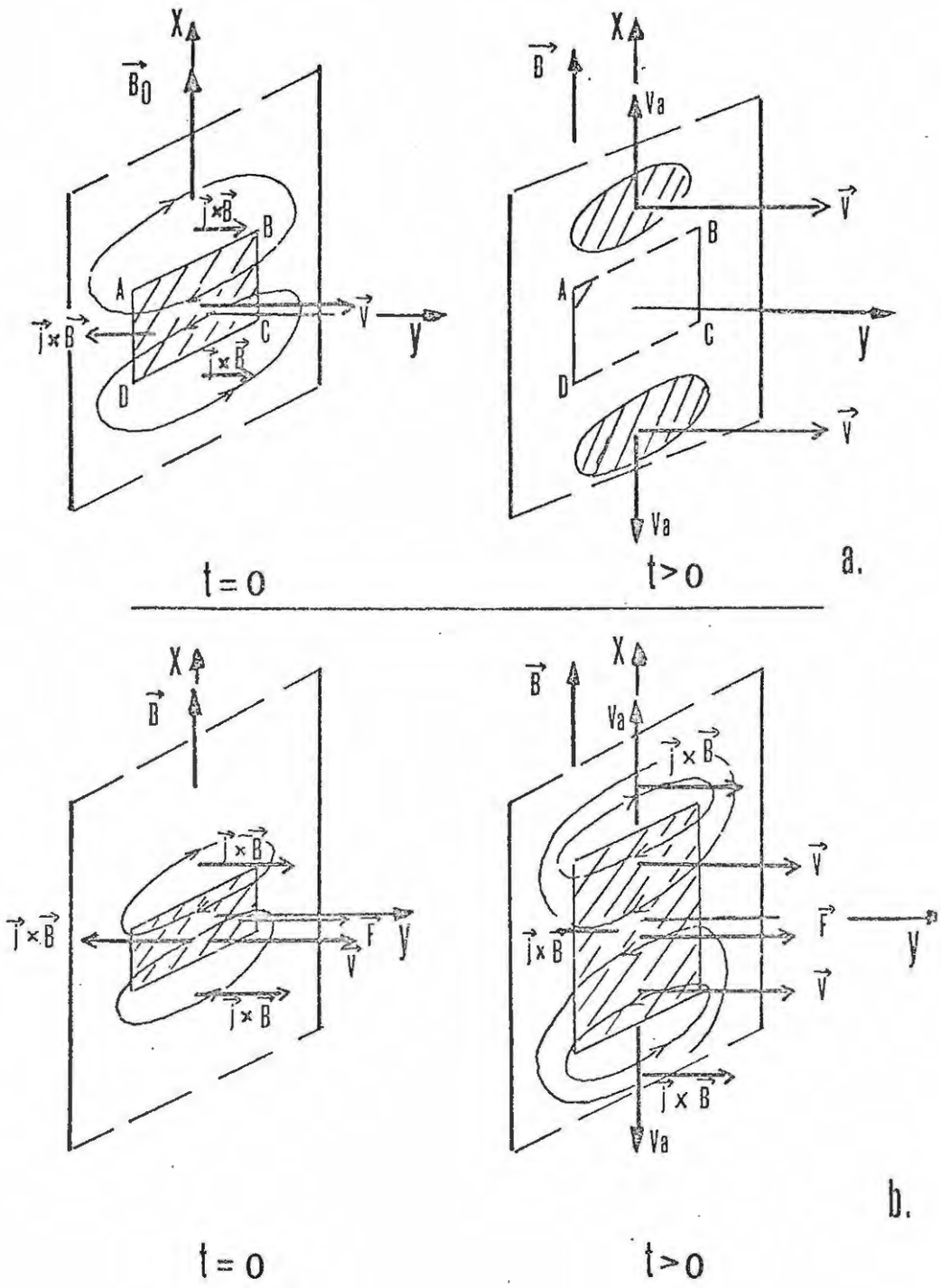

Figure 32: The generation of Alfvén waves.

a) The plasma is only momentarily displaced at x = 0.
b) The plasma is constantly displaced at x = 0. The constant force $\vec{F}$ is a contact force exerted on the plasma by Io.

string. Figure (32a) would then correspond to a displacement pulse of finite duration whereas figure (32b) would correspond to continuous displacement of the string at one end. The propagation of the Alfvén waves along the field line will accelerate the plasma near Io in the flux tube affected by Io until it acquires the velocity of the satellite. At the same time the magnetic field line is set at a tilt arctan $\phi = B_y/B_o$ where $B_y = \pm (v_s/V_A(x))\, B_o(x)$. The tilting of the field line is shown in figure (33c). In figure (33c) I have made the following approximations:

1. The underlying field line is assumed to be a straight line. Deift (1971) has shown that for the frequencies of the waves relevant in the Io - Jupiter situation ($f \approx \left(\frac{1}{v_y}\frac{\partial v_y}{\partial t}\right) \approx v_s/R_{Io} \approx 60/1600 \approx 1/30$ Hz) the curvature of the dipole field lines and the effects of the Coriolis force due to corotation can be neglected.

2. The local Alfvén velocity V_A was assumed to be constant. This is equivalent to a constant tilt angle ϕ. In reality the tilt of the field lines will vary considerably along Io's flux tube. After about t = 6 second ($t = \int_0^{x_{ion}} dx / V_A(x) \approx 6$ s) where the variation of Alfvén velocity is calculated from the density variation along IFT described in chapter (3) the Alfvén disturbance reaches the dense parts of the ionosphere. The flux tube has then attained a steady velocity $v_y = v_s$ (as measured in Jupiter's frame) at each point. The transverse velocity component v_y in the Alfvén disturbance will try to impart transverse momentum to the plasma in the ionosphere. But the ionosphere is very dense and hence immobile! Currents will be generated which eventually negate any movements of the ionospheric plasma with respect to Jupiter (Deift,

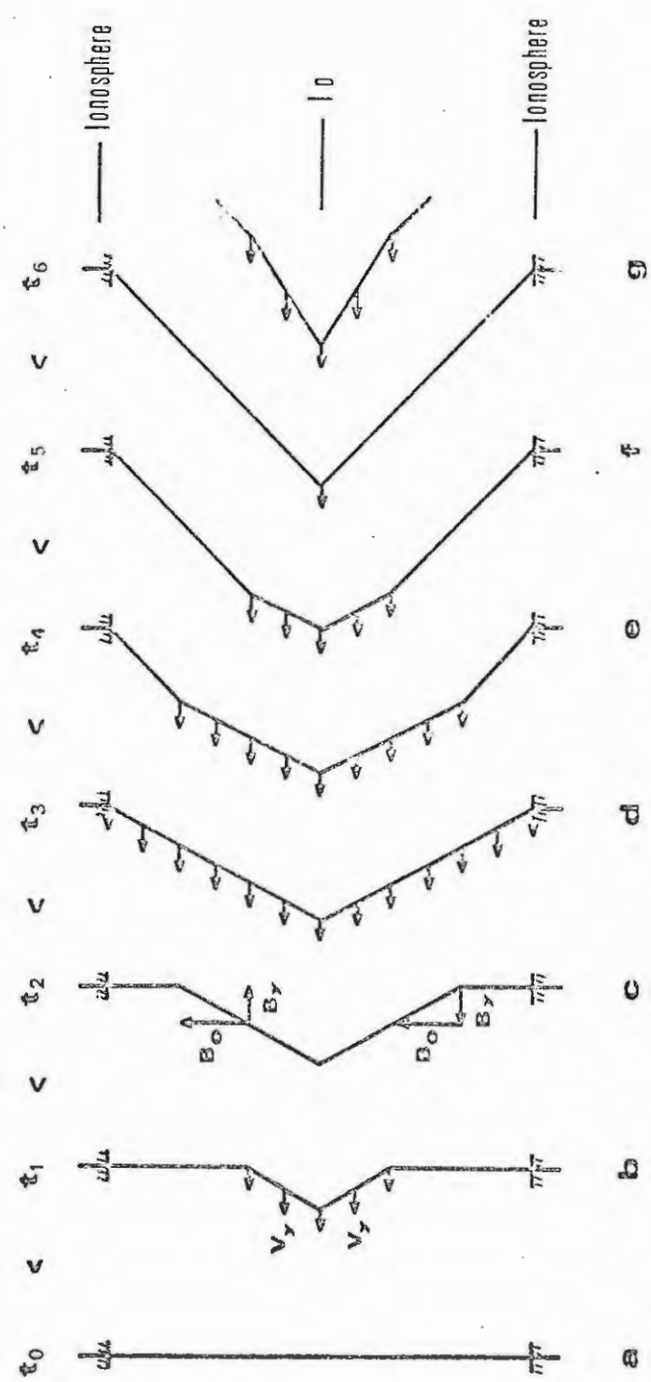

Figure 33: The propagation of Alfvén waves through an idealized magnetosphere.

1971). In order to keep $v_y = 0$ in the ionosphere a velocity pulse - v_s is generated in the ionosphere which travels back along IFT with its associated B_y field. In contrast to the original disturbance travelling in the direction of the underlying field with v_y and B_y in antiphase (this holds for $x > 0$; for $x < 0$ v_y and B_y are in phase) this return wave has v_y and B_y in phase for $x > 0$ (but in antiphase for $x < 0$). Thus the return wave cancels the transverse motion v_y at each point along IFT but doubles the magnetic tilt (see figure (33f)).

By the time the return wave reaches Io the whole of IFT will again corotate with Jupiter; i.e. move with respect to Io. But the trapped flux tube cannot move appreciably with respect to Io. Thus when the return wave reaches the satellite, an impulse is immediately imparted to the tube, accelerating it back to the velocity $v_y = v_s$. This situation is identical to the initial action, and a second Alfvén wave sets out from Io towards the ionosphere, where another return wave is generated etc. These waves will always add to the field B_y. Thus if B_y° is the disturbance of B in each wave then after n reflections there will be a tilt $n2(B_y^{\circ}/B_o)$ in the field.

Simultaneously with this process, however, the trapped flux tube diffuses through the satellite due to the latter's finite conductivity. The diffusion time $t_D = \mu \sigma_{Io} 4 R_{Io}^2$ (μ is the permeability of the satellite). More than one reflection of the type discussed above along one particular field line will occur only if t_D is greater than at least 2 x 6 = 12 seconds. For a non-magnetic satellite ($\mu = \mu_o = 4\pi \times 10^{-7}$ H/M) this requires a minimum conductivity for Io of

$\sigma_{min} = \frac{1}{4} \; 10^{-6} \; \Omega^{-1} \; m^{-1}$. I will assume that Io's conductivity is substantially larger than this: then many reflections occur along one field line. The discussion above is somewhat different from the treatment of Alfvén wave generation by Io as given by Schmahl (1970). He considers the case when Io has a strong induced magnetic dipole moment perpendicular to the direction of the undisturbed field. The movement of this dipole through the plasma constitutes a current source for the generation of Alfvén waves. He does, however, not consider the trapping of IFT by Io but rather assumes Io to move through the magnetized plasma without inducing any plasma currents. The currents constituting the magnetic dipole flow inside Io. They are caused by induction effects, that is: they are basically non-steady currents. Schmahl mentions the possiblity of currents generated in the plasma by Io's movement. He says that such currents will also generate Alfvén waves. In the discussion above exactly these currents in the plasma (or more precisely: the change of plasma flow velocity v_y) are the ones responsible for the generation of Alfvén waves. The non-steady currents inside Io have been neglected. If Io does, however, have an induced magnetic dipole moment, Schmahl's generation mechanism cannot be neglected.

4.4 The Formation of a Neutral Point

As the number of reflections increases along a particular magnetic field line it will be tilted more and more. As B_y has different signs for $x > 0$ and $x < 0$ respectively this will correspond to a curl B behind Io. A current $\vec{j}_p = \nabla \times \vec{B}$ must flow in the plasma (see figure 34). This current $\vec{j}_p$ will separate charges which

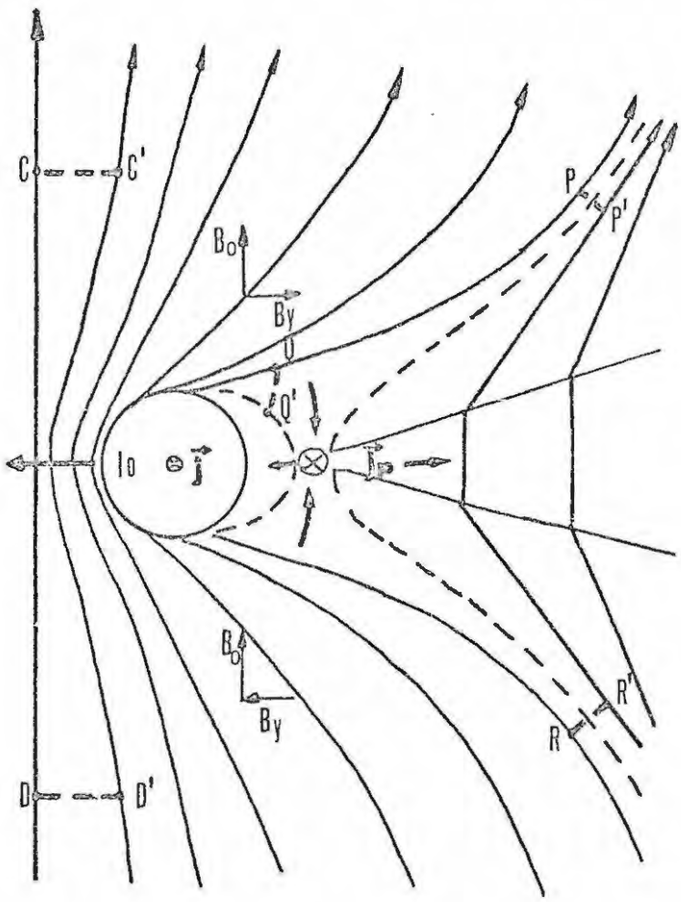

Figure 34: The magnetic field topology in Io's vicinity.

create an ohmic electric field $\vec{E} = \vec{j}_p/\sigma_M$ where σ_M is the conductivity of the plasma medium. This electric field $\vec{E}$ begins to drag the plasma across the field lines towards the current region at a velocity $\vec{E} \times \vec{B}/B^2$. These are precisely the conditions under which magnetic field energy can be dissipated at a neutral point (see Dungey, 1958 and Petschek, 1964). At this time it is necessary to state exactly what is meant by a magnetic field line. Consider the two points C and D in figure (34). Suppose that at a time t a three dimensional curve satisfying $\frac{dx}{B_x} = \frac{dy}{B_y} = \frac{dz}{B_z}$ passes through both points. We then say that this curve is the magnetic field line B (x,y,z) that connects C and D. Suppose the entire plasma evolves in time in such a way that at a time $t' > t$ the plasma at C moves to C' and that at D to D'. If the points C' and D' can still be connected by a curve $dx/B_x = dy/B_y = dz/B_z$ we say that the magnetic field line has moved with the plasma whereby, of course, its shape may be drastically distorted. This is the case for an infinitely conducting plasma. In this case the magnetic field line can be visualized as an elastic string extended between C and D. Connection of two points by a magnetic field line means that charged particles can move from one point to the other without violating the first adiabatic invariant. Thus if C and D remain magnetically connected the same particles will move between the two points. (This neglects violation of any adiabatic invariants due to e.g. magnetic field gradient or nonmagnetic forces). These particles can therefore be used to label the magnetic field line. If, however, it is not possible to connect C' and D' magnetically, we say that the field slips relative to the plasma. The rate of slip is inversely proportional

to the plasma conductivity.

The problem of the neutral point is best discussed by considering the growth of curl B to a very large value. The discussion follows the arguments given by Dungey (1958). Consider the field behind Io (see figure (34) and (35a)) in the vicinity of the neutral point. The neutral point is of the X - type. The field there can be expressed in a Taylor expansion about the neutral point as the origin of the co-ordinate system. To 1. order $\vec{B} = \frac{\partial B_i}{\partial x_j} \vec{\delta x_j}$ where $\vec{\delta x_j}$ is a position vector.

If curl $\vec{B} = 0$ the tensor $B_{ij} = \frac{\partial B_i}{\partial x_j}$ is symmetrical with its principal axes orthogonal. As div $\vec{B} = 0$ the 3 diagonal elements cannot all have the same sign. Assume B_{11} and B_{22} to have opposite signs. Suppose then that a current is started in the x_3 direction (this current may be due to an external generation of a small curl $\vec{B}$). In this case the lines of force will no longer be perpendicular to each other.

The current produces a magnetic field directed clockwise round it and the magnetic force density in $(\vec{B} \cdot \nabla)\vec{B} - \frac{1}{2}\nabla(B^2/\mu_o)$ forces the material to move as indicated by the arrows in figure (34) and (35b). As the field moves with the plasma (we are neglecting the resistivity of the plasma) the limiting magnetic field lines will be rotated towards each other which corresponds to an increase of curl $\vec{B}$ and hence $\vec{j}$. If the plasma was infinitely conducting the current density $\vec{j}$ would grow beyond all limits. This reversal of Lenz's law can be demonstrated as follows. The conservation of mass and equation of motion can be written as:

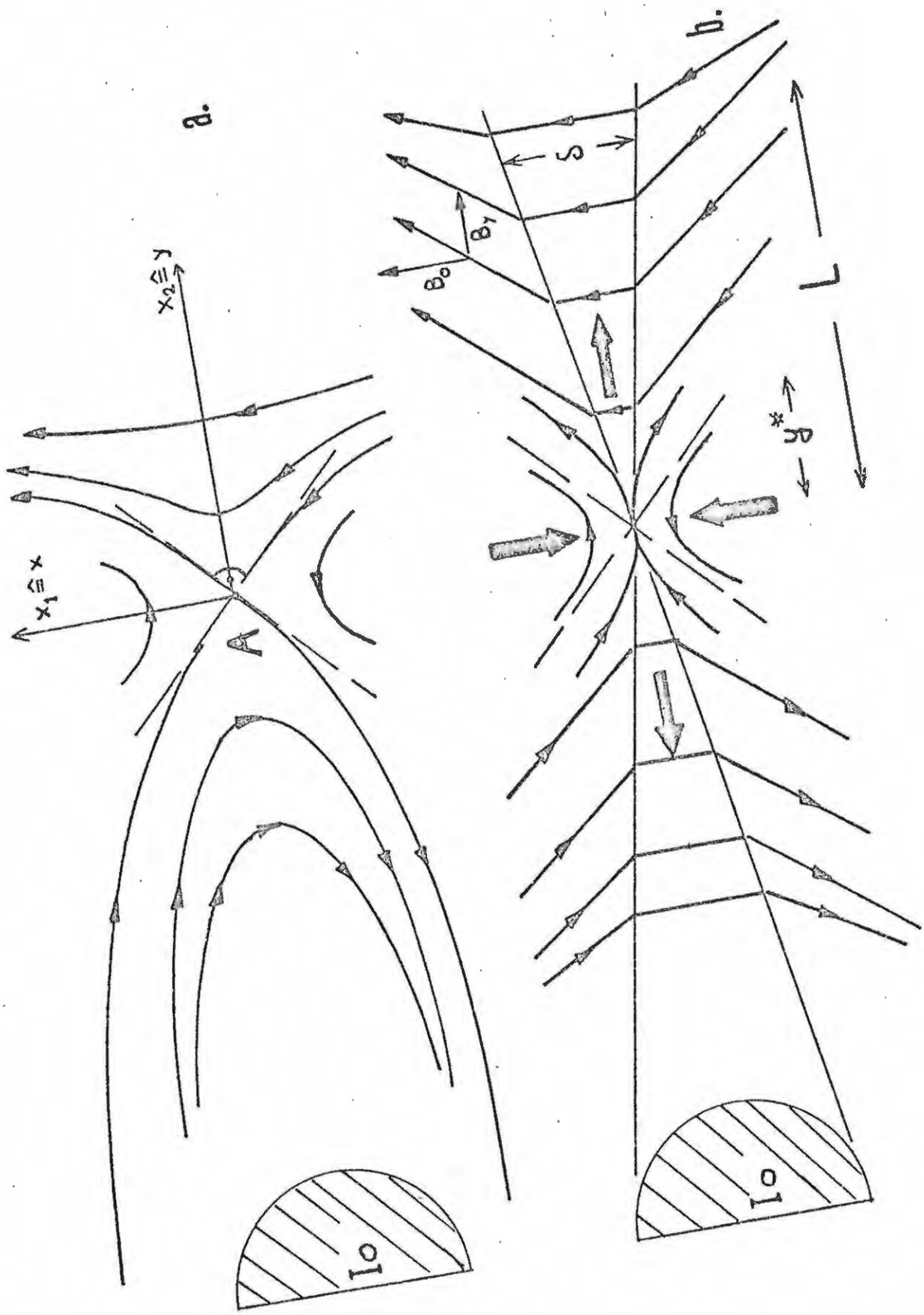

Figure 35: a) The zero order field behind Io.
b) The zero order field plus the B_y perturbation field.

$$(4.15)\qquad \frac{\partial \rho}{\partial t} = -\nabla(\rho \vec{v})$$

$$\rho \frac{Dv_i}{Dt} = \rho \frac{\partial v_i}{\partial t} + \rho v_i v_j = (\mu \vec{E} + \vec{j} \times B)$$

with

$$\nabla \times \vec{E} = -\frac{\partial B}{\partial t}$$

$$\nabla \times \vec{B} = -\mu_0 \vec{j}$$

where $\rho = n_i m_i + n_e m_e$ is the mass density, $\mu = e(n_e - n_i)$ the charge density, $\vec{j} = e(n_e \vec{v}_e - n_i \vec{v}_i)$ the current density and $\vec{v} = (n_i m_i \vec{v}_i + n_e m_e \vec{v}_e)/\rho$ is the mean mass velocity of the plasma. n stands for the particle concentration and m is the mass of the particle. The i and e subscripts indicate positive and negative particles. Mechanical stresses have been neglected.

Near the neutral point equations (4.15) give

$$(4.16)\qquad \frac{\partial B_{ij}}{\partial t} = -v_{kj} B_{ik} + B_{kj} v_{ik} - B_{ij} v_{kk}$$

assuming $\vec{E} + \vec{v} \times \vec{B} = 0$ (i.e. infinite conductivity)

$$(4.17)\qquad \frac{\partial v_{ij}}{\partial t} = -v_{kj} v_{ik} + (B_{ie} - B_{ei}) B_{ej} / \rho \mu_0$$

$$(4.18)\qquad \frac{\partial \rho}{\partial t} = -\rho v_{kk}$$

where the usual Einstein convention for summation is adopted. Now assume that $\frac{\partial}{\partial z} \triangleq \frac{\partial}{\partial x_3} = 0$ initially. Equations (4.16) and (4.17) then show that $\frac{\partial}{\partial z} = 0$ for all times. This can be seen by setting $j = 3$ and all quantities with subscripts $ij \hat{=} i3$, where i can be 1, 2 or 3, equal to zero on the right hand sides of (4.16) and (4.17). Both equations then show that $\frac{\partial B_{i3}}{\partial t} = 0$, i.e. $B_{i3} = 0$ (as was assumed), and likewise that $\frac{\partial V_{i3}}{\partial t} = 0$ i.e. $V_{i3} = \text{const} = 0$. The rest of the equations can then be written as:

(4.19) (1) $\partial B_{11}/\partial t = v_{12}B_{21} - v_{21}B_{12} - B_{11}(v_{11} + v_{22})$

(2) $\partial B_{22}/\partial t = -v_{12}B_{21} + v_{21}B_{12} - B_{22}(v_{11} + v_{22})$

(3) $\partial B_{12}/\partial t = v_{12}(B_{22} - B_{11}) - 2v_{22}B_{12}$

(4) $\partial B_{21}/\partial t = v_{21}(B_{11} - B_{22}) - 2v_{11}B_{21}$

(5) $\partial v_{11}/\partial t = -v_{11}^2 - v_{12}v_{21} + (B_{12} - B_{21})B_{21}/\rho\mu_0$

(6) $\partial v_{22}/\partial t = -v_{22}^2 - v_{21}v_{12} + (B_{21} - B_{12})B_{12}/\rho\mu_0$

(7) $\partial v_{12}/\partial t = -v_{12}(v_{11} + v_{22}) + (B_{12} - B_{21})B_{22}/\rho\mu_0$

(8) $\partial v_{21}/\partial t = -v_{21}(v_{22} + v_{11}) + (B_{21} - B_{12})B_{11}/\rho\mu_0$

Now assume that in the initial state, where $\vec{j} = 0$, the orthognal axes are chosen in such a way that $B_{12} = B_{21} = 0$. B_{11} is positive and B_{22} negative. Let all velocity gradients (v_{ij}) vanish initially. Consider now a perturbation of B_{12} (either positive or negative).

Let us write the changes in form of a table

B_{12}	B_{11}	B_{22}	B_{21}	v_{11}	v_{22}	v_{12}	v_{21}	
+	+	-	0	0	0	0	0	initially
+	+	-	0	0	0	-	-	by (7) and (8) of (4.19)
+	+	-	-	-	-	-	-	by (3) and (5) of (4.19)
or								
-	+	-	0	0	0	0	0	initially
-	+	-	0	0	0	+	+	by (7) and (8) of (4.19)
-	+	-	+	-	-	-	-	by (3) and (5) of (4.19)

We see that derivative of every component has the same sign as the component itself. Thus all components grow in magnitude. As $B_{21} \cdot B_{12} < 0$ always, curl $\vec{B}$ grows and hence the current density continues to grow. This is of course due to the assumptions made in

(4.15) and (4.16) of negligible mechanical forces and infinite conductivity.

It is obvious that this cannot be true. If the plasma has a conductivity σ_m the ohmic field $\vec{j}/\sigma_m$ causes a motion of plasma across the field lines with a velocity $\vec{v} = \vec{E} \times \vec{B}/B^2 = \vec{j} \times \vec{B}/\sigma_m B^2$. This velocity has a singularity at the neutral point where $B \to 0$. The effect of the motion is, that the plasma at points P,Q,R initially connected by a field line will move to the points P', Q', R' respectively of which only P' and R' are magnetically connected. In other words: the magnetic field line through P,Q,R appears to have been broken and reconnected to from the two lines, one of which connects P' and R' and the other forms a closed loop around Io. The effect of this rearrangement is to reduce curl $\vec{B}$ and hence $\vec{j}$. When the reduction of $\vec{j}$ by this process is balanced by an external motion of plasma across the magnetic field or by an external production of curl $\vec{B}$ the neutral point will be steady and the magnetic field in its vicinity will not vary in time. As the total length of the field line is reduced in this process the magnetic field energy $\iiint \frac{B^2}{2\mu_o} d\tau$ is also reduced. This magnetic field energy is thus dissipated in the neutral point, the energy being carried away either by accelerated particles, turbulent plasma motion or waves. The rate of energy dissipation depends on the rate of slippage of the plasma with respect to the field, which is dependent on the resistivity of the material. It has been suggested by Friedman and Hamberger (1968) and Bratenahl and Yeates (1970) that turbulent wave motions are mainly responsible for the increase of resistivity over the value for the resistivity due only to binary collisons. The increased

resistivity is necessary to explain the fast dissipation rate observed experimentally by Bratenahl and Yeates (1970) and others. Petschek (1964) and Petschek and Thorne (1967) explain the rapid dissipation as due to the emission of intermediate (Alfvén) waves and a slow wave shock as indicated in the figure (35b). This allows for a rapid transport of plasma across the field lines as will be shown below. Bratenahl and Yeates (1970) have found strong evidence for the emission of these waves. The dissipation of magnetic energy is due to a number of different processes, of which wave turbulence, particle acceleration (Tverskoi, 1962) and Alfvén wave emission are of major importance.

The importance of the reconnection and magnetic energy dissipation can be estimated in the following way. Petschek (1964, 1967) shows that the minimum time for reconnection of the magnetic field lines is given as

$$(4.20) \qquad \tau = \frac{L}{V_M}, \quad V_M = M_0 V_A'$$

where L is a scale length, V_m is the velocity of the plasma towards the neutral point, and V_A' is the Alfvén velocity calculated from the magnetic field outside the neutral point, taking only that component which is antiparallel across the neutral point (i.e. B_y). Mo is a number given for the compressible case by

$$(4.21) \qquad M_0 = \frac{\pi}{2(1+\alpha)\ln(M_0^2 2 R_M)}$$

where α is a number between 0 and 1 and R_M is the usual magnetic Reynolds number. ($R_M = \sigma \mu_0 V_A' L$)

$$(4.22) \qquad V_A' = \frac{B_y}{B_0} V_A = 2n \frac{B_y^0}{B_0} V_A = 2n V_S$$

and

$$(4.23) \qquad \tau = \frac{L}{2\pi v_s M_o} .$$

For the plasma at Io's orbit ($T \simeq 2\,000$ K, $N_e \simeq 10 \ldots\ldots 10^3$ electrons /cm^3) M_o is between 1/20 .... 1/40 for $L = \beta R_{Io}$ and $M_o \simeq 1/30$, τ is about $\tau = \beta 420$ n. β is a numerical factor between 1 and possibly 10 indicating the length of the neutral sheet (see figure (35b)). It should be noted that this time is almost independent of the plasma density and magnetic field at Io's orbit.

Certainly reconnection of a magnetic field line will become important if τ is less than a round trip time for the Alfvén waves. If $\tau < 12$ seconds reconnection will occur before the field line can be distorted further by the generation of Alfvén waves as described in the last section. Thus for $n > 35\ \beta$ reconnection cannot be neglected. This corresponds to $35 \times 12 \times \beta = 420 \times \beta$ seconds $= 7 \times \beta$ minutes from the time that a flux line first feels Io until it eventually reconnects at the neutral point. Or more accurately: 7 minutes is approximately the time for the points C and D (or the plasma at points C and D) which were initially magnetically connected to be disconnected by the advent of Io and then be reconnected in the neutral point.

The whole discussion is, of course, only valid if the field lines do not diffuse through Io in a time shorter than $7\ \beta$ minutes. Thus σ_{Io} should be greater than about $3\ \beta \times 10^{-5}\ \Omega^{-1}\ m^{-1}$. I will assume that Io is, indeed, such a good conductor.

In order to investigate the time scales involved in the magnetic field line reconnection across the

neutral point it is necessary to look into the neutral point generation in more detail. Suppose that Io's conductivity is as large as $5.10^{-4}\ \Omega^{-1}\ m^{-1}$. Then the currents through Io generate a magnetic field the magnitude of which is larger than the underlying magnetic field at Io's orbit (due to currents in Jupiter) at distances $r < 6\ R_{Io}$ from Io in the plane of Io's central meridian. (See formula 4.7)). There will thus be a point at $r \approx 6\ R_{Io}$ behind Io where the magnetic fields due to currents in Io and those in Jupiter cancel. Figure (35a) is a two dimensional representation of the field due to these currents. In three dimensions there will be a neutral line in the z - direction. (The neutral line is probably curved towards Io approaching Io at its sides M and N.) We have seen above that a change of $B_{21} \hat{=} \partial B_y/\partial_x$ due to some external agent will lead to an increase of curl $\vec{B}$ at the neutral point. The field lines will be rotated towards each other. In the limit of infinite conductivity the two limiting field lines will approach each other and form an infinitely thin sheet across which the field changes discontinuously. This requires an infinite current in the z direction; i.e. a mathematical current sheet. If, however, the conductivity of the plasma is not infinite the region of magnetic field change will have a thickness δ and the magnetic field topology will look something like the one shown in figure (35b). Sweet (1958) and Parker (1963) have shown that such a magnetic field configuration will lead to an ejection of plasma outward along the boundary. This is due to the fact that in the region where the magnetic field goes through zero the plasma pressure must be higher than that of the surrounding medium. The steady flow of plasma into the boundary and out along the

boundary is analysed easily. For a steady flow the balance of inflow of plasma requires

$$U_{xo} L = v \delta \tag{4.24}$$

where U_{xo} is the flow velocity outside and towards the boundary v is the velocity along the boundary, and L and δ are the length and thickness of the boundary respectively.

For the steady state we have ($\frac{\partial}{\partial t} = 0$) for the equation of motion:

$$(\vec{v}\cdot\nabla)\vec{v} = -\frac{1}{\rho}\nabla p + \frac{1}{\rho}\vec{j}\times\vec{B} \tag{4.25}$$

which is rewritten as (noting that $\vec{j} = \frac{1}{\mu_o}(\nabla \times \vec{B})$

$$(\vec{v}\cdot\nabla)\vec{v} = -\frac{1}{\rho}\nabla p + \frac{1}{\rho\mu_o}(\nabla\times\vec{B})\times\vec{B} \tag{4.26}$$

As both the magnetic field and velocity are small in the neighbourhood of the neutral point, Ohm's law is

$$\vec{j}_z = \sigma \vec{E}_z \tag{4.27}$$

(we are dealing with a 2 dimensional magnetic field configuration in which $B_z = 0$ and $\frac{\partial}{\partial z} = 0$)

Outside the boundary $\vec{j} = 0$, and as for steady flow $\nabla \times \vec{E} = 0$, we have E_z = const

$$|E_z| = U_{xo} B_{yo} \tag{4.28}$$

Where B_{yo} is the zero order magnetic field in the y-direction outside the boundary. $\nabla \times \vec{B}$ can be estimated from the fact that the field must change by 2 B_{yo} across the boundary which gives

$$(4.29) \qquad j_z \approx \frac{1}{\mu_o} 2 \frac{B_{yo}}{\delta}$$

Combining (4.27), (4.28) and (4.29) gives

$$(4.30) \qquad U_{xo} = \frac{2 B_{yo}}{\mu_o \sigma \delta}$$

In the vicinity of the neutral point we can neglect the second term in (4.26) and, noting that $\nabla p = - \nabla (B_{yo}^2 / 2\mu_o)$, and combining (4.24) to (4.30) we can write:

$$(4.31) \qquad U_{xo} = \left(\frac{B_{yo}}{\sqrt{\mu_o \rho}} \frac{2}{\mu_o \sigma L} \right)^{1/2} = \left(V_A(B_{yo}) \frac{2}{\mu_o \sigma L} \right)^{1/2}$$

where V_A is the Alfvén velocity for a magnetic field B_{yo}.

For the conditions at Io's orbit

$$\sigma = 10^2 \ [\Omega^{-1} \ m^{-1}]$$

$$L = 6 \ R_{Io} \simeq 10^7 \ m \quad \mu_o = 4 \ x \ 10^{-7} \ H/m$$

we get

$$U_{xo} = (1.5 \times 10^{-3} \ V_A \ (B_{yo}))^{\frac{1}{2}}$$

We have argued before that

$$B_{yo} \simeq 2n \ (vs/V_A \ (B_o)) \ B_o$$

For

$$n \simeq 110 \text{ and } V_A \ (B_o) = 0.1 \ c$$

$$U_{xo} = 140 \quad m \ s^{-1}$$

Thus we see that the flow of plasma towards the neutral point is very slow indeed.

Petschek has modified the picture by introducing a slow wave shock. In the following I will briefly describe Petschek's basic ideas and rewrite his

calculations in SI units. I do this rather than referring the reader to the excellent original paper, because I hope to point out some basic physical concepts which have been used earlier in this thesis and which are intimately related to Petschek's ideas.

In the compressible case ($p = NKT \ll B^2/2\mu_o$) the relevant shock is basically a switch-off shock across which the tangential magnet field component is switched off. The magnetic field topology is shown in figure (35b). The boundary splits up into two shocks across which the tangential magnetic field component vanishes. If B_{yo} (that is the y component of B) is independent of y and if the density in the boundary layer ρ_b is constant it follows from symmetry that the field between the waves is entirely in the X-direction. Switch-off shock waves propagate at a speed equal to the Alfvén speed based on the normal component of the magnetic field (i.e. B_x). Let us assume that the ratio of the density ρ_o far from the boundary to ρ_b is α. For a monoatomic perfect gas $\alpha = 2/5$ if energy is conserved. ($\alpha = 1$ for the incompressible case). The continuity equation is now written as

$$\alpha U_{xo}\, y = v\, \delta \tag{4.32}$$

and the y - component of the momentum equation is

$$\frac{d}{dy}\left(\rho_o v^2 \delta\right) = -\alpha \frac{B_{yo} B_x}{\mu_o} \tag{4.33}$$

From this we get:

$$M_o^2 \frac{d}{dy}\left(\alpha \frac{y^2}{\delta}\right) = -b_x \tag{4.34}$$

where M_o and b_x are defined as $M_o = \dfrac{U_{xo}}{V_A(B_{yo})}$, $b_x = \dfrac{B_x}{B_{yo}}$

The plasma moves towards the boundary with a velocity U_{xo} and is accelerated in the y direction in the shock front. In order to maintain a steady state flow the rate at which the plasma in the propagating slow wave shock is accelerated must be equal to the rate at which it is pushed in by the external flow.

$$|U_{xo}| = |V_A(B_x)| = V_A(B_{yo}) \frac{|B_x|}{B_{yo}} \tag{4.35}$$

or

$$M_o = |b_x|$$

We have taken the absolute value of B_x because the waves travelling in the direction of B_{yo} have B_x and U_x in antiphase whereas waves travelling in the opposite direction have them in phase. Substituting (4.35) into (4.34) we get

$$\delta = 2\alpha M_o |y| \tag{4.36}$$

If M_o is to be constant (which is true for small distortions of the external field) the magnitude of b_x must be constant. Now, for an X - type neutral point b_x must be an odd function of y. If $|b_x|$ is to be constant along the boundary this would require a discontinuity of b_x at the neutral point. This cannot be allowed for by the wave mechanism. This indicates that near the neutral point the magnetic field annhilation must be due to some other process than wave propagation, i.e. to diffusion, which can account for a continuous variation of b_x with y.

It may be convenient to point out the physics behind the mathematics at this point. In section 4.1 and 4.2 we have seen how Io traps the field lines

impinging on it. The currents through Io lead to the formation of a region of zero field behind Io, with B_x having different signs on both sides of the neutral point. The tilting of the field lines due to the emission of Alfvén waves by Io and their subsequent reflection in the ionosphere produces the B_{yo} fields, which have different signs on both sides of the neutral point. There is a curl $\vec{B}$ and hence a current $\vec{j}$ in the plasma. The associated $\vec{E}$ field pulls the plasma into the neutral point. The pressure and magnetic field gradients in the vicinity of the neutral point squeeze the plasma out along the boundary (i.e. in the y direction). This loss of plasma is balanced by an inflow of plasma towards the neutral point in the x direction. This velocity is correlated with the velocity in the y direction by the continuity equation. Sweet's model give U_{xo} only as due to an $\vec{E} \times \vec{B}/B^2 = \frac{1}{\sigma\mu_o} \nabla \times \vec{B} \times \vec{B}/B^2$ drift. Petschek's mechanism fixes U_{xo} essentially by allowing the plasma to be convected along the y direction by the propagation of a hydromagnetic wave. This is very similar to the situation described in section 4.2. There we had a velocity gradient being cancelled by a hydromagnetic wave producing a magnetic field component perpendicular to the underlying field. Here we have a magnetic field gradient being cancelled by a hydromagnetic wave producing a velocity component perpendicular to the underlying field. This velocity is independent of the conductivity and only related to the change of the magnetic field across the wave front and the rate of magnetic field cancellation is proportional to the wave velocity i.e. to the magnetic field component normal to the wave front. In the vicinity of the neutral point this component is essentially zero and the rate of field cancellation due to this process is very

small. Sweet's mechanism is, however, independent of this field and will thus be more important (i.e. faster) than the field cancellation due to the wave propagation. The wave mechanism will, however, become faster when the normal component is large enough. The interplay of the two processes will thus decrease the length L over which diffusion must produce the magnetic field annihilation.

Close to the neutral point we have from (4.31)

$$M_o = \frac{2}{V_A \mu \sigma_m \delta} \tag{4.37}$$

which replaces (4.35) for small y. We assume that δ is nearly constant in this region. Substituting (4.32) into (4.34) gives

$$b_x = -M_o^3 V_A(B_{yo}) \mu_o \sigma \alpha y \tag{4.38}$$

Thus we see that for small y b_x varies linearly with y. Now wave propagation will become important when b_x according to (4.38) is equal to b_x according to (4.35). This gives the length of the region controlled by diffusion y*.

$$y^* = \frac{1}{M_o^2 \mu_o \sigma_m \alpha V_A(B_{yo})} \tag{4.39}$$

Equation (4.39) is similar to (4.31) if y* and L are interchanged. As $y^* < L$ we see that the rate of plasma flow into the boundary (M_o) is greatly enhanced.

The above discussion relates entirely to the flow in the region between the shocks. The flow towards the boundary was taken into account by introducing M_o. (More or less as an unspecified variable.) (4.39)

contains two unknown's M_o and y* in contrast to (4.31) which allows for the calculation of M_o for a specified L. In Petschek's model L is only of minor significance. It is the unknown quantity y* which determines the rate of plasma flow into the neutral point. It is thus essential to find conditions which either fix y* or M_o. In the vicinity of Io we have the following situation. In a frame of reference moving with Io the zero order magnetic field is the superposition of Jupiter's magnetic field and that due to the currents through Io. The field lines cannot diffuse through Io and cannot be carried around Io by the plasma motion (or currents in the plasma) or at least not completely. This trapping results in the emission of hmd waves propagating into the ionosphere and back. The field lines are tied to massive conducting bodies at both ends and in the process of Io's motion relative to the ionosphere they will be stretched. In Io's frame this is seen as an addition of a B_y component to the zero order field. The more reflections the larger will this component become. The stretching will be stopped either by a diffusion of the field line through Io or its diffusion through the neutral point. Diffusion through Io is a gradual process, whereas diffusion through the neutral point is a rapid one. The plasma in the neutral boundary traverses the distance L ($\sim 6 R_{Io}$) in a time $t = L/v = L/V_A(B_{yo}) = L/2n\ V_s$ where n indicates the number of reflections which occur along a particular field line between the time of the first encounter between the field line and Io and its subsequent reconnection in the neutral point. The inverse of t gives a characteristic frequency of the Alfvén waves involved in the merging process in the neutral region. In the following n is related to M_o which indicates the flow velocity into the neutral

point.

Petschek finds the maximum value of M_o by calculating the x component of the magnetic field perturbation at the boundary required for large enough flow velocities so that y* can be smaller than L. He then uses this B_x to specify a distribution of magnetic sources along the y-axis. As the perturbation of the zero order magnetic field must satisfy Laplace's equation in Petschek's model, he then solves for the y component of the perturbation field B'_y. Adopting a maximum value for B'_y at the neutral point as $B'_y(0) = \frac{1}{2} B_{yo}$ then fixes M_o to a value given by (4.21). In the case of Io we know the variation of the x component of the zero order field along the y axis. The zero order field is due to the currents through Io and the underlying magnetic field of Jupiter.

$$(4.40) \qquad B_{xo} = B_o \left(1 - \frac{c}{y'}\right) \quad \text{for } x = 0$$

where

$$c = \frac{\mu_o \sigma_{Io} V_s R_{Io}^2}{2}$$

The zero order y component B_{yo} near the neutral point has the same magnitude as B_{xo}. (The zero-order field has curl $\vec{B}_o = 0$ at the neutral point.) Now, in the steady state, the perturbation of the field must be produced by the external flow or an external perturbation of the field. We have seen in section 4.2 that the trapping of the magnetic field lines by Io will lead to a generation of B_y. We equate this with the perturbation necessary to maintain the steady state flow

$$(4.41) \qquad B_{yo} = B_{xo} + B_y \approx B_{xo} + 2n \frac{V_s}{V_A} B_o$$

thus

$$(4.42)\qquad b_x = \frac{B_x}{B_{yo}} = \frac{B_o\left(1-\frac{c}{y'}\right)}{B_o\left(1-\frac{c}{y'}+2n\,V_S/V_A\right)}$$

Near the neutral point this can be expanded as

$$y_o = y' - y_o' = 0$$

$$(4.43)\qquad b_x(y) = \frac{V_A}{c2nV_S}\,(y'-y_o') = \frac{V_A}{c2nV_S}\,y = \frac{V_A}{R_{Io}^2\mu_o\sigma_{Io}V_S^2}\cdot\frac{y}{n}$$

Combining this with (4.38) gives

$$(4.44)\qquad M_o^3\,V_A(B_{yo})\,\mu_o\,\sigma_m\,\alpha = \frac{V_A}{R_{Io}^2\,V_S^2\,\mu_o\,\sigma_{Io}}\cdot\frac{1}{n}$$

or, as

$$V_A(B_{yo}) \approx 2nV_S$$

$$(4.45)\qquad n^2 = \frac{V_A}{2R_{Io}^2V_S^3\mu_o^2\sigma_{Io}\sigma_m\alpha}\cdot\frac{1}{M_o^3}$$

For $V_A = 3 \times 10^7$ m s^{-1}, $R_{Io} = 1.7 \times 10^6$ m, $V_S = 5{,}6 \times 10^4$ m s^{-1}, $\sigma_{Io} = 5 \times 10^{-4}\ \Omega^{-1}$ m^{-1} and $\sigma_m = 10^2\ \Omega^{-1}$ m^{-1} this reads $n^2 = 4{,}4 \times 10^{-7}\ \frac{1}{M_o^3}$.

From (4.45) we see that even for n = 1 the necessary M_o will be smaller than the maximum reconnection rate for steady flow in Petschek's model. ($M_{o\,max} \approx 1/30$ for $\sigma_m = 10^2\ \Omega^{-1}$ m^{-1} and $L \approx 6R_{Io}$). We conclude that if more than one reflection occurs along one particular field line before it reconnects through the neutral point, the merging rate M_o will adjust to a value less than that given by Petschek.

The characteristic frequency of the Alfvén wave emitted from the neutral point was shown above to be:

$$(4.46)\qquad f = \frac{2nV_S}{L} \approx \frac{1{,}35\times10^{-3}}{M_o^{3/2}}\cdot\frac{V_S}{L} \propto V_A^{1/2}$$

It is difficult to estimate the steady state value of M_o. It is probably smaller than Petschek's maximum value of 1/30. In the following we will adopt a value for M_o which gives the best agreement between the model of the Io controlled decametric radiation and the observations of that radiation and check whether that value leads to a consistent model. In chapter 5 we will show that the maximum frequency of the Alfvén waves from the neutral point should be of the order of 1-3Hz. This value should correspond to the maximum value of V_A encountered along Io's orbit ($V_A = 3 \times 10^{+7}$ m/s). This gives M_o between 4×10^{-4} and 2×10^{-4}. These values are smaller than Petschek's maximum values by a factor of about 100.

Let us adopt a mean value $M_o = 3 \times 10^{-4}$ ($f = 1,5$ Hz) in the following calculations. According to (4.48) this gives $n \approx 130$ which means that there will be about 130 reflections along a particular field line between the time of the first Alfvén wave emission by Io along this line and its final reconnection through the neutral boundary. 130 reflections take place in a time $130 \times 12 = 1\ 560$ secs = 26 min. Jupiter's angular velocity is $\Omega = 1,77 \times 10^{-4}\ s^{-1}$ and Io's mean motion is $n = 4,13 \times 10^{-5}\ s^{-1}$. Thus Io's motion relative to Jupiter is $\omega = (\Omega - n) = 1.36 \times 10^{-4}\ s^{-1}$. In 1 560 secs Io will have moved $\omega \times 1\ 560 = 0.212 \approx 12,5^{\circ}$. Thus the Alfvén waves generated in the neutral point will impinge onto the ionosphere at a longitude which is about $12,5^{\circ}$ away from Io. This is in good agreement with the required lead of the foot of IFT by about 12° - 15° (see chapter 1 and 5). Thus the adopted value of M_o leads to a consistent picture.

The above discussion is, of course, only valid if the diffusion time of the magnetic field lines through

Io ($t_D \approx 4\mu_o \sigma_{Io} R_{Io}^2$) is larger than the time between first encounter and reconnection (i.e. $t_D > nt$, where t is the time for one reflection $\approx$ 12 secs). This condition reads:

$$4 \sigma_{Io} R_{Io}^2 \mu_o = \sigma_{Io} \times 1.6 \times 10^7 > nt$$

with

$$M_o = 2 \times 10^{-4} \quad V_A = 3 \times 10^7 \text{ m s}^{-1}$$

we get

$$\sigma_{Io} > 5 \times 10^{-5} \ \Omega^{-1} \text{ m}^{-1}$$

Our calculations were based on $\sigma_{Io} \approx 5 \times 10^{-4} \ \Omega^{-1} \text{ m}^{-1}$.

A serious shortcoming of Petschek's model is the fact that with the maximum recombination rate M_o the diffusion length y* (see (4.39)) becomes very small, smaller even than an ion gyroradius. With our estimate of M_o we get $y^* = 2.6 \times 10^3$m which is larger than the electron and proton gyroradii of the thermal particles at Io's orbit. Thus the treatment of the neutral point in the way described above seems to be valid.

4.5 Results

In the last sections it was shown that hmd waves will be generated by Io. These waves travel in the form of pulses along the field lines into the ionosphere of Jupiter. The characteristic frequency $f \approx 1/v \ dv/dt$ in the pulses is given by (4.46). This frequency changes while Io moves around Jupiter through regions of varying plasma density (see figure 26a). The variation of f normlized to the value at $\lambda Io = 220^\circ$ as a function of sub Io longitude λIo is shown in figure (36b) for different magnetic dipole displacements. The waves will be incident on the top of the ionosphere at a longitude which is ϕ degrees ahead of Io. This lead angle ϕ is simply related to n. Figure (36c) shows the

variation of ϕ as a function of the sub Io longitude λ_{Io} again for different magnetic dipole-displacements.

The waves are emitted at Io with a (magnetic) amplitude $b = B_y = 2n \frac{Vs}{V_A} B_o$. It was shown above (equation 4.45) that $n \propto V_A^{\frac{1}{2}}$. Thus the amplitude b should vary as $b \propto V_A^{-\frac{1}{2}} B_o$. Figure (36a) shows the variation of b normalized to the value at $\lambda_{Io} = 220^o$. The average power contained in these waves can be easily estimated as

$$P = (L \times 2 R_{Io}) (\tfrac{1}{2} \mu_o) (b^2) V_A \qquad /W/$$

The amplitude b has a minimum at $\lambda_{Io} = 220^o$ of about 2.5×10^{-6} T. With the area $2LR_{Io} = 12 R_{Io}^2 = 36 \times 10^{12}$ m^2 the power P is at least $P = 9 \times 10^7 V_A = 2.7 \times 10^{15}$ /W/. This is much larger than the power involved in an average decametric storm, which is about 10^8 W (see section 2.1).

In the following we will argue that the decametric radiation derives its energy from the magnetic energy of the hydromagnetic waves. We will therefore be interested in the amplitude b of the hmd waves when they are incident on the Jovian ionosphere where the decametric radiation is generated. In the next chapter the propagation of the hmd waves through the magnetosphere of Jupiter is described.

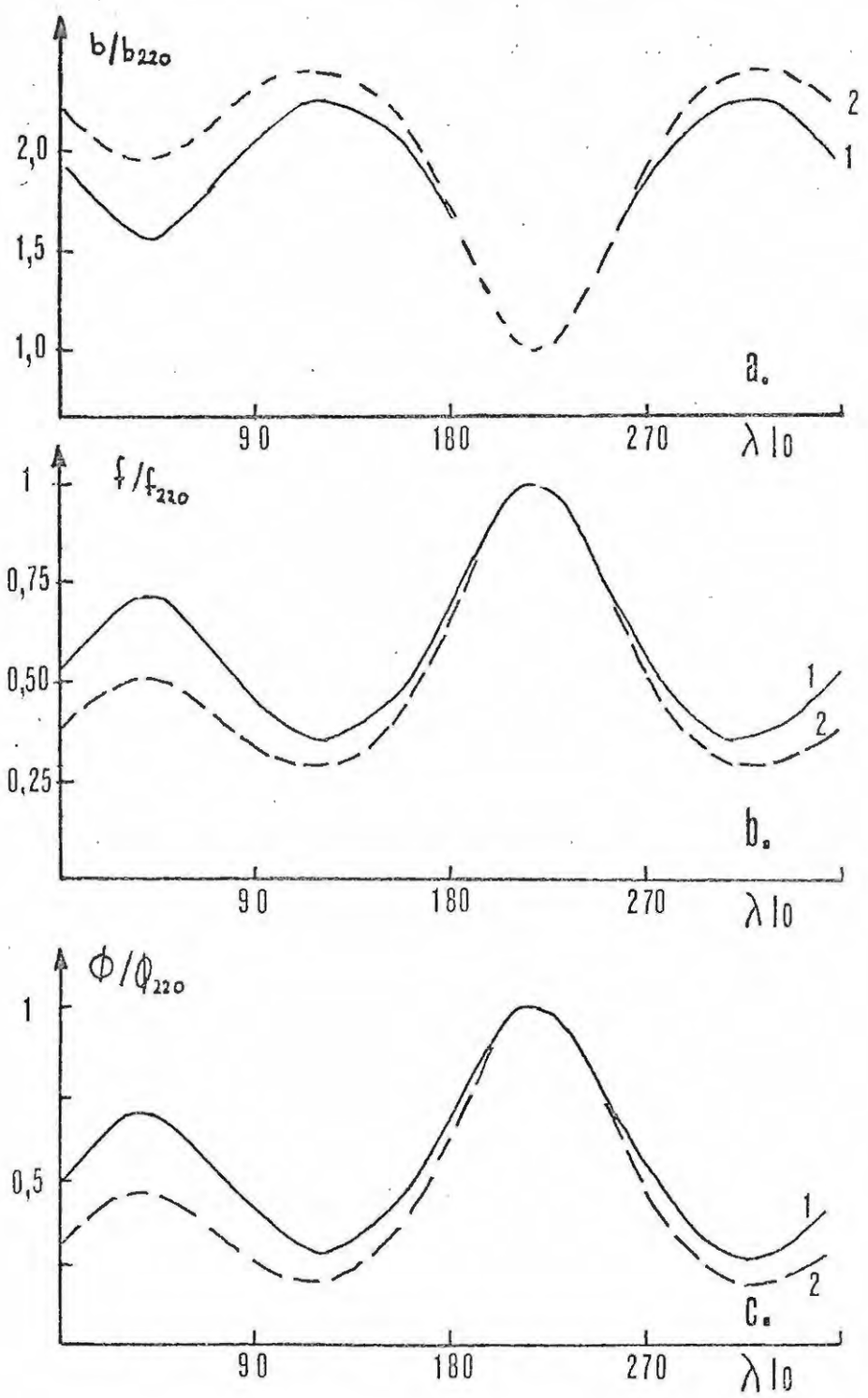

Figure 36: a) Magnetic amplitude (b) of the Alfvén waves as a function of λ Io normalised to the value of b at λIo = 220°. For both curves λ_o = 235, λ_T = 210, α = 10.
1: δ = 0,05, s = -0,1.
2: δ = 0,15, s = -0,2.
b) Variation of normalized frequency with λ Io.
c) Variation of normalized lead angle (ϕ) with λ Io.

5. Propagation of Alfvén Waves Along Field Lines

Schmahl (1970) shows that transverse Alfvén waves can be damped. The damping rate k_i is given by him as:

$$k_i = \frac{\sqrt{\pi}}{2} \frac{\omega_{pi}}{c} \left(1 + \Omega_i^2/\omega_{pi}^2\right)^{-1/2} a\, e^{-a^2} \tag{5.1}$$

where

$$a = -\left(\frac{m_i}{2kT}\right)^{1/2} \frac{\Omega_i}{k_x} = -V_A \left(\frac{m_i}{2kT}\right)^{1/2} \frac{\Omega_i}{\omega}$$

k_x is the wavenumber of the Alfvén wave travelling along the direction of the underlying field $B = (B_o, 0, 0)$. At Io's orbit, where a is a minimum and hence k_i is a maximum, the damping rate is ($\omega = 2\pi f \approx 10\ s^{-1}$)
$k_i \sim \exp(-10^{10})\ m^{-1}$.
Collisionless damping, to which (5.1) applies, should therefore be entirely negligible. Schmahl (1970) and Deift (1971) have also investigated the effect of the magnetic field line curvature on the propagation of Alfvén waves. Schmahl (1970) derives a critical angular frequency $\omega \approx 0.5\ s^{-1}$ (for slightly different plasma parameters at Io's orbit) below which hmd waves will not propagate their energy beyond the bend of the field line. Waves of much lower frequency will be partially reflected and set up a standing wave pattern in the outer parts of the magnetic field tube. As the waves generated in the neutral point have larger frequencies than 0.5 sec^{-1}, the standing wave pattern will not be formed and the energy can propagate around the bend of the magnetic field line from Io down into Jupiter's ionosphere.

Thus in the approximation of the waves propagating through an incompressible, inviscid and perfectly conducting medium the hmd disturbance propagates only along the magnetic field lines which pass through it.

These waves should not suffer any attenuation with distance. Non-collisional effects, however, alter the unidirectional, unattenuated propagation of the waves. Lighthill (1959) has included the (non-collisional) effects of resistivity, compressibility and Hall current. He investigated the directional distribution of Alfvén waves from a local source. The Hall-current effect was shown to be much more important than the electrical resistivity when the magnetic field is so large that the electron gyro-frequency greatly exceeds the collision frequency. This condition reads $B \gg 10^{-6} N_e T_e^{-3/2}$ where N_e is the electron density in cm^{-3}, T_e the electron temperature in K, and B the magnetic field in G. Everywhere along IFT B is always larger than $10^{-6} N_e T_e^{-3/2}$. The effect of finite compressibility introduces two new hmd waves, the fast wave which propagates with a velocity $v = \sqrt{V_A^2 + b^2}$ and the slow wave which propagates with $v = b$ (b is the velocity of sound $b^2 = \gamma KT/m_i$). The intermediate wave propagating with $v = V_A$ still propagates in a unidirectional way along the field line. We are interested in this wave and neglect the other waves which are geometrically attenuated, because they do not propagate uni-directionally but in all directions. In the case of negligible resistivity the relations between the disturbances of v and B are in 1. order

$$(5.2) \quad -\nabla \times \vec{E} = \frac{\partial \vec{B}}{\partial t} = \frac{\partial}{\partial t}\left(\nabla \times \left(\vec{v} - \frac{\nabla \times \vec{B}}{\mu_0 e N_e}\right) \times \vec{B}\right)$$

$$(5.3) \quad \rho_0 \frac{\partial \vec{v}}{\partial t} = -\nabla p + \frac{(\nabla \times \vec{B}) \times \vec{B}_0}{\mu_0} = -\nabla\left(p + \frac{\vec{B}_0 \cdot \vec{B}}{\mu_0}\right) + \frac{\vec{B}_0 \cdot \nabla \vec{B}}{\mu_0}$$

Where B_0 is the undisturbed magnetic field and $B = B_0 + b$ is the disturbed field. Since we are only interested in the intermediate waves we can ignore the

compressibility and analyse the waves by assuming $\rho = \text{const} = \rho_0$. From the continuity equation

$$\frac{\partial \rho}{\partial t} + \operatorname{div}(\rho \vec{v}) = 0 \tag{5.4}$$

we get

$$\operatorname{div}(\vec{v}) = 0 \tag{5.5}$$

Taking the divergence of equation (5.3) yields

$$\nabla^2 \left(p + \frac{\vec{B}_0 \cdot \vec{B}}{\mu_0} \right) = 0 \tag{5.6}$$

Now, as $B_0 = (B_0, 0, 0)$, we get

$$\frac{\partial \vec{B}}{\partial t} = B_0 \frac{\partial}{\partial x}\left(\vec{v} - \frac{\nabla \times \vec{B}}{\mu_0 e N_e} \right), \quad \frac{\partial \vec{v}}{\partial t} = \frac{B_0}{\mu_0 \rho} \frac{\partial \vec{B}}{\partial x} \tag{5.7}$$

$$\frac{\partial}{\partial t}\left(\frac{\partial}{\partial t} + \frac{B_0}{\mu_0 e N_e} \frac{\partial}{\partial x} \operatorname{curl} \right) \vec{v} = \frac{B_0^2}{\mu_0 \rho} \frac{\partial^2 \vec{v}}{\partial x^2} = V_A^2 \frac{\partial^2 \vec{v}}{\partial x^2} \tag{5.8}$$

$$\frac{B_0}{\mu_0 e N_e} = \frac{V_A^2}{\Omega_i}$$

Following Lighthill (1956) we introduce the x component of the vorticity, curl $\vec{v}$

$$\zeta = \frac{\partial v_z}{\partial y} - \frac{\partial v_y}{\partial z} \tag{5.10}$$

and

$$\Delta = \operatorname{div} \vec{v} = 0 \qquad \Gamma = \frac{\partial v_x}{\partial x} \tag{5.11}$$

With these equations (5.9) reads

$$\frac{\partial^2 \zeta}{\partial t^2} - \frac{V_A^2}{\Omega_i} \frac{\partial}{\partial t} \nabla^2 \Gamma = V_A^2 \frac{\partial^2 \zeta}{\partial x^2} \tag{5.12}$$

$$(5.13)\quad \frac{\partial^2 \Gamma}{\partial t^2} + \frac{V_A^2}{\Omega_i} \frac{\partial^3 \zeta}{\partial t\, \partial x^2} = V_A^2 \frac{\partial^2 \Gamma}{\partial x^2}$$

$$(5.14)\quad \left\{ \left(\frac{\partial^2}{\partial t^2} - V_A^2 \frac{\partial^2}{\partial x^2} \right)^2 + \frac{V_A^4}{\Omega_i^2} \frac{\partial^2}{\partial t^2} \frac{\partial^2}{\partial x^2} \nabla^2 \right\} \zeta = 0$$

The second term on the left hand side of (5.14) represents the Hall-current effect and indicates that the vorticity component ζ cannot be propagated one-dimensionally. Assuming a periodic solution for ζ of the form $\zeta \propto \exp(i\omega t) \exp(i(\alpha x + \beta y + \gamma z)$ we get

$$(5.15)\quad G = (\omega^2 - V_A^2 \alpha^2)^2 - V_A^4 \alpha^2 k^2 (\omega^2/\Omega_i^2) = 0$$

or

$$(5.16)\quad \beta^2 + \gamma^2 = k^2 - \alpha^2 = \frac{\Omega_i^2}{\omega^2} \frac{1}{\alpha^2} \left(\frac{\omega^2}{V_A^2} - \alpha^2 \right)^2 - \alpha^2$$

Thus the wave number surface G = 0, (S), is the plane $\alpha = \omega/V_A$ only if $\omega/\Omega_i = 0$. This corresponds to the case of "the perfectly conducting fluid", transmitting waves one-dimensionally in the x-direction. In this case the group velocity of the wave $\vec{V}_G = \nabla G/(\partial G/\partial \omega)$ is $\vec{V}_G = V_A \hat{x}$ where $\hat{x}$ is a unit vector in the x-direction. If $\omega/\Omega_i > 0$, the wave number surface splits into two surfaces and the resulting two waves will propagate their energy (in the direction of the group velocity) into two cones the semi-angles Θ_1, and Θ_2 of which are given by Lighthill (1956) as:

$$(5.17)\quad \frac{\omega}{\Omega_i} = \frac{2 \tan \Theta_1}{(1 - 2\tan^{2/3}\Theta_1)(1 + \tan^{2/3}\Theta_1)^{1/2}} = \sin \Theta_2$$

For the waves emitted by Io ω is smaller than 10 $\sec^{-1}$ and Ω_i is larger than 5×10^2 $\sec^{-1}$. Thus $\omega/\Omega_i < 2 \times 10^{-2}$, and (5.17) can be approximated as

(5.18) $$\frac{\omega}{\Omega_i} = \sin\Theta_2 \approx 2\tan\Theta_1$$

The cone angle of the waves (subscripted) 2 is twice as large as that of the waves (subscripted) 1. The derivations above are for purely harmonic waves. Lighthill (1953) has shown, that the results for waves of finite duration are not basically changed. The wave packet at any point can be obtained by a superposition of waves with different frequencies so that the initial disturbance $a(t) = \int_{-\infty}^{\infty} d\omega f(\omega)\, e^{-i\omega t}$ where $f(\omega)$ is the frequency spectrum of the disturbance. Each individual wave component will spread into a cone the semi-angle of which will be given by (5.17). The resultant amplitude will, of course, decrease accordingly.

The waves emitted by Io will thus not follow the magnetic field lines exactly but they will be spread over an area, the diameter of which can be calculated in the following way. Assume the field lines to be straight (the effects of curvature have been shown to negligible above). The direction of B is taken as x, with Io at x = 0 and the top of Jupiter's ionosphere at $x = x_o$. Any direction perpendicular to x is y. The cone angle Θ (given by (5.17)) will change because Ω_i changes along x. The waves will thus follow a path y = y (x) where y(x) is given bx.

(5.19) $$\frac{dy}{dx} = \tan\Theta = \frac{1}{2}\frac{\omega}{\Omega_i} = \frac{1}{2}\frac{f\, m_i\, 2\pi}{eB}$$

We can integrate this equation along x if B is assumed to vary as the field of a magnetic dipole $B(r) = B_E (R_J/r)^3 (1 + 3\cos^2\Theta')^{\frac{1}{2}}$ where B_E is the magnetic field strength at Jupiter's surface. Inserting this into (5.19) and noting that

$$dx = (dx'^2 + dy'^2)^{1/2}$$

$$x' = r \sin\Theta' \,, \quad y' = r\cos\Theta'$$

and $$r = L R_J \sin^2\Theta'$$

where Θ' is the magnetic colatitude, we obtain

$$(5.20) \quad y = y_o + \left(\frac{K}{\cos^8\Theta'}\left(\sin^7\Theta' - \sin^7\Theta_{Io}\right)\right) L R_J$$

with $K = \frac{1}{2}(\omega/\Omega_i)$ evaluated at the point where the waves are generated. The integration constant y_o is the distance of the initial disturbance from the x-axis. Assume that the waves are generated on all magnetic field lines in IFT. The radius of IFT at Io is approximately R_{Io} whereas IFT has an average radius of 100 km in the ionosphere. Then $y_o \approx$ 100 km in and at the top of the ionosphere. The diameter of the area over which the energy contained in the waves is spread is thus

$$(5.21) \quad A = y^2$$

Deift (1971) has shown that the propagation of Alfvén waves with frequencies of the order of several Hz can be treated, in the magnetosphere, to a high degree of accuracy by using WKB solution. This can be seen quite easily by the following argument. In the low frequency limit ($\omega/\Omega_i \ll 1$) (5.17) and (5.8) reduce to the well-known Alfvén (wave) equations

$$(5.22) \quad \rho \frac{\partial v}{\partial t} = \frac{B_o}{\mu_o} \frac{\partial b}{\partial x}$$

$$\frac{\partial b}{\partial t} = B_o \frac{\partial v}{\partial x}$$

which give (assuming a linear polarized wave v = (0,v,0))

$$(5.23) \quad \frac{\partial^2 v}{\partial x^2} = \frac{\mu_o \rho}{B_o^2} \frac{\partial^2 v}{\partial t^2} = \frac{1}{V_A^2} \frac{\partial^2 v}{\partial t^2}$$

The solutions are supposed to have the form $v = e^{i\omega t} U(x)$ thus:

$$(5.24) \quad \frac{d^2U}{dx^2} + \left(\frac{\omega}{V_A}\right)^2 U = 0$$

If $U = e^{+i\phi}$ we get

$$(5.25 \quad -\left|\phi'\right|^2 + i\phi'' + \left(\frac{\omega}{V_A}\right)^2 = 0$$

where $\phi' = \frac{d\phi}{dx}$ and $\phi'' = \frac{d^2\phi}{dx^2}$

if $\phi'' \ll \left(\frac{\omega}{V_A}\right)^2$, we get the familiar WKB solution

$$\phi = \pm \int \frac{\omega}{V_A}\, dx$$

The condition $|\phi''| \ll \left(\frac{\omega}{V_A}\right)^2$ is then

or : $\omega \frac{d(1/V_A)}{dx} \ll \left(\omega/V_A\right)^2$

$$(5.26) \quad \frac{dV_A}{dx} \ll \omega$$

Now in the magnetosphere $\frac{d\,V_A}{dx}$ is a maximum at the edge of the plasma disk, where it has the value (See formula (3.54))

$$\frac{dV_A}{dx} \simeq \frac{d(1/N^{1/2})}{dx} \frac{B_o}{(\mu_o m_i)^{1/2}} = \frac{B_o}{(\mu_o N_{eo} m_i)^{1/2}} \frac{d\, e^{(B'/4kT)x^2}}{dx}$$

$$= V_{AO} \left(\frac{B'}{2kT} x\right) e^{(B'/4kT)x^2}$$

$$\simeq 0.1\ [s^{-1}] \quad \text{at } x = 5 \times 10^7 \text{ m}$$

assuming

$T = 2\ 500$ K; $V_{AO} = 3\ 000$ km s^{-1}

In the magnetosphere the WKB solution should thus be completely adequate. The WKB solution for the velocity and magnetic field amplitude of the wave is:

$$\begin{bmatrix} v \\ b \end{bmatrix} = \text{const. } B^{-1} \begin{bmatrix} \rho^{-1/4} \\ \rho^{1/4} \end{bmatrix} \exp i\omega\left(t \pm \int \frac{dx}{V_A}\right)$$

(Parker, 1955), where B is the (varying) magnetic field.

If we assume that the power is conserved we get for the amplitude of the wave impinging on the ionosphere of Jupiter.

$$(5.28)\quad A_{Io}\left(\frac{1}{2}\rho_{Io}v_{Io}^2+\frac{b_{Io}^2}{\mu_o}\right)(V_A)_{Io}=A_{ion}\left(\frac{1}{2}\rho_{ion}v_{ion}^2+\frac{b_{ion}^2}{\mu_o}\right)(V_A)_{ion}$$

where A is the area over which the wave is spread. The subscript "Io" indicates that the value is to be taken at Io's position and the subscript "ion" indicates the value at the top of the ionosphere. With (5.29) this gives for the flux F (energy per unit area) incident on the top of the ionosphere and the amplitude b at the top of the ionosphere.

$$(5.29)\quad F_{ion}=F_{Io}\;A_{Io}/A_{ion}\qquad /J\ m^2\ s^{-1}/$$

$$b_{ion}=b_{Io}\left(\frac{B_{Io}}{B_{ion}}\right)\left(\frac{\rho_{ion}}{\rho_{Io}}\right)^{1/4}\left(\frac{A_{Io}}{A_{ion}}\right)^{1/2}$$

Figure (37) shows the variation of flux F and the amplitude b of the wave incident on the top of the ionosphere as a function of sub-Io longitude, again normalised to the value at $\lambda Io = 220^{\circ}$.

In the ionosphere, $\left|\frac{dV_A}{dx}\right|$ can be larger than ω. In this case $|\phi'|$ is small and we get from (5.25) that $\phi = i\iint\left(\frac{\omega}{V_A}\right)^2 d\omega^2$. The condition $|\phi'|$ small is

$$|\phi'| = \left|\int(\omega/V_A)^2 dx\right| \ll \omega/V_A \quad \text{i.e.}$$

$$(5.30)\quad \left|\int\frac{\omega}{V_A^2}\,dx\right| \ll \frac{1}{V_A}$$

When (5.26) holds, ϕ is real and one obtains elementary solutions to the Alfvén wave equation (5.23) which are travelling waves. If, however, (5.30) holds, ϕ is pure imaginary and the solution to (5.23) represent

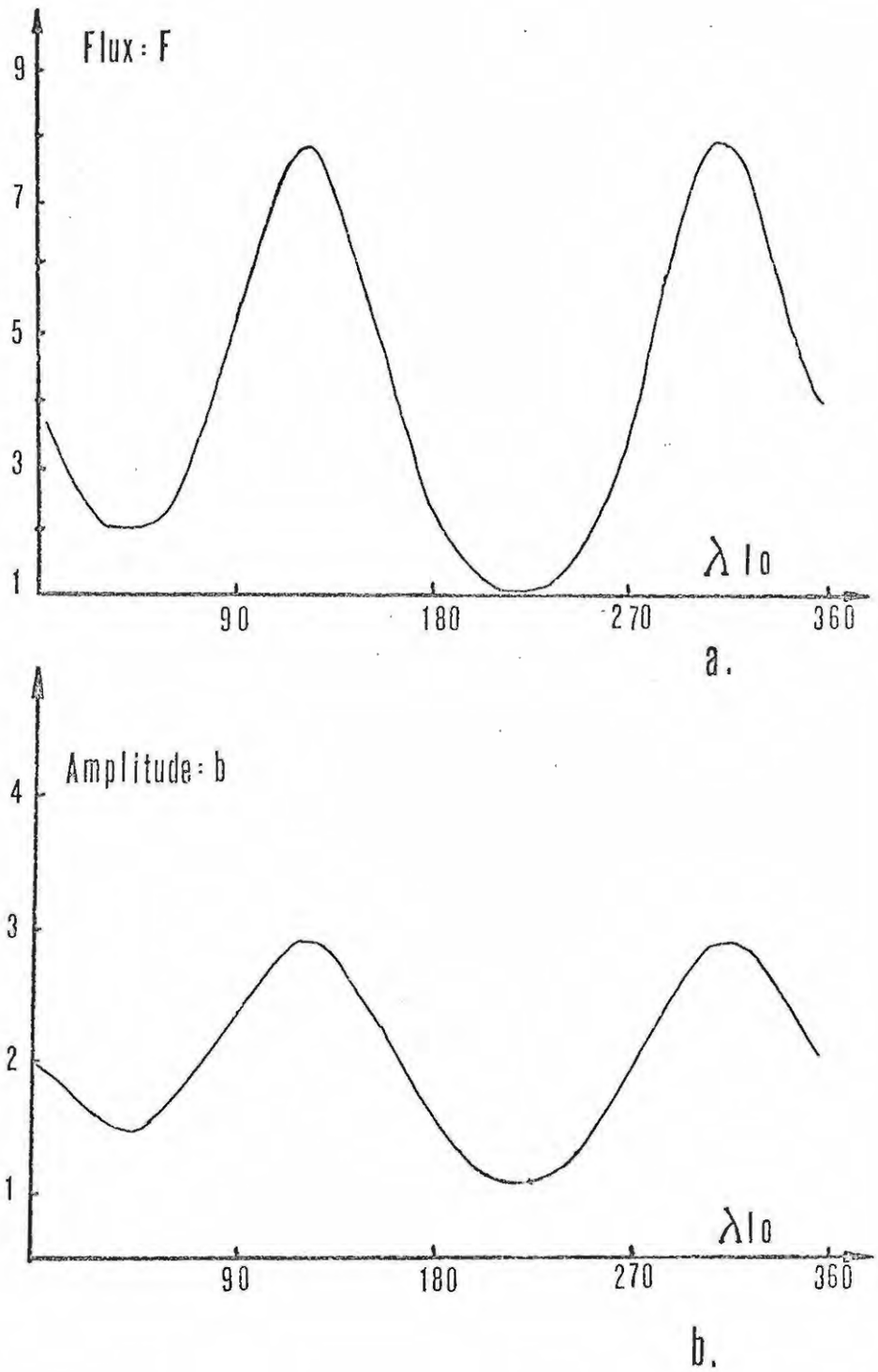

Figure 37: a) Normalized Alfvén wave flux incident on the top of the ionosphere as a function of λ Io.
b) Normalized magnetic amplitude at the top of the ionosphere as a function of λ Io.

standing waves. One may interpret this in the following way: when a wave (or pulse) impinges on a region in which V_A changes gradually (so that 5.26 holds) the wave generates (WKB) waves in the medium which can carry the energy through the medium. When, on the other hand, the change of V_A is precipitous (and (5.30) holds) standing waves will be established in the medium (in a time of order $1/\omega$) and all the energy incident on the medium will be reflected.

Deift (1971) has investigated the transmission and reflection of hmd waves at the Jovian ionosphere. For frequencies of several Hz the magnetosphere allows the propagation of (WKB) travelling waves. The ionosphere, however, is pervious only to waves of high enough frequencies (that is in excess of 1 Hz). Deift (1971) has approximated the variation of Alfvén velocity in the ionosphere by power laws.

$$V_A(x) = V_A(x_o)\left(\frac{x}{x_o}\right)^m \tag{5.31}$$

where x_o is the height of the top of the ionosphere above the cloud level, and $V_A(x_o)$ is the Alfvén speed at thav level. He has investigated three cases, for $m = 1$, $m = 2/3$, $m = 2$. He derived a transmission coefficient for the energy flux defined as

$$T = F_i / F_{ion} \tag{5.32}$$

where F_i is the energy flux transmitted into the ionosphere and F_{ion} the energy flux incident on the top of the ionosphere. In figure (38) the variation of V_A as a function of height above the cloud level according to the model developed in chapter 3 is shown. Also included are the model variations of V_A for different

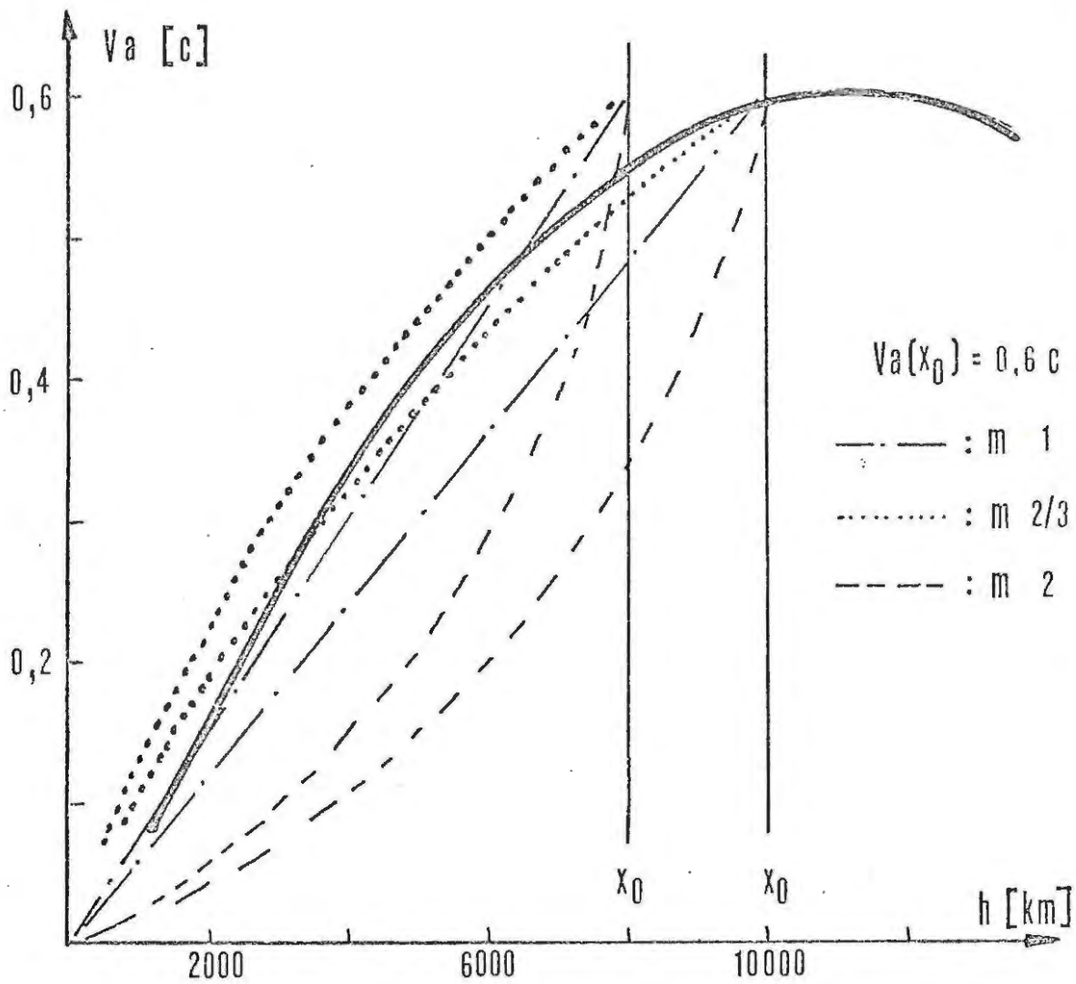

Figure 38: Comparison of the variation of the Alfvén velocity in the model ionosphere with various power law variations (assuming x_o either to be 8 000 km or 10 000 km).

m. It is seen that the best agreement between a power law and the actual variation is obtained for m = 2/3.

The transmission coefficients (5.32) are functions of frequency and are given by

(5.33) $T = 1 - \omega + (\omega^2 - 1)^{1/2} \quad \omega > 1$
$T = 0 \quad \omega < 1$ for m = 1

(5.34) $T = \frac{9\omega^4}{4 + 4\omega^2 + 9\omega^4}$ for m = 2/3

(5.35) $T = \frac{\omega^2}{1 + \omega^2}$ for m = 2

where $\omega = \frac{2\pi f 2x_0}{V_A(x_0)}$ is a normalised frequency with f the real frequency of the waves.

It is seen from (5.33) that for the variation of V_A with m = 1 there is a (normalised) cut-off frequency $\omega = 1$. Waves with frequencies f for which $\omega < 1$, will be totally reflected and no energy will be transmitted into the ionosphere.

Combining (5.29) and one of (5.33) to (5.35) allows for the calculation of power transmitted into the ionosphere as a function of sub-Io longitude. The variation of frequency f of the waves as a function of sub-Io longitude is taken from figure (36a). For the calculations below f_{220} was taken as 1,5 Hz. Figure (39) is based on the following magnetic field parameters (see section 2.2.2).

$\delta = 0.15\ R_J$
$\lambda_o = 235^\circ$
$B_E = 10\ G$
$S = -0.20\ R_J$
$\alpha = 10^\circ$
$\lambda_T = 200^\circ$

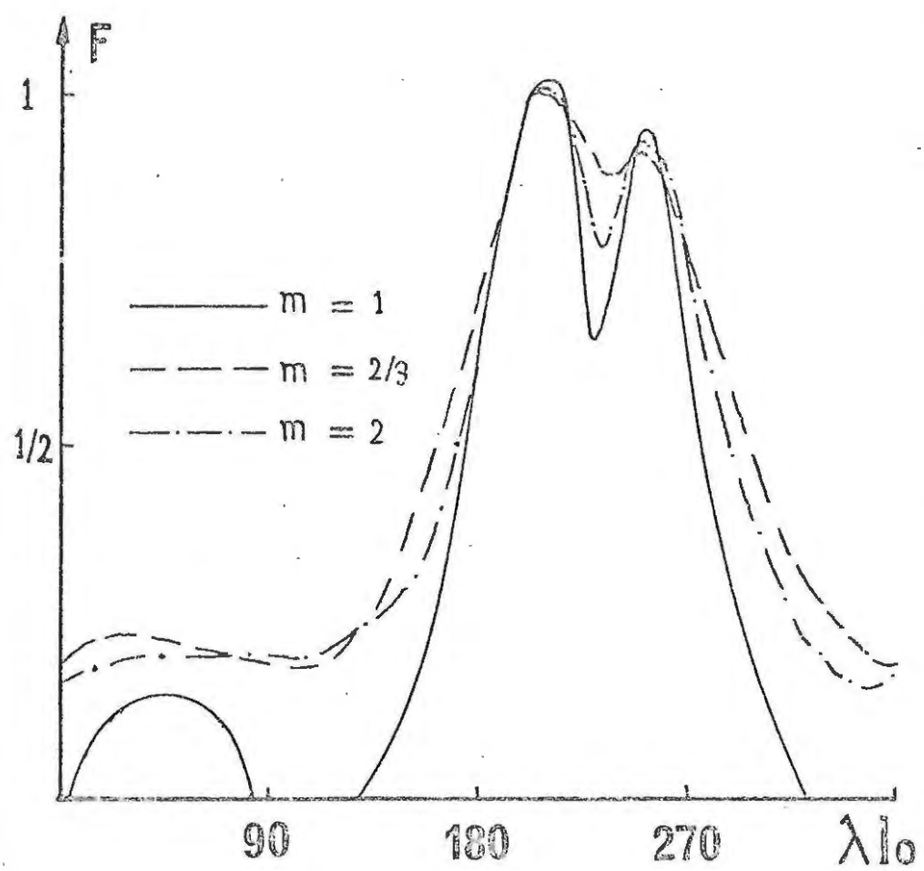

Figure 39: Normalized Alfvén wave flux transmitted into the ionosphere.

It is obvious that the energy flux transmitted into the ionosphere shows two distinct peaks for all variations of V_A. Figure (39) includes the lead angle ϕ which was defined in section 3.4. The x-axis of figure (39) indicates the longitude above which Io is, when the hmd waves propagate in the dense parts of the ionosphere. Thus the longitude at which the hmd disturbance reaches the ionosphere is $\lambda_{Io}-\phi$, (it should be noted that ϕ is a function of λ_{Io}). In the next chapter we will relate these results to the observed "sources" of the Io controlled radiation.

6. The Relation Between the Model and Observations

In chapter 4 it was shown, how Io interacts with Jupiter's magnetosphere. Io emits hmd wave pulses, the characteristic frequency of which varies as Io orbits the planet in a way shown in figure (36). These waves do not strictly propagate along the magnetic field but spread over an area, which depends on their frequency. The energy flux contained in these waves incident on the top of the ionosphere at a height h_o above the cloud level, is then partly transmitted into the ionosphere and partly reflected. The energy flux which is transmitted into the dense parts of the ionosphere varies as Io moves around Jupiter. The variation shows two distinct peaks when the sub-Io longitude is close to the longitude to which the northern end of the magnetic dipole is tilted (λ_T).

In this chapter we will relate the energy flux of the hmd waves to the activity of decametric radiation observed on earth. We will, however, not attempt a detailed description of the actual generation mechanism of the decametric radiation. It has been suggested by various authors, that the plasma distribution function in the front of a large amplitude Alfvén wave pulse will be considerably different from a Maxwellian one. One would hence expect the existence of microinstabilities in the steep front of such waves which may be able to amplify EM radiation either at the plasma frequency ($\omega_p/2\pi$) or gyrofrequency ($\Omega/2\pi$) or harmonics and combinations (e.g. upper hybrid) thereof. The following is meant as an indication of the type of instability that could be expected in the front of a propagating hmd wave.

In the frame of reference moving with the wave the (cold) background plasma is incident on the wave-front with the Alfvén velocity. An individual particle moves under the influence of the $q(\vec{V} \times \vec{B})$ force. It describes a semi circular path, as indicated in figure (40a), and will hence be reflected. Incident protons have much larger momentum than the electrons and will penetrate into the hmd wave much further than the electrons. The resulting charge separation produces an electric field which has the effect of slowing down the protons and accelerating the electrons. Then both particles penetrate to almost the same depth into the hmd wave as indicated in figure (40b). The electrons gain energy in this process nearly equal to that of the protons outside the hmd pulse. Thus the electrons will move with considerable velocity through the almost stationary protons (as seen in the frame of the moving hmd wave). The velocity of the electrons may even attain relativistic values. The process outlined is very similar to what is supposed to happen in the geomagnetic boundary of the magnetosphere (Piddington, 1969). One would therefore expect the plasma in the hmd front to consist of slowly moving protons and fast electrons. Assume the magnetic field in the wave to be uniform. $\vec{B} = (B_o, b_y, b_z)$, where b is the amplitude of the wave and $B_o \gg b$ the magnetic field produced by currents in Jupiter. Tverskoi (1962) and Trakhtengerts (1965) have investigated the motion of electrons and ions in the front of such a hmd wave propagating along the undisturbed magnetic field $\vec{B} = (B_o, 0,0)$. Both show that the electrons acquire velocities of the order of $V \approx V_A \frac{b}{B_o} (\frac{mi}{me})^{\frac{1}{2}}$ in the frame moving with the wave, $(b = (b_y^2 + b_z^2)^{\frac{1}{2}})$. Their treatment is valid for mildly relativistic Alfvén velocities $(V_A^2 < C^2)$ and for wave

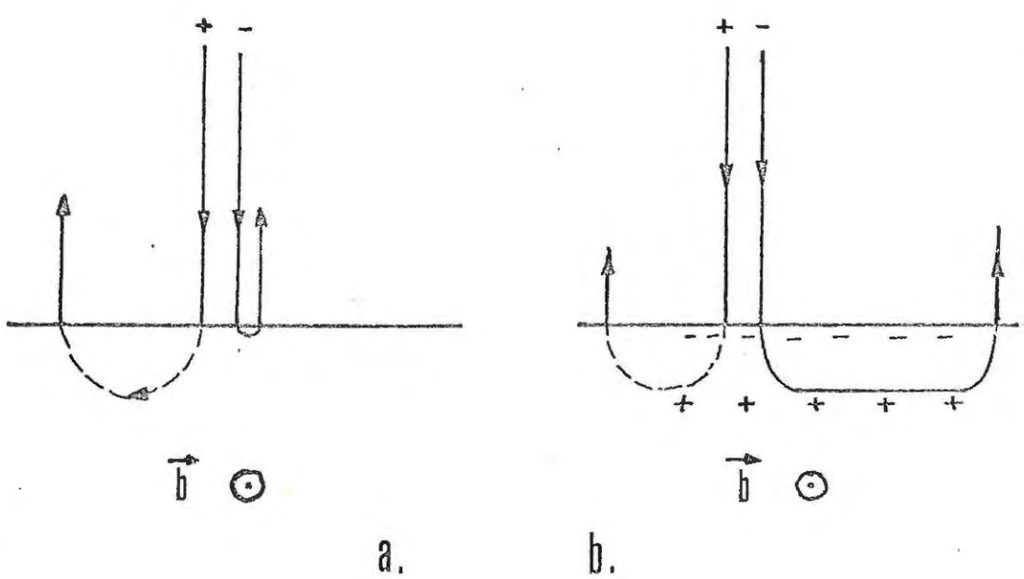

Figure 40: Path of electrons and protons in the front of the Alfvén wave pulse.

pulses of thickness smaller than the mean free path of the electrons. Both conditions are met at the time the Alfvén waves impinge onto the top of the Jovian ionosphere ($V_A^2 \leq 0.3\ c^2$). The waves will also have steepened their fronts on their way through the magnetosphere. Montgomery (1958), showed that the front of a plane-polarised Alfvén wave will become infintely steep in a time $t_s \simeq 2B_o(1+b^2/B_o^2)^{3/4}(\mu_o\rho)^{1/2}/(b(db/dx)_o)$ where $\frac{db}{dx}$ is evaluated at t = o. At Io $b \simeq (2n\ V_s/V_A)\ B_o$ (see chapter 4). If b/B_o were constant along the path of the wave as well as B_o and ρ, t_s would be ($db/dx \approx b/R_{Io}$) $t_s \geq 9 \times 10^{-3}\ V_A/V_s$ [s] which is always less than 6 secs, the travel time of the waves from Io to the ionosphere. Thus Alfvén waves impinging onto Jupiter's ionosphere will have developed steep fronts. Far from the front of the advancing waves the ionospheric plasma will be relatively undisturbed (it consists of the background plasma plus particles reflected from the wave front.) Inside the front one would find energetic electrons, moving perpendicular to the undisturbed field B_o, and slow protons. Trakhtengerts (1965) points out that electrostatic oscillation at the plasma frequency should develop. This is an instability very much of the same type as described in section 3.3. Goldreich and Lyden-Bell (1969) have pointed out that a beam of electrons whose momentum distribution is a function in both $P_{\parallel}$ and $P_{\perp}$ is unstable to waves at the electron gyrofrequency. The coherent cyclotron instability has a linear growth rate

$$(6.1) \qquad \omega_i = (3)^{1/2}\frac{\Omega}{4}\left(\frac{\omega_{po}}{\Omega}\frac{p_\perp}{mc}\sin\Theta\right)^{2/3}(1+\cos^2\Theta)^{1/3}$$

where Θ is the angle between the propagation vector of the unstable (extraordinary mode) wave and B_o.

It was shown above that

$$(6.2) \qquad p_\perp = m_e v_\perp \simeq m_e V_A \left(\frac{b}{B}\right)\left(\frac{m_i}{m_e}\right)^{1/2}$$

The amplitude b of the wave is

$$(6.3) \qquad b = b_{Io} \left(\frac{\rho}{\rho_{Io}}\right)^{1/4} \left(\frac{B_{Io}}{B}\right)^{1/2}$$

The subscript "Io" indicates that the subscripted quantity has to be evaluated in the vicinity of Io, where the hmd waves are generated. Inserting (6.2) and (6.3) into (6.1) it can be seen that along a magnetic field line

$$(6.4) \qquad \omega_i \propto B^{2/3} N^{1/6}.$$

Along this field line the growth rate of the unstable extraordinary wave will increase when the Alfvén wave moves into regions of increasing magnetic field and density; i.e. when it moves into the dense parts of the ionosphere. The emission of the electromagnetic radiation does of course decrease the amplitude b of the wave and hence the growth rate. The exact variation of the growth along a field line can only be determined by a nonlinear extension of the theory of the coherent cyclotron instability. This would, however, require an exact knowledge of the distribution of electrons in the hmd wave front. In order for the instability to lead to a sufficiently rapid growth of the cyclotron radiation so that it can be detected on earth ω_i should exceed a certain critical limit, say ω_i'. Only when $\omega_i \geq \omega_i'$, will an observer on earth detect decametric radiation.

An order of magnitude calculation shows that the absorption coefficient $k = \omega_i/c$ is typically of the order

$k = 7 \times 10^{-6}$ cm^{-1}. The total amplification over a length L $\simeq$ 100 km is then $e^{kL} \simeq e^{70}$. Of course, this figure, based on a very crude model, neglecting non-linearities, inhomogenities of ρ and B, can only indicate that there is an amplification which could explain the high intensity of the observed decametric radiation. In this thesis, we will be satisfied by noting that an instability may exist in the front of the hmd waves which may lead to a fairly rapid growth of extraordinary electromagnetic waves.

The following results are important:

1. The growth rate is proportional to the 6th root of the plasma density, and also to $B^{2/3}$.

2. In the frame of reference moving with the Alfvén wave the growth is restricted to directions of propagation very nearly perpendicular to B_o. (see Goldreich and Lynden-Bell, 1969).

3. The amplified wave is in the extra-ordinary mode. The frequency of the amplified wave as seen in a frame moving with the Alfvén wave is the (relativistic) electron gyrofrequency.

4. The amplification is proportional to the magnetic field amplitude of the Alfvén wave (because $v_\perp \propto b$).

From these we can deduce a number of important consequences.

In chapter 3 it was shown that the amplitude of the Alfvén wave generated at Io is $b = B_o \frac{2n V_s}{V_A}$. It was also shown that $n \propto V_A^{\frac{1}{2}}$, where V_A is the Alfvén velocity at Io's orbit. Thus $b \propto B/V_A^{\frac{1}{2}}$. Also: at a perpendicular level in the ionosphere where ρ has a certain value ρ_o, the amplitude b of the Alfvén wave depends on the ratio $(\rho_o/\rho_{Io})^{\frac{1}{4}}$. As ρ_{Io} varies with

λ_{Io} (see figure (26a)), whereas B_{Io} remains almost constant, the amplitude b of the Alfvén wave at a particular level in the ionosphere (that is where $\rho = \rho_o$ = const) should be independent of λ_{Io} ($V_A^{\frac{1}{2}} \propto \rho^{-1/4}$) if the energy flux and hence b were not reduced by:

(a) the spreading of the Alfvén wave due to Hall-current and

(b) by partial reflection at the top of the ionosphere. Thus the growth rate of the electromagnetic wave should by $e^{\alpha} = e^{kL}$, where $k = \frac{\text{const } T^{2/3}}{L^{4/3}} B^{2/3}$ thus:

$$\alpha = \text{const. } T^{2/3} B^{2/3} L^{-1/3} \qquad (6.5)$$

at a particular level

where ρ is ρ_o T,L, and B vary as a function of λ_{Io}. (B varies if the magnetic dipole is displaced from the centre of the planet.) The transmission coefficient T is given by one of the formulae (5.33) to (5.35). The (average) diameter L of the region over which the Alfvén disturbance is spread is given by (5.21). Figure (41a) shows the variation of α as a function of λ_{Io} for the magnetic dipole displacement indicated in the figure. The three curves shown are based on the three different forms of T. This figure shows the variation of the logarithmic decrement of the decametric radiation for waves generated in the northern hemisphere of the planet. (T and L were calculated for Alfvén waves travelling to the northern hemisphere) Figure (41b) shows the variation of α for decametric radiation generated in the southern hemisphere. Both figures indicate that there should be a large variation of Io controlled decametric radiation intensity as Io orbits around Jupiter. The two main peaks of α around

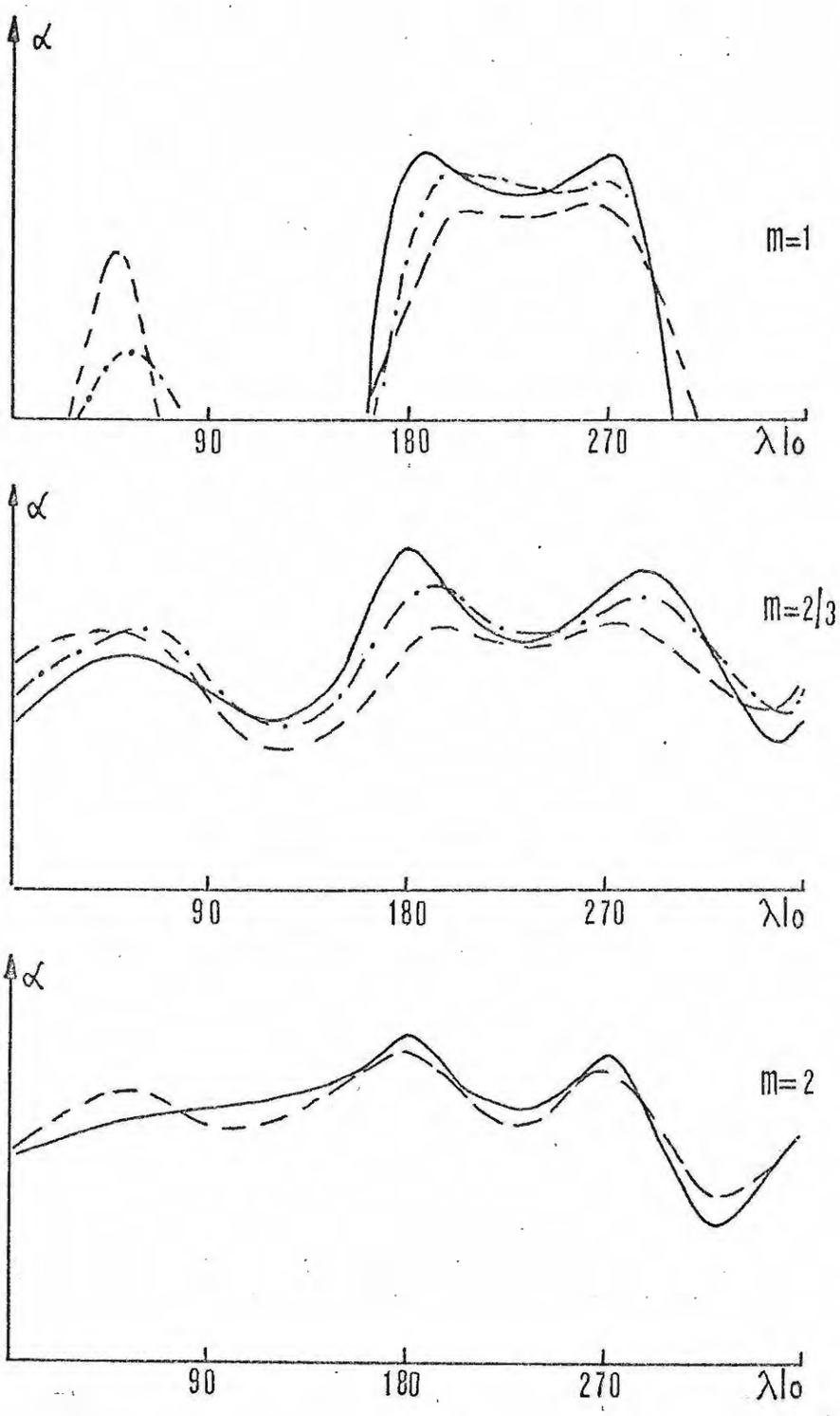

Figure 41: a) Variation of α as a function of λ_{Io}. x_o = 8 000 km. Waves go to northern hemisphere. $\lambda_o = 235^\circ$, $\lambda_T = 210^\circ$, $\alpha = 10^\circ$.

——— $\delta = 0{,}15\ R_J$, $s = -0{,}20\ R_J$

—·— $\delta = 0{,}10\ R_J$, $s = -0{,}10\ R_J$

— — — $\delta = 0{,}10\ R_J$, $s = -0{,}05\ R_J$

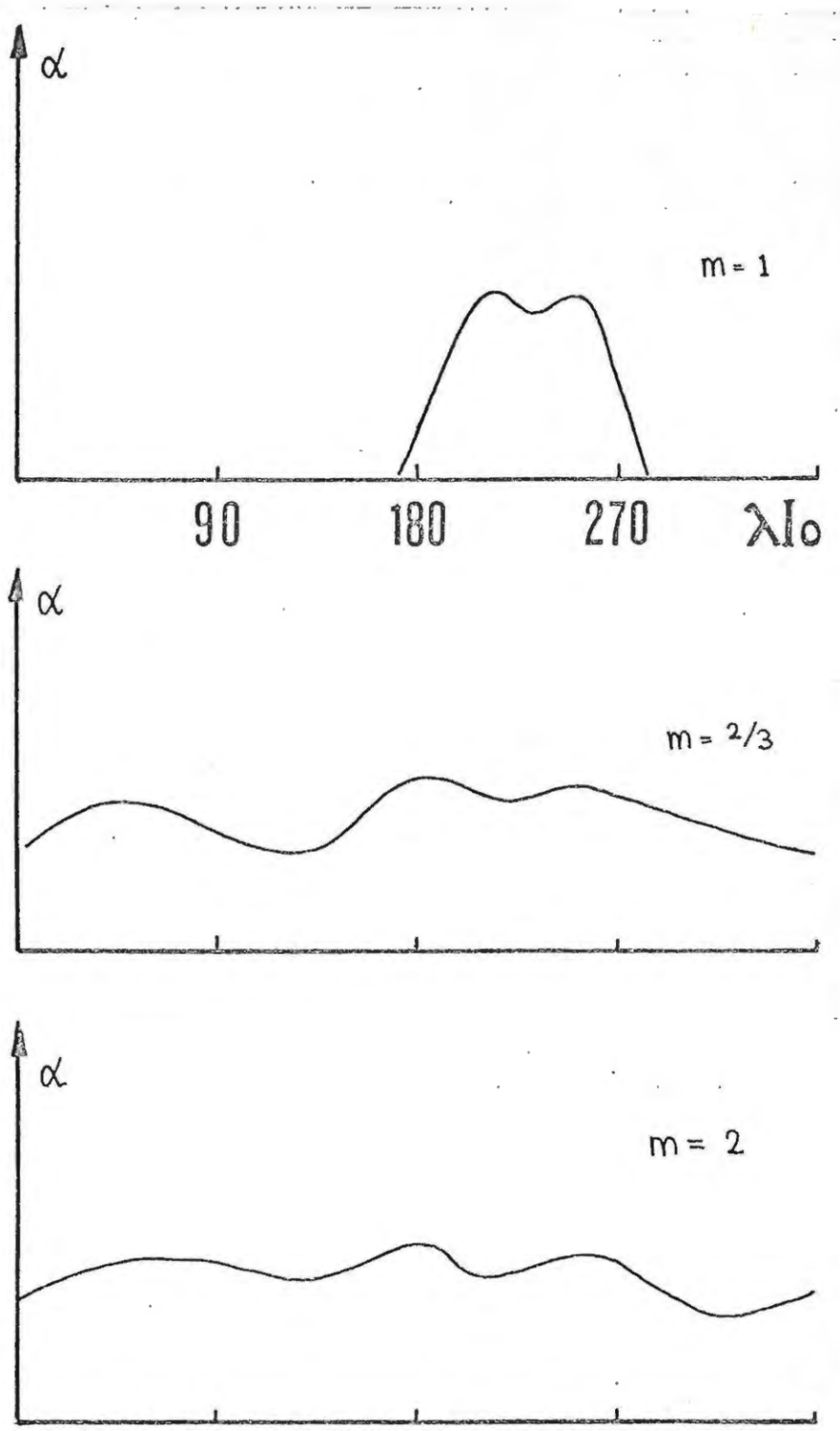

Figure 41: b) Variation of α as a function of λ Io. X_o = 8 000 km. Waves go to southern hemisphere. For explanation of curves see figure 41a.

$\lambda_{Io} \simeq 210^{o}$ are prominent. It must be noted that the lead angle ϕ has been taken into account. When Io is above λIo the radiation is actuall generated at a longitude λIo - ϕ,B and T are evaluated at this longitude, whereas the value of the Alfvén wave frequency was calculated at a position corresponding to λIo. Figures (42) and (43) show the variation of α for a different thickness of the ionosphere. (The thickness of the ionosphere determines T.) When Io is above the morning side of Jupiter, i.e. when radiation is received from the B1 or B2 source, the Alfvén waves impinge onto a cold and hence thin ionosphere. When Io triggers the A or C source the Alfvén waves impinge onto a warm afternoon, and hence thick, ionosphere. If we relate the peaks in the α vs λIo curves to the "sources", we expect the B1 and B2 sources to be closer together than the A and C sources. This is indeed observed (see section 2.2.1). Figure (44) shows the variation of the number of Io controlled storms as a function of sub-Io longitude (λIo). The two peaks around λIo = 210^{o} are clearly visible.

6.1 Sources

The relation between these figures and the four Io controlled "sources" is now easily established. The amplification of the E.M. radiation considered above was treated in a frame moving with the Alfvén velocity. In this frame the radiation propagates predominantly at right angles to the undisturbed magnetic field. In Jupiter's frame the radiation is confined to a conical sheet above the magnetic field direction with opening angle $\gamma = \frac{\pi}{2} - \frac{V_A}{c}$, (see also Goldreich and Lynden-Bell, 1969). The radiation is beamed towards the planet. It is reflected at levels where the upper

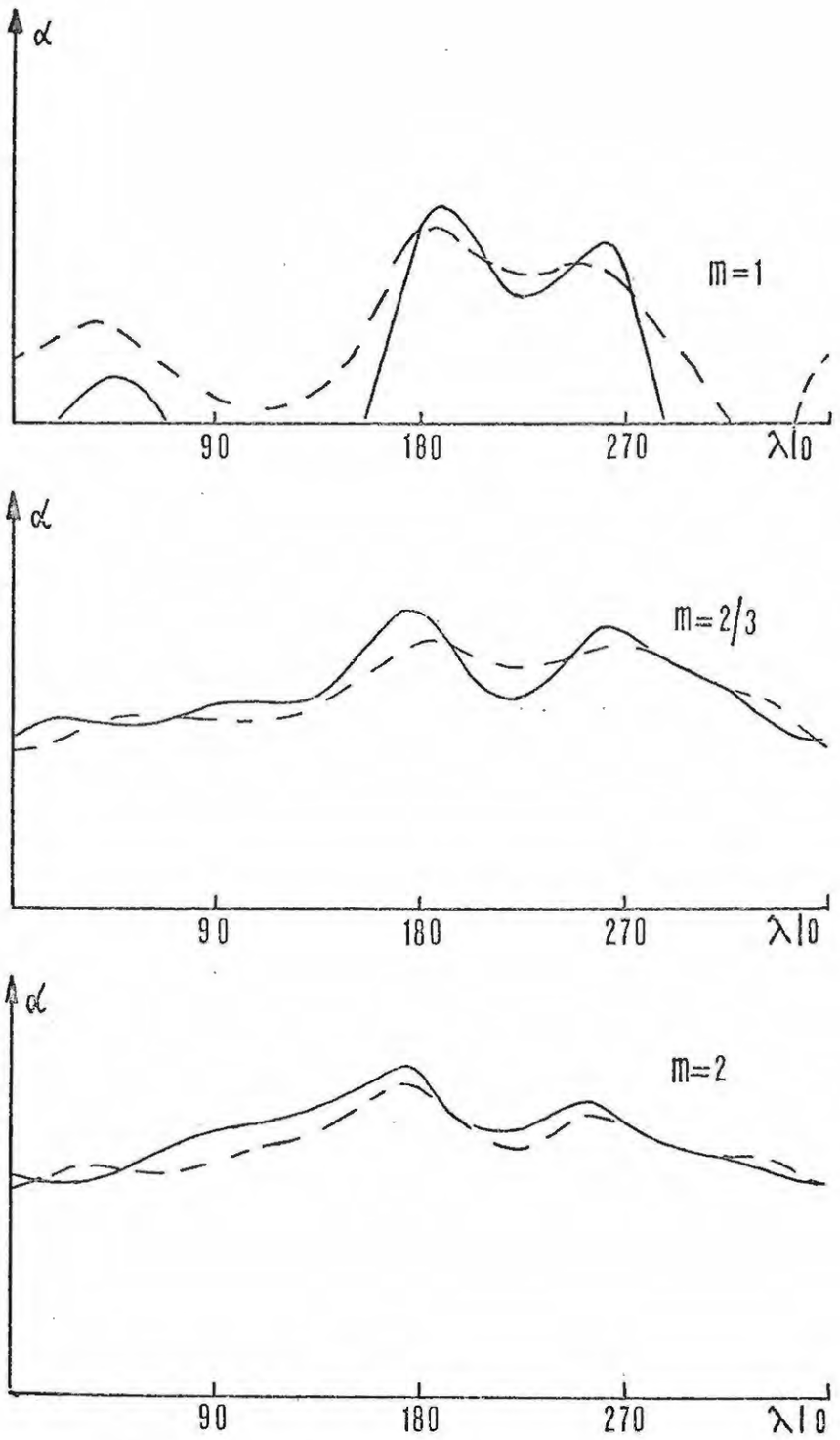

Figure 42: Variation of α as a function of λ Io. X_o = 10 000 km. For explanation of curves see figure 41a.

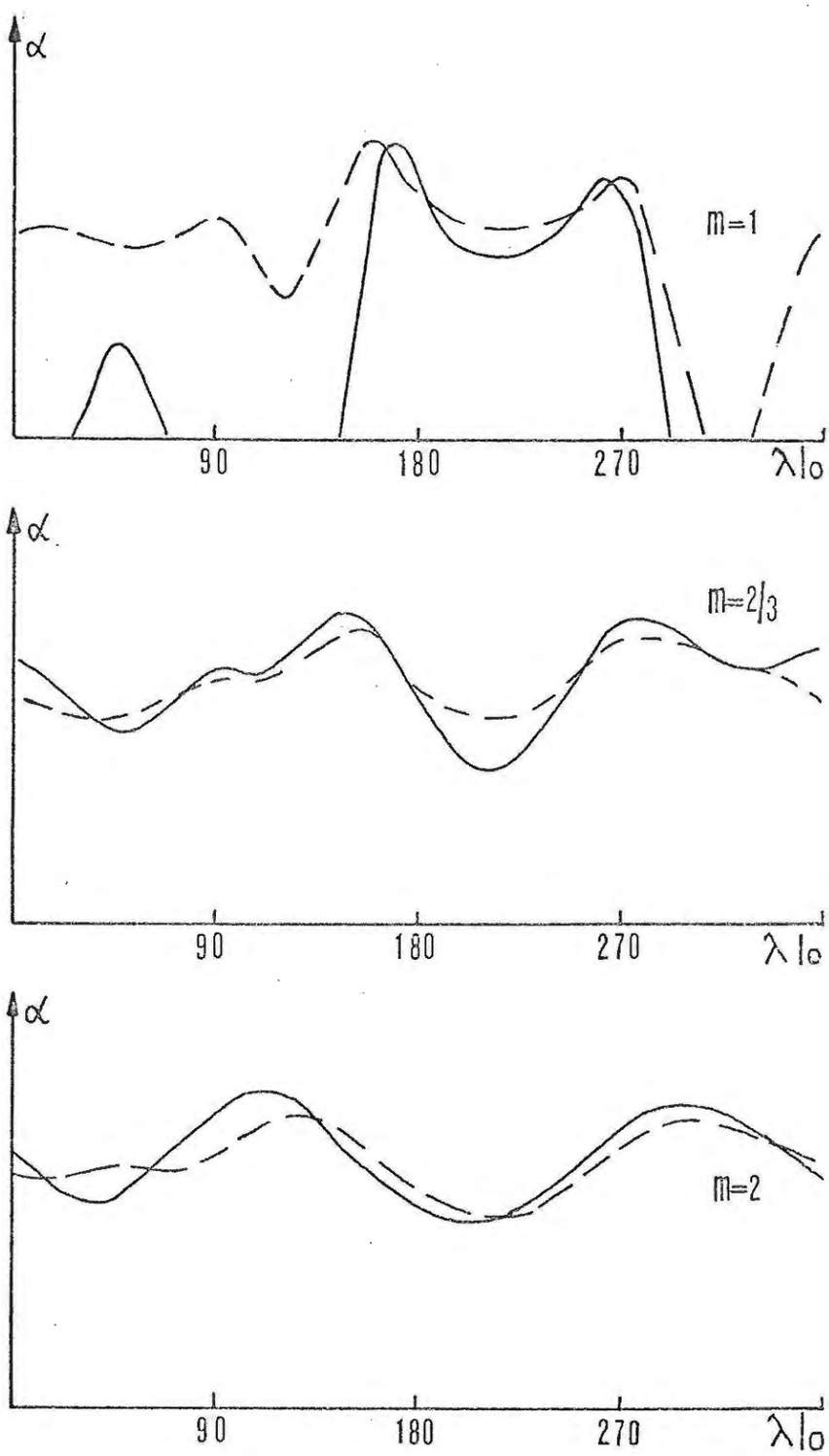

Figure 43: Variation of α as a function of λIo. X_o = 12 000 km. For explanation of curves see figure 41a.

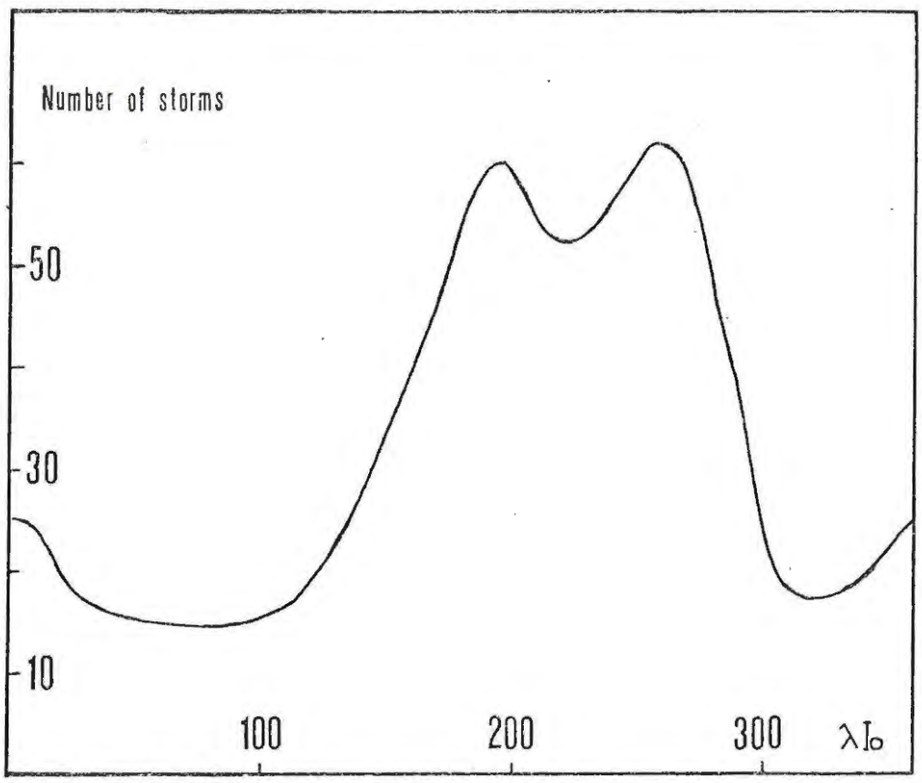

Figure 44: Number of decametric storms (all frequencies) as a function of λ Io.

hybrid frequency $\omega_H = \frac{\Omega}{2} + (\Omega^2/4 + \omega_{po}^2)^{1/2}$ is the same as the Doppler shifted frequency $\omega = \Omega(1 + V_A^2/c^2)$. Since $\frac{\omega_{po}^2}{\Omega^2} = \frac{c^2}{V_A^2}\frac{m_e}{m_i}$, the condition for the escape of the Doppler-shifted radiation ($\omega > \omega_H$) is $V_A > 3 \times 10^{-2} c$. This is true everywhere in the ionosphere except very near the level where the electron density has a maximum.

After reflection the decametric radiation propagates away from the planet in a conical sheet with the same opening angle γ. (There may also be some refraction of the decametric radiation when it propagates away from the planet. An evaluation of this effect would require a detailed ray tracing through the Jovian ionosphere. The results would only be as "good" as the model of the ionosphere.) These ideas are exactly the same as those incorporated by Goldreich and Lynden-Bell (1969) in their model of the Io controlled radiation. The essentail difference between their model and the present one is the following. In their model electrons are accelerated at Io whereas here the electrons are accelerated in the Jovian ionosphere. The actual amplification mechanism of the observed decametric radiation is the same, namely the coherent cyclotron instability. In both models the radiation is beamed into a conical sheet. The sheet, shown in figure (45), intersects the ecliptic plane along two lines making an angle 2μ, which is related to the angle γ by

$$\tan\mu = (\tan^2\gamma \cos^2\tau - \sin^2\tau)^{1/2} \qquad (6.6)$$

where the angle τ is the angle between the axis of the cone (the magnetic field direction at the point of emission) and the ecliptic (essentially the Jovian equatorial plane). τ is related to the colatitude Θ by

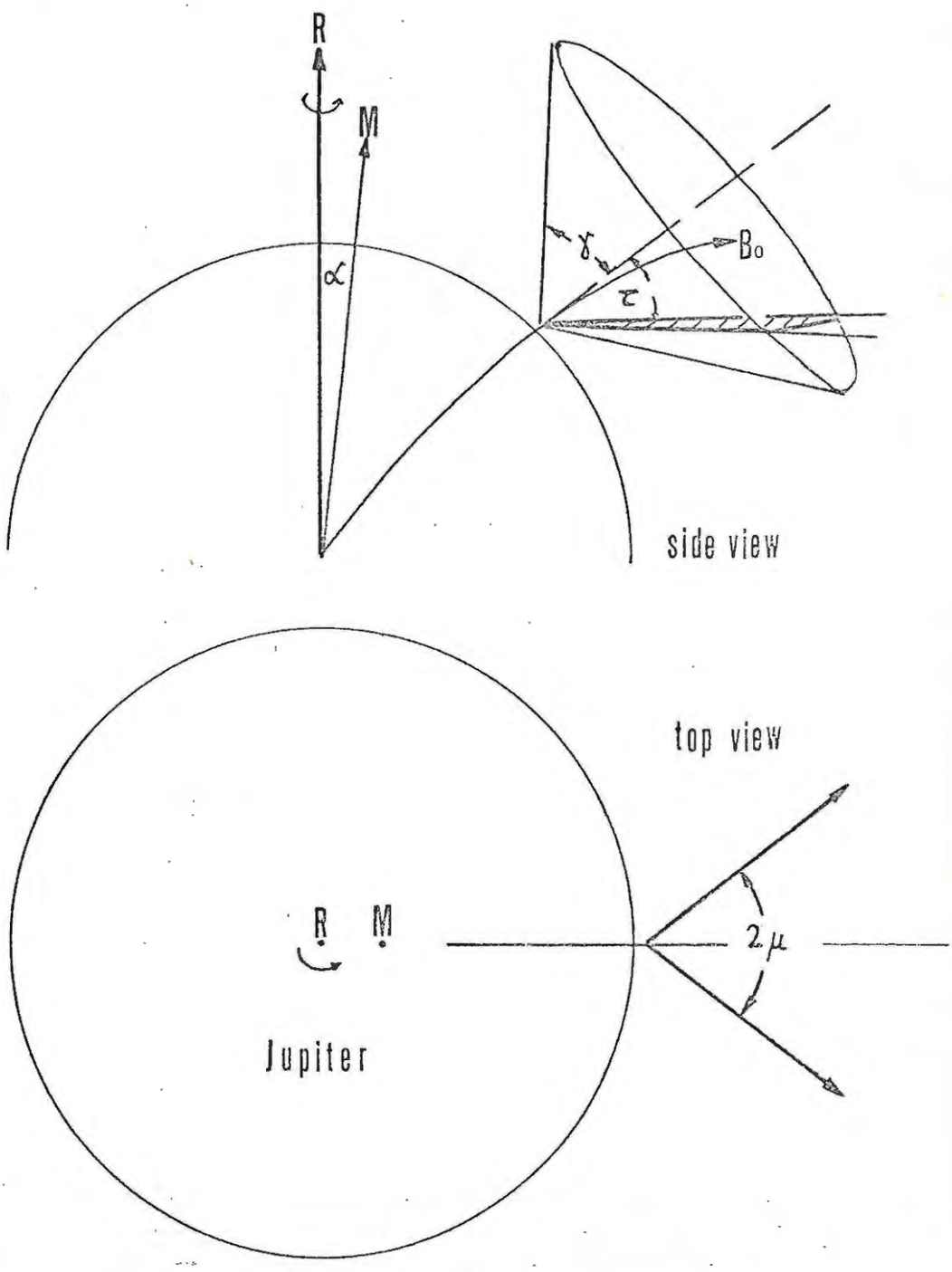

Figure 45: Emission geometry. See text for explanation.

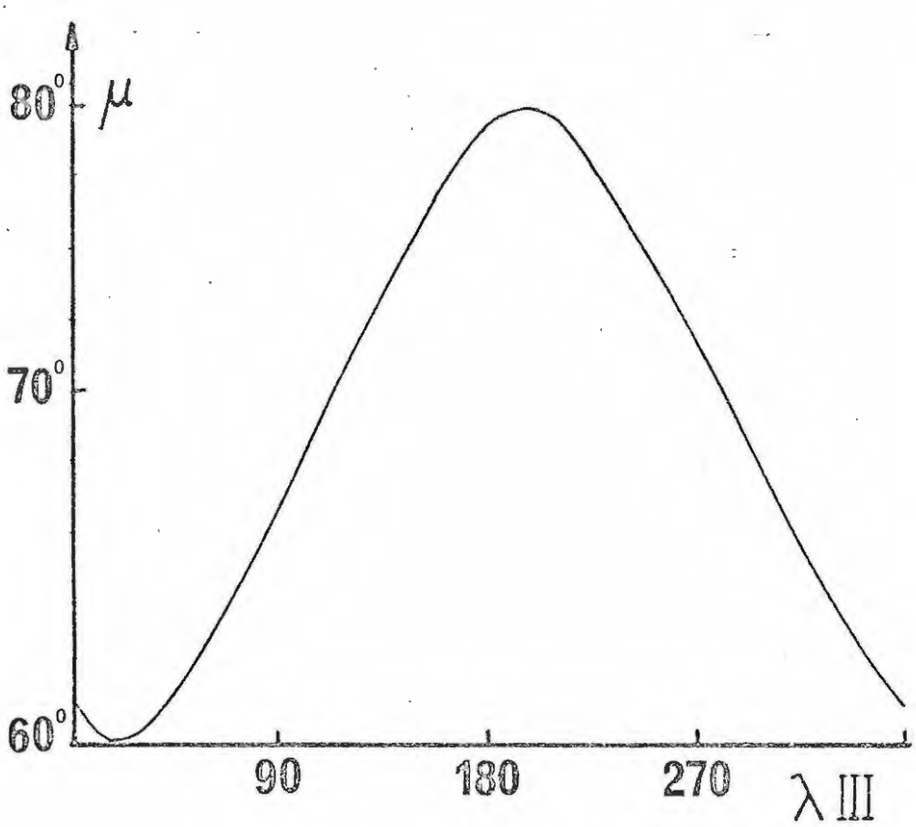

Figure 46: μ as a function of Jovian longitude (λIII) for radiation generated in the northern hemisphere.

(6.7) $\cos \tau = 3 \sin\Theta \cos\Theta / (1 + 3\cos^2\Theta)^{1/2}$

In the ionosphere V_A is typically $V_A = 0.1\ c \ldots 0.5\ c$. In the northern hemisphere $\Theta \geq \Theta_i \simeq 24^\circ$. For $V_A = 0.3\ c$, $\gamma = 75^\circ$ this gives $\mu \gtrsim 69^\circ$. Since the magnetic dipole is tilted by $\alpha \simeq 10^\circ$, μ varies between 78° and 60°. Figure (46) shows the variation of μ as a function of Jovian longitude, assuming that the dipole is tilted towards 210° λ III.

The radiation is beamed towards the earth if Io is either $\mu + \phi$ or $\mu - \phi$ on either side of CML. ϕ is the lead angle which varies as a function of λ Io, (see section 4.6). Thus we can immediately calculate the position at which Io lies relative to earth (i.e. its angular deviation from SGC : β) when radiation is received on earth as a function of λ Io. The result is shown in figure (47). There are two regions of Io's position at which radiation can be received on earth. Figures (41-43) show that the decametric radiation will be generated with large amplitude in certain λ Io ranges. These are marked in figure (47) by shading. I have assumed that the thickness of the ionosphere is somewhat larger in the afternoon side of Jupiter than in the morning. This is to be expected because the plasma temperature Tp, which determines the thickness of the ionosphere, should be higher in the afternoon. Note that figure (47) is relevant for waves generated in the northern hemisphere. Figure (48) shows the same for waves generated in the southern hemisphere. The CML value given by

(6.8) $CML = \lambda Io - (180 - \beta) = \phi \pm \mu + 180$

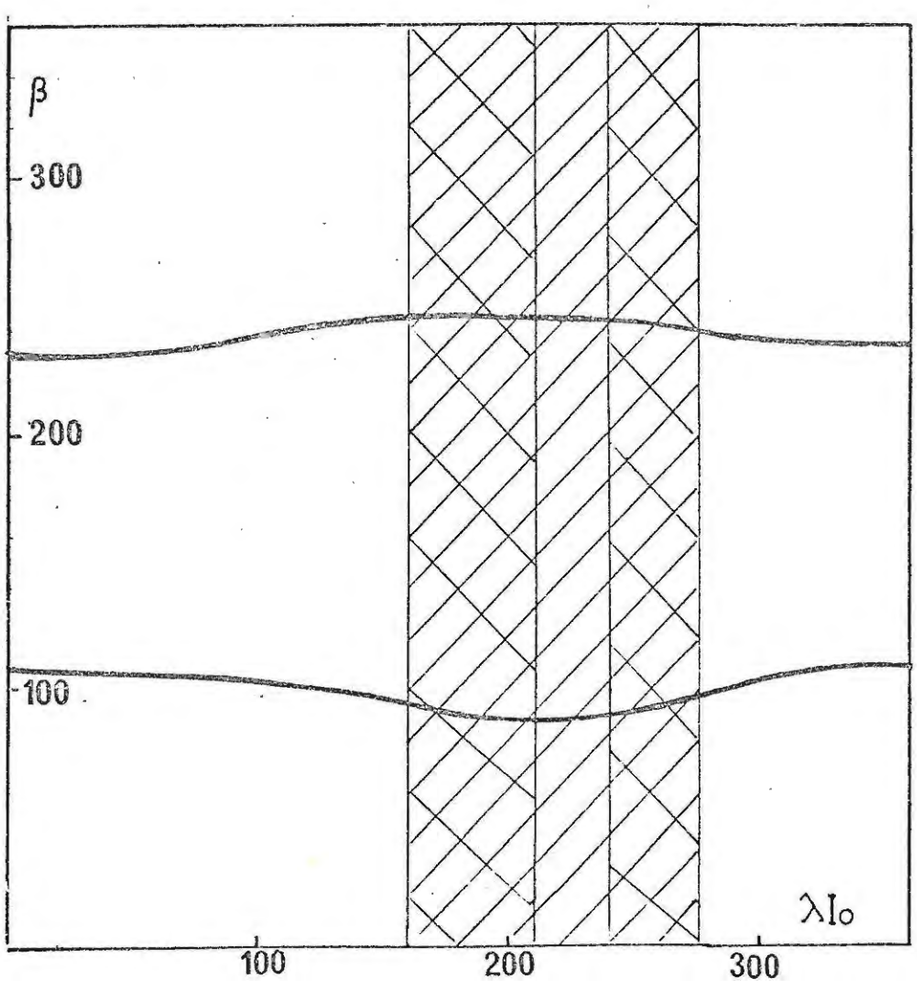

Figure 47: β as a function of λI_o for radiation emitted in the northern hemisphere. The shaded areas correspond to regions of large α.

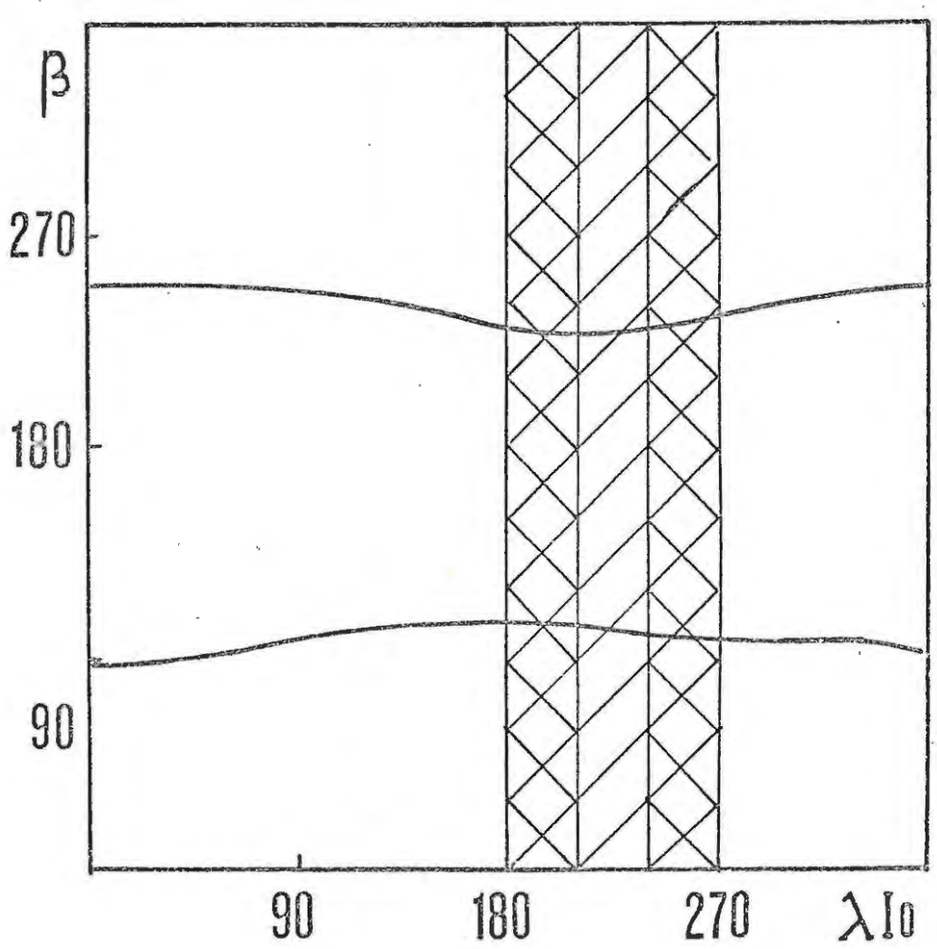

Figure 48: β as a function of λ Io for radiation emitted in the southern hemisphere. The shaded areas correspond to regions of large α.

where the + stands for the B_1 and B_2 sources and the - for the A and C sources.

We can construct a plot of lines of constant receiving probability like the one shown in figure (5) if the probability is assumed to be proportional to α (see formula (6.1)). Figure (49) includes radiation both from the northern and southern hemisphere. The agreement between figure (49) and figure (5) is very good.

6.2 The Maximum Frequency Variation

The control of Io over the maximum observed frequency of the decametric radiation can be explained quite easily in terms of the present model. In section 2.2.2 it was shown that the variation of f_M can be explained in terms of variation of height above Jupiter's cloud level at which f_M is emitted (see figure 8).

The discussion in the last sections dealt with average conditions. Only Alfvén waves which have large enough frequencies can enter the dense parts of the ionosphere. But, independently of the frequency, all Alfvén waves will propagate until they reach the top of the ionosphere. Waves which are transmitted lose energy in the ionosphere. But sometimes the power contained in these waves may be so large that they can travel through the ionosphere and still retain enough energy to trigger the generation of decametric radiation at the bottom of the ionosphere. Hence the Alfvén waves are either reflected at the top of the ionosphere or they may go down to the bottom (if they are generated at Io with large enough power or if they do not lose too much energy on their path through the ionosphere). The transmission coefficient T determines

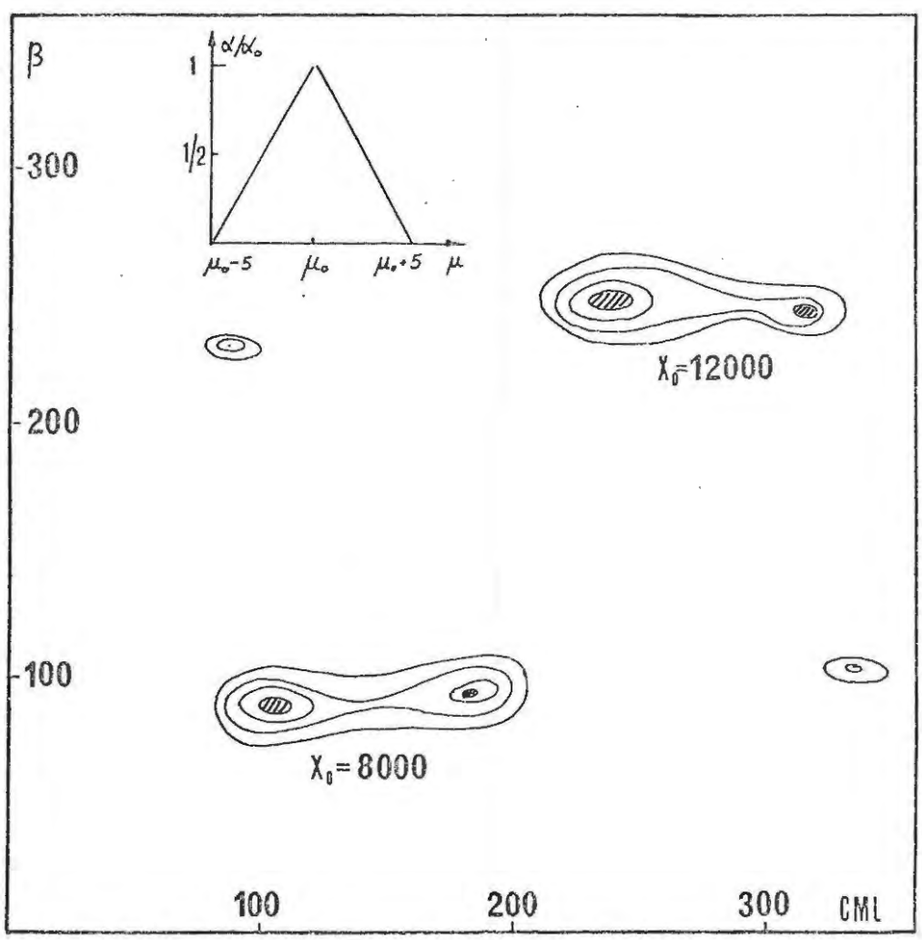

Figure 49: Contours of equal α. Radiation is assumed to be generated in the northern hemisphere alone.

whether they are reflected or not. When T is small the waves will be mostly reflected at the height h_o and hardly any decametric radiation will be received from within the ionosphere. If T is large, radiation will be received from within the ionosphere and perhaps one or two times per apparition also from the bottom of the ionosphere.

Figure (8) shows the variation of height above Jupiter's cloud level (h) where the maximum frequency is generated. In terms of the present model a large height should correspond to a small T and a small height to a large T. Figure (50) shows the variation of T and h superimposed. The expected anticorrelation between h and T is indeed shown by this figure. Also: the maximum height of h, h_m = 12 000 km, is in very good agreement with the thickness of the ionosphere (h_o) described in chapter 3.

6.3 Polarization

The present model predicts the radiation to be in the extraordinary mode. (This conclusion has also been reached by many other authors.) Radiation from the northern hemisphere should be more frequent than from the southern. (Compare figures (41a) and (41b).) The present model does predict, however, that for certain sub-Io longitudes the radiation should contain radiation from both hemispheres (not necessarily at the same frequency). The ratio of the two should be related to a polarization ratio. Figure (51) shows the predicted variation of R.H. to L.H. polarization as a function of λ Io, assuming that the radiation from the northern hemisphere is right hand (R.H.) polarized and the radiation from the southern hemisphere to be polarized

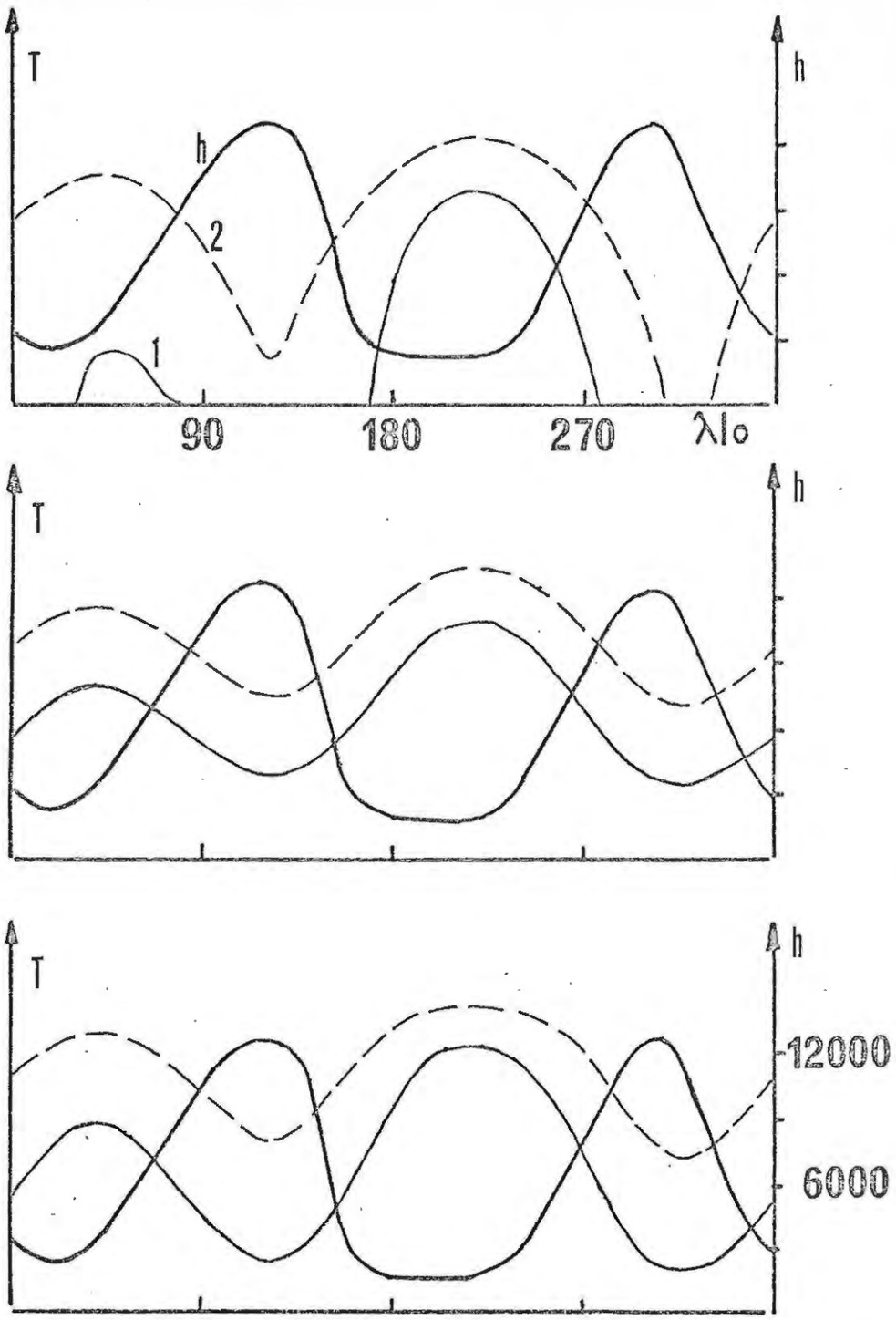

Figure 50: Variation of T and h as a function of λ Io. The variation of h is taken from figure 8 (curve 4). The variations of T are for

1: $\delta = 0{,}10\ R_J$, $s = -0{,}05\ R_J$, $\lambda_o = 235$, $\lambda_T = 210$, $\alpha = 10$.

2: $\delta = 0{,}15\ R_J$, $s = -0{,}20\ R_J$, $\lambda_o = 235$, $\lambda_T = 210$, $\alpha = 10$.

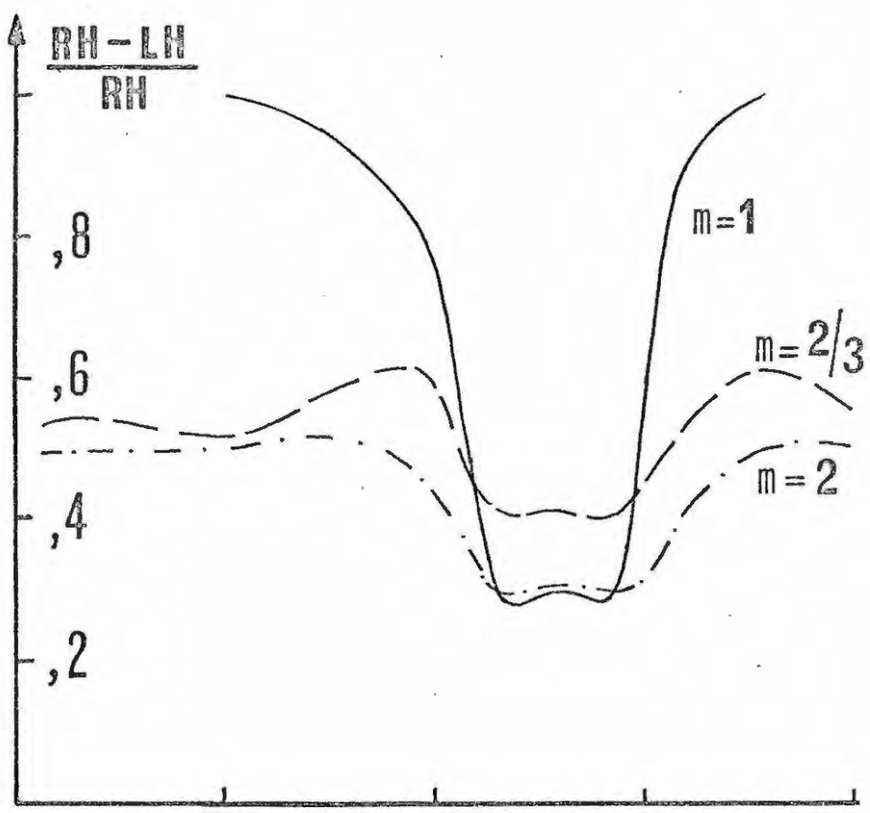

Figure 51: The predicted ratio of right hand polarisation (RH) to left hand polarization (LH) as a function of Io.

in the opposite sense. To the present author's knowledge no investigation of the polarization as a function of λ Io has been published.

6.4 The Time Structure of the Storms

In the last sections it was shown how the decametric radiation may be generated in the steep front of the Alfvén waves propagating through the ionosphere. Radiation of sufficient amplitude to be detected on earth will be emitted when the amplification controlling quantity α is large enough. α increases with increasing magnetic field strength and plasma density. Only those Alfvén waves which reach the denser parts of the ionosphere could trigger intense decametric radiation. The frequency at which the radio waves are emitted is the Doppler shifted gyrofrequency $f = f_e (1 + V_A^2/c^2)$. The fact that f depends on V_A is significant. In chapter 3 we have seen, that V_A varies with height in the ionosphere. Along a field line V_A decreases towards the planet. Thus, although $f_e = \frac{1}{2} \frac{e B}{m_e}$ increases towards the planet, the frequency of the radiation leaving Jupiter after reflection may actually decrease while the Alfvén wave moves towards the planet. The Alfvén waves moving towards the planet's surface emit EM radiation at a frequency the time variation of which can be written as

$$(6.9) \quad \frac{1}{f}\frac{df}{dt} = \frac{c^2}{c^2+V_A^2}\frac{1}{B}\frac{dB}{dt} + \frac{2V_A}{c^2+V_A^2}\frac{dV_A}{dt}$$

Now: $\frac{d}{dt} = V_A \frac{d}{dx}$ for the advancing hmd wave. (x is counted positive towards the planet.) Thus $dx = - dh$, where h is the height above the cloud levels. (6.5) is then rewritten as:

$$(6.10)\quad \frac{1}{f}\frac{df}{dt} = \frac{V_A}{V_A^2+c^2}\left(-\frac{1}{B}\frac{dB}{dh}(c^2+2V_A^2) + V_A^2\frac{1}{N}\frac{dN}{dh}\right)$$

where we have used the relation between V_A and plasma density N ($V_A = B\,(\mu_o\, N m_i)^{-\frac{1}{2}}$). Along a field line of a magnetic dipole field

$$\frac{1}{B}\frac{dB}{dh} \approx \frac{3}{h+R_J}$$

In the ionosphere N decreases nearly exponentially with height. Thus:

$$\frac{1}{N}\frac{dN}{dh} \approx -H$$

where H is a characteristic scale height (6.6) is then:

$$(6.11)\quad \frac{1}{f}\frac{df}{dt} \approx \frac{V_A}{V_A^2+c^2}\left(\frac{3(c^2+2V_A^2)}{h+R_J} - \frac{V_A^2}{H}\right)$$

The relative frequency drift rate ($\frac{1}{f}\frac{df}{dt}$) can be positive or negative, depending on whether $(h + R_J)$ is smaller or larger than $3H\,(1 + 2\,c^2/V_A^2)$. The Alfvén velocity at the top of the ionosphere is 0.5c. The frequency drift is thus negative since $3H\,(1 + 2\,c^2/V_A^2)$ is then always less than R_J. As the Alfvén waves travel downwards, the Alfvén speed decreases and the frequency drift becomes positive. The frequency of a decametric storm should thus exhibit first a negative and then a reversal to positive frequency drift. As the negative frequency drift should occur at height levels where the plasma density and magnetic field intensity are low, the amplification (α) may not be large there and the negative frequency drift may not be observed on earth. The range of decametric frequencies excited in one storm depends both on the width of the Alfvén wave front (which is probably of the order of the mean free path of a plasma particle with thermal velocities) and the rate at which the energy of the Alfvén wave is dissipated. In order to evaluate the second effect a non-linear

analysis of the generation mechanism of the coherent cyclotron radiation would be required. It seems, however, likely that the length over which the energy of the Alfvén wave is dissipated is larger than the width of the Alfvén wave, because the mean free path of the thermal protons in the ionosphere is of the order of 10^6 /N [km]. For N = 10^4 cm^{-3} the width of the front is about 100 km. Assuming that all the electrons in the front radiate at the local gyrofrequency this corresponds to a range of frequency $\frac{\Delta f}{f} \simeq 4 \times 10^{-3}$ or $\Delta f \simeq 0.1$ MHz. This is the average bandwidth of a decametric storm.

The frequency time spectra on earth represent a superposition of many events, because Io continuously emits hmd waves. Assume that the growth rate of the decametric radiation becomes large enough for the radiation to be detected on earth, when the density increases above a value ϱ'_o. Denote the height at which $\varrho = \varrho'_o$ as h'. If the magnetic dipole is displaced towards a longitude $\lambda_o = 235^o$ then the magnetic field at h' will vary as a function of longitude. Thus the frequency f at which the radiation is observed ($f = \frac{e B}{2\pi m_e} (1 + V_A^2/c^2)$) will also vary. It will be a maximum when the radiation is generated at the longitude λ_o and a minimum 180^o away. When the radiation is generated at λ_o, Io is above $\lambda_o + \phi$ longitude. When Io moves away from this position the frequency at which the Io controlled storms start decreases. Now, the frequency range which can be excited depends on the length over which the energy of the Alfvén waves is dissipated. Certainly this is related to the energy contained in the hmd wave when it enters the dense parts of the ionosphere. Since the energy flux of the

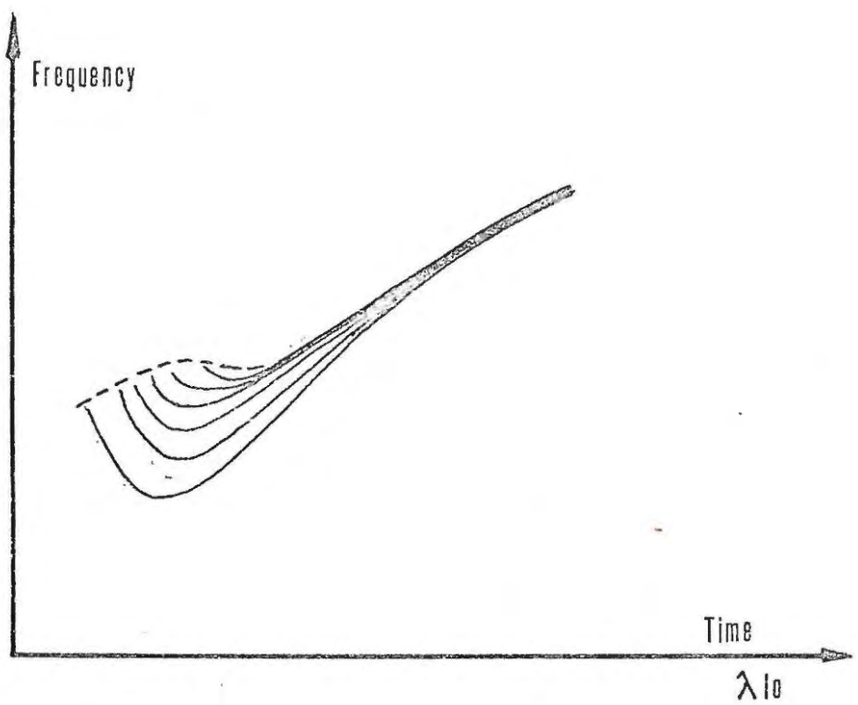

Figure 52: Theoretical frequency-time structure of a decametric storm.

hmd waves has a maximum value when Io is above 200° λ III (in the morning side of Jupiter) the range of decametric frequencies excited should be large at this λ Io and smaller everywhere else. Thus one would expect a frequency-λIo spectrum from the early (B) source as shown in figure (52). This is indeed observed. (Warwick 1967, Carr and Gulkis, 1967.) The main (A) source does not show this effect very clearly, although it should be expected in terms of this model. The lack of this characteristic frequency spectrum in the A source is probably due to the fact that the A source does not only contain Io controlled radiation but also a large amount of radiation independent of Io.

6.4.1 S-Pulses

One of the most puzzling aspects of the Jovian decametric radiation is the existence of drifting millisecond (S) bursts. The drift rate of $\frac{df}{dt} \lesssim -25$ MHZ s^{-1} may be explained as due to keV electrons spiralling through Jupiter's magnetic field (Ellis, 1965). If the observed frequency is related to the local magnetic field, i.e. if the radiation is assumed to be emitted at the electron cyclotron frequency, then the negative drift rate requires electrons moving away from Jupiter. The velocity of these electrons parallel to the magnetic field lines must be about 0.2 c (Warwick, 1970). There are, however, some objections to this interpretation of drifting millisecond pulses as Warwick (1970) pointed out.

There are 6 major characteristic features connected with the S-bursts, which any satisfactory model should be able to explain.

1. The duration of a single S-burst at a fixed frequency is 4 ms or even much less.

2. The repetition rate of the bursts at a fixed frequency is about 100 s^{-1}.

3. The bursts drift in frequency with a drift rate between -10 and -50 MHz s^{-1}

4. S-bursts are of extremely high intensity; their intensity is greater than that of ordinary Jovian emission by a large factor.

5. The S-burst activity is restricted to a narrow Io - Jupiter - Earth geometry range. They are only observed when Io is close to the Jovian longitude of 230°. (Riihimaa et al, 1970).

6. Some S-burst events show the phenomena of polarization diversity (Gordon and Warwick, 1967).

The fact that S-bursts often appear to be superimposed on normal Jovian emission makes it unlikely that S-bursts are due to a completely different generation mechanism from that of normal emission events.
The first aspect can be explained as due to the narrow bandwidth of the S-bursts and their drift rate. The bandwidth of the millisecond bursts seems to be 100 kHz or less. Thus the bursts will appear for less than 4 ms (df/dt = -25 MHz/s) on a fixed frequency receiver with bandwidth less than 100 kHz. Thus, if one can explain the narrow bandwidth and the drift rate of S-bursts, one can also explain their short duration.

The high intensity of the S-pulses appears to be either due to a focusing or beaming effect of normal radiation. This together with point 5 indicates that S-pulses could be normal events taking place in a certain region of Jovian longitude which allows for a particular kind of focusing or beaming. Only when Io is

above this longitude range will the disturbance created by Io cause radiation which appears as S-burst activity.

The polarization diversity could be due to mode coupling of the extraordinary mode in regions of a rapid change of the index of refraction and subsequent Y - 1 Faraday effect. (Warwick, 1970.)

The following is a rather speculative attempt to explain the major features of the S-bursts in terms of the present model.

In the last sections it was shown that the decametric radiation is emitted into a conical sheet making an angle of $\vartheta = 75^{\circ}$ with the direction of the magnetic field, as seen from Jupiter. The angular thickness of that cone may be large or small ($\Delta\vartheta: 0^{\circ} \ldots 20^{\circ}$). The radiation is travelling towards the planet. In order to be observed by an observer on earth it has to be reflected at the level where the Doppler shifted frequency f equals the upper hybrid frequency. If the radiation is reflected at one level, the radiation cone will just reverse its direction without a major change of intensity (if anything the intensity will decrease) or beaming characteristic. If, however, the plasma exhibits some kind of regular stratification, i.e. layers of increased plasma density (or increased magnetic field intensity) perpendicular to the magnetic field, one would expect multiple reflections from the different layers. The waves reflected at different layers will form a far field interference pattern which sweeps across the antenna of an observer on earth. The far field interference pattern can be described by treating the layer structure as a kind of "lattice". The condition for an interference maximum to be observed at an

angle β in the frame can be written as (see figure 53)).

$$(6.12) \qquad 2L\mu \sin\beta = n\lambda_0 = nc/f$$

where μ is the index of refraction, L the "lattice constant" and λ_0 the wavelength of the radiation. We thus get

$$(6.13) \qquad f = \frac{c}{2L\mu \sin\beta}\, n$$

For $\mu \simeq 1$ and β between 5° ..... 20° one will pick up only a limited number of interference maxima at a particular frequency. Formula (6.12) allows us to calculate the frequency drift an observer would observe, when the far field interference pattern moves across his telescope.

$$(6.14) \qquad \frac{1}{f}\frac{df}{dt} = -\frac{1}{L}\frac{dL}{dt} - \cot\beta\,\frac{d\beta}{dt}$$

Formulae (6.12) to (6.14) relate the frequency and its drift to a change of either the "lattice constant" L or the diffraction angle β. They are valid in the frame in which the lattice is stationary. Then the far field interference pattern consists of two parts: the first is due to the superposition of the radiation transmitted at each layer (corresponding to lattice diffraction in transmission) and the other is due to the superposition of the reflected beams. The reflected radiation, however, will be reflected into the source of the radiation where it interacts with the plasma in a way determined by the plasma. It will either be reflected or re-emitted. The interference pattern will probably be destroyed in this process. Hence only the transmitted radiation will form an interference pattern.

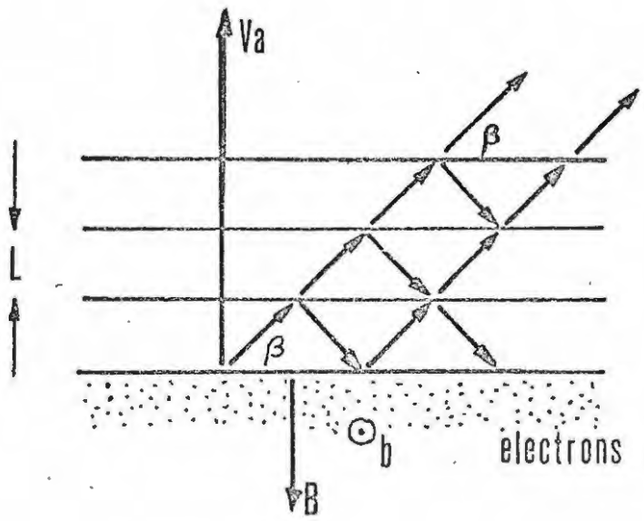

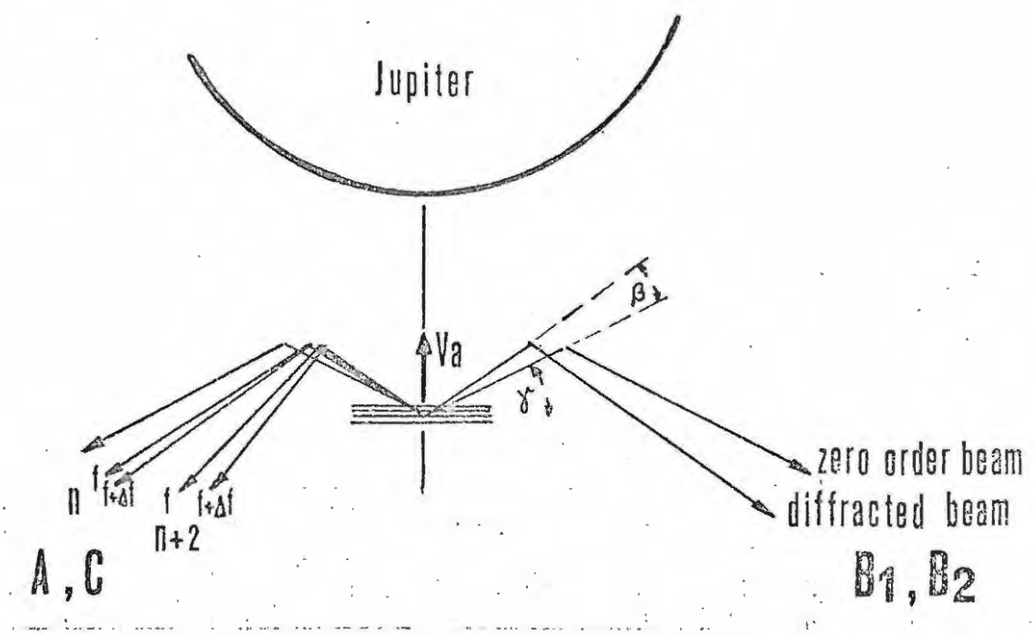

Figure 53: The generation of S-bursts. See text for explanation.

This beam will find a conical sheet in Jupiter's frame with an opening angle $\gamma = \frac{\pi}{2} - (\frac{V_A}{c} + \beta)$. The zeroth order beam has $\gamma_0 = \frac{\pi}{2} - \frac{V_A}{c}$. The beam reflected from the "lattice" will be contained in the zeroth order beam. When the Alfvén waves move towards the planet V_A decreases and γ increases. γ is related to μ in such a way that increasing γ increases μ. An observer on earth receives radiation only when the radiation is beamed towards him. Neglecting the rotation of Jupiter on time scales of milliseconds, the observer on earth will only remain in the beam if the increase of γ due to the decrease of V_A is cancelled by a change of or by a change of β. For the interference pattern β must increase and according to (6.13) the frequency f must decrease. Thus if an observer on earth is in the transmitted beam he would observe a negative frequency drift.

A frequency drift can also be produced by the rotation of Jupiter (then $\frac{d\beta}{dt} = 1.6 \times 10^{-4}$ rad/s). For S-bursts $\frac{1}{f} \frac{df}{dt} \simeq -1$. Thus $\frac{d\beta}{dt}$ due to the rotation of Jupiter is much too small to explain the S-bursts. It may, however, be large enough to explain the slow frequency drift observed by Riihimaa et al. (1970). Furthermore, $\frac{d\beta}{dt}$ is of different sign for the B and C source, which both show a negative frequency drift. In order to evaluate (6.14) we must look for a mechanism which could produce the required stratification of the plasma in front of the advancing wave. It is known that in the front of large amplitude hydromagnetic wave pulses the magnetic field intensity does not change continuously from its undisturbed value to the value in the wave but rather exhibits an oscillatory structure (Karpman, 1964, and Cavaliere and Engelmann, 1967).

The magnetic profile of the wavefronts starts with small oscillations which are converted into a series of rarefaction waves. These convert the magnetic field from the undisturbed value to the value in the wave pulse. The separation of the crests in these rarefaction waves is of the order (Tverskoi, 1962 also Karpman, 1964).

$$L \approx \frac{V_A}{\Omega_i} = \text{const. } N^{-1/2} \tag{6.15}$$

The rarefaction waves are damped due to electron-ion collision. The length over which the amplitude of the rarefaction waves decreases by 1/e is

$$\ell \simeq \frac{V_A}{\nu_{ei}} \frac{m_e}{m_i} \tag{6.16}$$

ν_{ei} is the electron ion collision frequency. A well-defined stratification will only be formed if $L \ll 1$, i.e. if $\Omega_i \gg \nu_{ei} \frac{m_i}{m_e}$. In the ionosphere $\nu_{ei} \approx 10^{-3} N$ (for a temperature of $T_e = T_i = 1\,500$ K), where N is the particle density in cm^{-3}. The condition for the stratification in front of the Alfvén to exist is thus

$$\Omega_i \gg 2N \tag{6.17}$$

when Ω_i is measured in $/s^{-1}/$ and N in $/cm^{-3}/$

If the magnetic dipole is displaced towards the longitude 235° λ III the ratio Ω_i/N at a particular height above the planet's surface (that is where N has a certain value independent of longitude) has a maximum at the longitude 235°. If the regular stratification forms at all, it will form when the Alfvén waves impinge onto the ionosphere at a longitude 235° λ III. Io is then above 235° + $\phi \approx$ 250° λ III. If the S-pulses are related to the diffraction at the

regular stratification, they should predominantly occur around 250° λ Io. This is indeed the case (see figure (12)). As the Alfvén waves move towards the planet Ω_i/N becomes smaller, and the condition (6.17) may not be fulfilled when the waves pass a certain level. This indicates that S-bursts should only appear within a certain frequency range, the upper limit of which is determined by (6.17) and the lower is determined by the condition $\alpha > \alpha_{cr}$ (α is the amplification coefficient of the cyclotron instability).

The drift rate of the S-bursts which is to be expected from (6.14) and (6.13) and (6.15)

$$d\beta = -\frac{1}{c} V_A$$

$$\frac{1}{f}\frac{df}{dt} = \left\{ \frac{1}{2}\frac{1}{N}\frac{dN}{dt} \right\} + \frac{\cot\beta}{c}\frac{dV_A}{dt}$$

Now:

$$\frac{d}{dt} = V_A \frac{d}{dx} = -V_A \frac{d}{dh}$$

(6.18)
$$\frac{1}{f}\frac{df}{dt} = -\frac{1}{2}\frac{V_A}{N}\frac{dN}{dh} - \frac{V_A}{c}\cot\beta\frac{dV_A}{dh}$$

In the ionosphere the variation of V_A is mainly determined by the variation of N ($V_A \propto N^{-\frac{1}{2}}$) because the magnetic field intensity B changes only by a factor of 2 in the ionosphere as compared with a factor of 10^3 for the density variation. Assuming B to be constant in the ionosphere (6.18) is then rewritten as:

(6.19)
$$\frac{1}{f}\frac{df}{dt} = \frac{dV_A}{dh}\left(1 - \frac{V_A}{c}\cot\beta\right)$$

The drift rate is negative when $\frac{V_A}{c}\cot\beta > 1$. β can be estimated as follows:

The observed S-pulses appear at different frequencies at the same time. The separation in frequency of two pulses is $\Delta f = \left|\frac{df}{dt}\right| \tau$ where τ is the time between the appearance of two pulses at a fixed frequency. $\left|\frac{df}{dt}\right| = 25\ \mathrm{MHzs}^{-1}$ and $\tau \approx 10^{-2}\mathrm{S}$ gives $\Delta f = 0.25$ MHz. Then $\frac{\Delta f}{f} = \frac{\Delta n}{n} \approx \frac{1}{100}$ with $\Delta n = 1$ this yields $n = 100$.

From (6.12) $$\frac{1}{\sin\beta} = \frac{2Lf}{cn} = \frac{V_A}{\pi nc}\,\frac{m_i}{m_e} = 6\,\frac{V_A}{c}$$

for $n = 100$. Then the drift rate is according to (6.19))

$$\frac{1}{f}\,\frac{df}{dt} = \frac{d\,V_A}{dh}\left(1 - 6\left(\frac{V_A}{c}\right)^2\right)$$

An observer on earth will, however, see the Doppler shifted frequency $f = f_e\left(1 + {V_A}^2/c^2\right)$ and a drift rate

$$(6.20)\quad \frac{1}{f}\,\frac{df}{dt} = \frac{dV_A}{dh}\left(1 - 2\left(3 + \frac{2}{1+x}\right)x\right)$$

where $x = \left({V_A}/{c}\right)^2$. The drift rate will be negative only for large values of x, i.e. at the top of the ionosphere, where $x \simeq 0.16$ and $\frac{dV_A}{dh} \approx 3.....5$ /sec^{-1}/.

The drift rate calculated from (6.20) is then

$$\frac{1}{f}\,\frac{df}{dt} = -1.6 ..... -2.6 \quad /s^{-1}/$$

This is only slightly larger than the observed drift rate. The observed drift rate seems to be constant throughout a particular S-pulse event. The predicted drift rate (6.20) is not constant along a particular field line. The change in drift rate predicted by (6.20) may, however, not be observable because the generation of S-bursts is restricted to a narrow range of heights over which the change of $\frac{df}{dt}$ is small. The determination of the drift rate from swept-frequency

recordings of the decametric radiation is not very accurate and a slight change of $\frac{df}{dt}$ may well have been overlooked. The narrow band width of the S-bursts can be related to the "resolving power" of the "lattice". If there are m planes at which reflection of the radiation occurs the frequency resolution in the nth diffraction maximum is $\frac{\delta f}{f} = \frac{1}{nm}$. The bandwidth must be much smaller than Δf in order for the S-bursts to be observable. The bandwidth of S-pulses seems to be smaller than 100kHz. That is $\frac{\delta f}{f} < 1/250$. n was estimated at 100. In order to account for the narrow bandwidth there must be at least 3 well defined layers in front of the hydromagnetic waves, i.e. $\ell \geq 3L$. Since this explanation of the S pulses involves the superposition of many waves as any interference phenomenon does, the increased intensity of the S-burst is to be expected. It has been mentioned by Warwick (1970) that the polarization diversity of the S-pulses may be due to mode coupling at steep gradients of the plasma density or the magnetic field intensity. Exactly this is encountered in the layers. The S-pulses occur on time scales of milliseconds and are possibly due to interference effects in the front of a single advancing hmd wave. But Io continuously emits hmd waves. There may also be effects producing far-field interference pattern which are stable on time scales of minutes. These may, of course, contain the interference pattern stable only on time scales of milliseconds. If the interference pattern produced by many hmd waves is indeed stable over minutes; that is: if there is coherence between the Alfvén waves emitted by Io over the times of the order of minutes, we expect the interference pattern to be swept across the antenna beam of an observer on earth by Jupiter's rotation. In this case $\frac{d\beta}{dt} = 1.6 \times 10^{-4}\ s^{-1}$.

It is tempting to relate this to the lanes in the frequency time spectra observed by Riihimaa et al. (1970). They have been observed $\Delta f/f = 1/75$; i.e. n = 75. The lanes are observed in the frequency range 20 - 25 MHz. In the ionosphere this corresponds to a level where $V_A > 0.4$ c. Thus $\cot\beta \sim 10$ and the drift rate $\frac{1}{f}\frac{df}{dt} = \cot\beta \frac{d\beta}{dt} \simeq 1.6 \times 10^{-3}$ s^{-1} . This is slightly less than the observed drift rate but not entirely wrong. The drift rate for the B1 and B2 source should be positive and negative for the A and C source. This is indeed observed. The lanes have a larger bandwidth than the S-bursts. Thus the requirement that there should be a sufficient number of layers in front of the Alfvén waves does not apply here. The lanes are then not restricted to sub-Io longitudes where Ω_i/N is large. They also appear when the Alfvén waves excite cyclotron radiation in regions where Ω_i/N is small.

It should be mentioned, that diffraction at a lattice-like stratification of the Jovian ionosphere, has already been suggested by Riihimaa et al. (1970), as a possible explanation of the lanes in the frequency time spectra. The present model does allow for this "lattice" in a simple way, whereas it was only postulated by Riihimaa et al. There is also a difference between the two models in so far as the present model is based on a moving "lattice" whereas the "lattice" is stationary in the model by Riihimaa et al.

The explanation of the S-bursts described above has many weak points. The drift rate should not be strictly constant. The exact value for the drift rate is derived from the model only through squeezing the right numbers. It is also questionable that the oscillatory structure in front of the Alfvén wave pulse

produces strong diffraction effects. The reason for the inclusion of the above speculation into this thesis is only the fact that the explanation of many of S-bursts would be possible if the described stratification has the correct size and produces strong diffraction effects.

SUMMARY

A new model of the Io-controlled Jovian decametric radiation is proposed. The model incorporates the following ideas

1. The Jovian ionosphere is not isothermal and cold. Due to absorption of solar U.V.-radiation the temperature of the plasma increases with height in a way similar to the increase of plasma temperature in the terrestrial ionosphere. The maximum plasma density in the ionosphere is about 3×10^6 particles cm^{-3}. The plasma temperature in the top-side ionosphere may be as high as 1 500 K.

2. There is a considerable loss of thermal plasma from the topside ionosphere. This loss must be balanced by an upward diffusion of particles. The Jovian ionosphere is not in static equilibrium.

3. The thermal plasma in Jupiter's magnetosphere is unstable against the two-stream instability. Growing waves feed on the streaming energy of the plasma. This energy loss of the plasma leads to a trapping of plasma in the outer parts of the magnetosphere.

4. The trapped plasma forms a Gledhill disk corotating with Jupiter. The plasma density in the disk is limited by recombination. At Io's orbit the plasma density may be as high as 10^3 particles cm^{-3}. The magnetosphere so derived is stable against interchange motions.

5. Io's interaction with the magnetosphere is considered. Io impedes the corotating plasma and magnetic field. Low frequency Alfvén waves transmit the information about Io's contact with the magnetic

field line along the field line into the ionosphere. The Alfvén waves are reflected there and propagate back to Io, where they are regenerated again and so forth. The magnetic field lines intersected by Io will be tilted in this process. This tilting continues until the field lines either diffuse through Io or are reconnected through a neutral point formed on the downstream side of the satellite. If Io's conductivity is larger than $5 \times 10^{-5}\ \Omega^{-1}\ m^{-1}$ reconnection will take place before diffusion. The reconnection rate is enhanced by the emission of large amplitude Alfvén waves with frequencies of the order of one Hz.

6. The amplitude and frequency of these Alfvén waves generated at the neutral point vary as Io orbits around Jupiter due to the varying plasma density encountered by Io along its orbit.

7. The propagation of these Alfvén waves through the magnetosphere along the field lines is investigated. The magnetosphere can be trated as a WKB medium. The inclusion of the Hall effect predicts a spreading of the energy contained in the Alfvén waves into a conical sheet about the magnetic field line. This spreading together with the WKB solution of the Alfvén wave equation is used to determine the (magnetic) amplitude of the Alfvén waves by the time they reach the topside ionosphere.

8. The Alfvén waves will be partly reflected at and partly transmitted across the boundary region between the ionosphere and magnetosphere. Transmission coefficients are used to predict the (magnetic) amplitude of the Alfvén waves transmitted into the dense parts of the ionosphere. The ionosphere is pervious only to high frequencies.

9. The amplitude is then related to the growth rate of coherent cyclotron radiation in the fronts of the Alfvén waves propagating through the ionosphere. The variation of the growth rate as a function of sub-Io longitude is then calculated. This is compared with the observed "sources" of the Io-controlled decametric radiation. The agreement is found to be good.

10. The variation of highest cut-off frequency is explained in terms of the model. Observed frequency-time spectra are also found to be in agreement with the predictions of the model.

11. It is tentatively proposed that there are regular stratifications in the fronts of the advancing Alfvén waves. These stratifications may give rise to interference effects which could explain the S-bursts and the lanes observed in the frequency-time spectra of the decametric radiation. It is shown that the model predicts the observed duration, band-width and frequency drift of the S-bursts. The restriction of S-bursts to the B2 and C "sources" can also be accounted for by the model.

LIST OF REFERENCES

ANGERAMI, J.J. and THOMAS, J.O. 1964, J.G.R. 69, 4537.

BAART, E.E., GREENER, J.G. and WULFF, A. 1971, submitted to Astrophys. Letters.

BAILEY, V.A. 1950, Phys. Rev. 78, 428.

BAUM, W.A. and CODE, A.D. 1953, Astr. J. 58, 108.

BRATENAHL, A. and YEATES, C.M. 1970, Phys. Fluids, 13, 2696.

BRICE, N.M. 1968, Cornell University, CSUAC Rept. 124.

BROWN, G.W., CARR, T.D. and BLOCK, W.F. 1968, Ap. Letters, 1, 89.

BULLARD, E. 1967, Quart. J. Roy. Astr. Soc, 8, 143.

BURKE, B.F. and FRANKLIN, K.L. 1955, J.G.R. 60, 213.

CARR, T.D. and GULKIS, S. 1970. Ann. Rev. of Astron. and Astrophys. 8, 577.

CAVALIERE, A. and ENGELMANN, F. 1967, Nuclear Fusion, 7, 137.

CLEMMOW, P.C. and DOUGHERTY, J.P. 1969, Electrodynamics of Particles and Plasmas, Addison-Wesley, London.

DEIFT, P.A. 1971, M.Sc. thesis, Rhodes University, S.A.

DONIVAN, F.F. and CARR, T.D. 1969, Astrophys. J. (Letters), 157, L65.

DOUGLAS, J.N. and SMITH, H.J. 1967, Astrophys. J. 148, 885.

DULK, G.A. 1969, Astrophys. J. 159, 671.

DUNGEY, J.W. 1968, Cosmic Electrodynamics, C.U.P.

ELLIS, G.R.A. 1965, Radio Science 69D, 1513.

ENCRENAZ, Th., GAUTIER, D., VAPILLON, L. and VERDET, J.P. 1970, Astron. and Astrophys. 11, 431.

FRIEDMAN, M. and HAMBERGER, S.M. 1968, Astrophys. J. 152, 667.

GEISLER, J.E. and BOWHILL, S.A. 1965, J. Atmosph. Terr. Phys. 27, 457.

GILLET, F.C., LOW, F.J. and STEIN, W.A. 1969, Astrophys. J. 157, 925.

GLEDHILL, J.A. 1967, GSFC Rept. X-615-296.

GOERTZ, C.K. 1971, Nature P.S. 229, 151.

GOLDREICH, P. and LYNDEN-BELL, D. 1969, Astrophys. J. 156, 59.

GREEN, T.C. and SHERRILL, W.M. 1969. Astrophys. J. 158, 351.

GROSS, S.H. and RASOOL, S.I. 1964, Icarus, 3, 311.

GRUBER, G.M. 1966, Ph.D. Thesis, Rhodes University, S.A.

HASCHICK, A. 1970. Honours Project, Rhodes University, S.A.

HERMAN, J.R. and CHANDRA, S. 1969, Planet. Space Sci. 17, 815 and 1247.

HERMAN, J.R., HARTLE R.E. and BAUER, S.J. 1971, Plan. Space Sci, 19, 443.

HILL, I. 1969, M.Sc. Thesis, Rhodes University, S.A.

HOGAN, J.S., RASOOL, S.I. and ENCRENAZ, Th. 1969, J. of Atm. Sci. 26, 898.

JEFIMENKO, O.D. 1966, Electricity and Magnetism, Appleton-Century-Crofts, New York.

JOHNSON, F.S. 1961, Astrophys. J. 133, 701.

KARPMAN, V.I. 1964, Sov. Phys.-Techn. Phys. 8, 715.

KRAUSS, J.D. 1966, Radio Astronomy, McGraw Hill, New York.

LIGHTHILL, M.J. 1960, Phil. Trans. Roy. Soc. London A, 252, 397.

MARSHALL, L. and LIBBY, W.F. 1967, Nature, 214, 126.

MARUBASHI, K. 1970, Rept. Ionosphere Space Res. Japan, 24, 322.

McELROY, M.B. 1969, J. of Atm. Sci. 26, 798.

MELROSE, D.B. 1967, Planet. Sp. Sci. 15, 381.

MONTGOMERY, D. 1959, Phys. Rev. Letters, 2, 36.

NESS, N.F. BEHANNON, K.W., SCEARCE, C.S. and CANTARANO, S.C. 1967, J.G.R. 72, 5769.

NEUFELD, J. and WRIGHT, H. 1963, Phys. Rev. 129, 1489.

PARKER, E.N. 1960, Astrophys. J. 132, 821.

PETSCHEK, H.E. 1964, in AAS-NASA Symposium on the Physics of Solar Flares, edited by W. Hess, NASA)SP50, 425.

PETSCHEK, H.E. and THORNE, R.M. 1967, Astrophys. J. 147, 1154.

PIDDINGTON, J.H. 1967, U. of Iowa Rept. 67-63.

PIDDINGTON, J.H. and DRAKE, J.F. 1968, Nature, 217, 935.

PIDDINGTON, J.H. 1969, Cosmic Electrodynamics, Wiley, New York.

RIHIMAA, J.D., DULK, G.A. and WARWICK, J.W. 1970, Astrophys. J. Supplement Series No. 172, 19, 175.

SCHMAHL, E.J. 1970, Ph.D. thesis, U. of Colorado, U.S.A.

SHERRILL, W.M. 1965, Astrophys. J. 142, 1171.

SLEE, O.B. and HIGGINS, C.S. 1966, Australian J. Phys. 19, 67.

SWEET, P.A. 1958, NUOVO Cimento Suppl. 8, Ser. X, 188.

TRAFTON, L.M. 1967, Astrophys. J. 147, 765.

TRAKHTENGERTS, V. Yu. 1966, Sov. Astr.-AJ, 10, 281.

TVERSKOI, B.A. 1962, Sov. Phys.-JETP, 15, 581.

WARWICK, J.W. 1961, Ann. N.Y. Acad. Sci. 95, 39.

WARWICK, J.W. 1964, Ann. Rev. of Astron. and Astrophys. 2, 1.

WARWICK, J.W. 1967, Space Sci. Rev. 6, 841.

WARWICK, J.W. 1970. NASA CR-1685.

WILSON, R.G., WARWICK J.W., DULK, G.A. and LIBBY, W.F. 1968, Nature, 220, 1218.

ZHELEZNYAKOV, V.V. 1970, Radio Emission of the Sun and the Planets, Pergamon Press, Oxford.

APPENDIX A

If we assume that f_M is the electron gyrofrequency at the point of emission, we can calculate from the observed variation of f_M with λ Io the variation of emission radius r. Let us first calculate r in a coordinate system S" with the magnetic dipole as the origin. In this frame the equation of a magnetic line of force for a dipole field is:

$$(1) \quad r = L R_J \sin^2 \ominus$$

where L is a constant which gives the distance from the dipole axis, in equatorial planetary radii (R_J), at which the line of force cuts the (magnetic) equatorial plane. $\ominus$ is the (magnetic) colatitude. For IFT L varies as a function of λIo due to the tilt of the magnetic dipole axis (M) with respect to the rotational axis (R) of the planet (see figure 54). The distance (r") from Io to the centre of the magnetic dipole is given by

$$(2) \quad r''^2 = ((5,9)^2 + \delta^2 - (2 \times 5,9) \times \delta \cos(\lambda_{Io} - \lambda_o)) R_J^2$$

(Io orbits Jupiter at a distance $5,9R_J$)

The magnetic colatitude of Io varies as the satellite orbits around the planet in the following way

$$(3) \quad \cos \ominus = \sin \alpha \sin(\lambda_{Io} - \lambda_T)$$

From (1), (2), and (3) L_{IFT} can be calculated as

$$(4) \quad L_{IFT} = \frac{r''}{R_J} \frac{1}{1 - \sin^2 \alpha \sin^2(\lambda_{Io} - \lambda_T)}$$

For a dipole field the magnetic field intensity B at a point $(r, \ominus)$ along IFT is given by

$$(5) \quad B = B_o \left(\frac{R_J}{r}\right)^3 (1 + 3 \cos^2 \ominus)^{\frac{1}{2}}$$

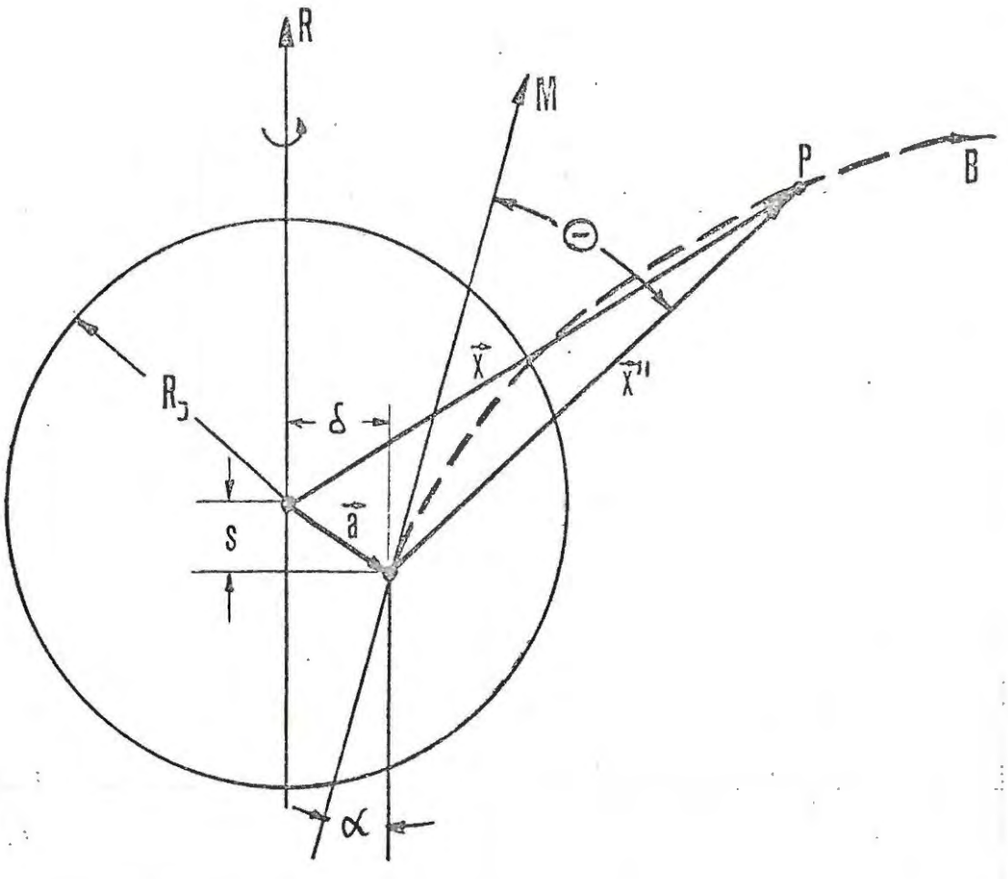

Figure 54.

with (1) this can be rewritten as

$$(6) \quad B = B_o \left(\frac{R_J}{r}\right)^3 \left(1 + 3(1 - r''/L_{IFT} R_J)\right)^{\frac{1}{2}}$$

B_o is the magnetic field intensity at the magnetic equator. As f_M is assumed to be proportional to B we can write

$$(7) \quad \frac{f_M}{f_o} = \frac{B}{B_o} = \left(\frac{R_J}{r}\right)^3 \left(1 + 3(1 - r''/L_{IFT} R_J)\right)^{\frac{1}{2}}$$

From (7) the variation of r" with λ_{Io} can be determined from the observed variation of f_M with λ_{Io} if a particular f_o (usually f_o = 40 MHz) is assumed. The point of emission P has the position (X") in the cartesian coordinate system with the magnetic axis (M) as the 2 axis, the y and 2 axes define the meriodianal plane λ_T. The x axis completes a normal cartesian coordinate system. Then :

$$(8) \quad \vec{X}'' = \begin{Bmatrix} r \sin\Theta \sin(\lambda_T - \lambda_{Io}) \\ r \sin\Theta \cos(\lambda_T - \lambda_{Io}) \\ r \cos\Theta \end{Bmatrix}$$

The position (X) of P in a coordinate system (S) with the planet's centre as the origin can be determined easily by noting that S" is derived from S by a displacement through ($\vec{a}$) and a tilt by α about the x axis of S". In the system S' which is untilted but displaced P has the position X'

$$(9) \quad \vec{X}' = \begin{pmatrix} 1 & 0 & 0 \\ 0 & \cos\alpha & 0 \\ 0 & 0 & \cos\alpha \end{pmatrix} \vec{X}''$$

In the system S P has the position $\vec{X}$

$$(10) \quad \vec{X} = \vec{X}' + \vec{a}$$

where $\vec{a}$ is the position of the magnetic dipole centre in the system S (see figure 54):

$$(11) \qquad \vec{a} = \begin{Bmatrix} \sin(\lambda_T - \lambda_o)\ \delta \\ \cos(\lambda_T - \lambda_o)\ \delta \\ S \end{Bmatrix}$$

The height (h) of P above Jupiter's surface is then

$$(12) \qquad h = \left|\vec{x}\right| - R_J$$

APPENDIX B

Gross and Rasool (1964) give the following reactions as important in the Jovian ionosphere:

1) $H_2 + h\nu \rightarrow H_2^+ + e^-$ $\quad \sigma(H_2) = (4.10^{-18})\ cm^2 \quad \sigma = \sigma(\lambda)$

2) $H + h\nu \rightarrow H^+ + e^-$ $\quad \sigma(H) = (2.10^{-18})\ cm^2 \quad \sigma = \sigma(\lambda)$

3) $H_e + h\nu \rightarrow He^+ + e^-$ $\quad \sigma(He) = (3.10^{-18})\ cm^2 \quad \sigma = \sigma(\lambda)$

4) $He^+ + H_2 \rightarrow He + H_2^+$ $\quad \alpha_4 = 10^{-13}\ cm^3\ s^{-1}$

5) $He^+ + H_2 \rightarrow HeH^+ + H$ $\quad \alpha_5 = 10^{-12}\ cm^3\ s^{-1}$

6) $H_2^+ + H_2 \rightarrow H_3^+ + H$ $\quad \alpha_6 = 5 \times 10^{-10}\ cm^3\ s^{-1}$

7) $H_2^+ + H \rightarrow H^+ + H_2$ $\quad \alpha_7 = 10^{-10}\ cm^3\ s^{-1}$

8) $H_2^+ + He \rightarrow HeH^+ + H$ $\quad \alpha_8 = 10^{-10}\ cm^3\ s^{-1}$

9) $H_2^+ + e \rightarrow H' + H''$ $\quad \alpha_9 = 10^{-8}\ cm^3\ s^{-1}$

10) $HeH^+ + e \rightarrow He + H$ $\quad \alpha_{10} = 10^{-8}\ cm^3\ s^{-1}$

11) $He^+ + e \rightarrow He + h\nu$ $\quad \alpha_{11} = 5 \times 10^{-12}\ cm^3\ s^{-1}$

12) $H_3^+ + e \rightarrow H_2 + h\nu$ $\quad \alpha_{12} = 10^{-8}\ cm^3\ s^{-1}$

13) $H^+ + e \rightarrow H + h\nu$ $\quad \alpha_{13} = 5 \times 10^{-12}\ cm^3\ s^{-1}$

14) $H + H + X \rightarrow H_2 + X$ $\quad \alpha_{14} = 10^{-32}\ cm^6\ s^{-1}$

The amount of H produced by the absorption of solar UV radiation can be calculated by noting that each ionized H_2 and He will produce 2 H atoms (reactions 5, 6, 8, 10, 12). The variation of neutral density with height z is calculated by assuming diffusive equilibrium for each component. This may lead to densities which are too large at large heights. (The decrease of density due to escape from the planet is neglected.) At these heights the ionization is however determined mainly by diffusion.

The continuity equation has the general form for a static ionosphere below the level of maximum density.

15) $\frac{\partial n_s}{\partial t} = Q(X_s) - L(X_s) = 0$ for equilibrium

where $Q(X_s)$ is the ionization rate of the component X_s and L is the loss rate by one of the reactions (4) - (14). For equilibrium ($\frac{\partial n}{\partial t} = 0$) the electron density is given by (see Gross and Rasool (1964)).

16) $$N_e = \left(10^8 \left(Q(He) + \frac{Q(H_2)\ 5n(H_2) + n(He)}{5n(H_2) + n(H) + n(He)} \right) + 10^{12} \left(Q(He) + \frac{n(H)\ Q(H_2)}{5n(H_2) + n(H)} \right) \right)^{1/2}$$

where the ionization rate is given by

17) $$Q(Xs) = \int_0^{\lambda_{cr}} n_z(X_s)\ \sigma_\lambda(X_s)\ \Phi_\infty(\lambda)\ e^{-\tau_z(\lambda)}\ d\lambda$$

$n_z(X_s)$ density of component X_s at level z $[cm^{-3}]$

$\sigma_\lambda(X_s)$ Ionization cross section at the wavelength $[cm^2]$

$\Phi_\infty(\lambda)$ Solar UV flux incident on top of ionosphere $[photons\ cm^{-2}\ s^{-1}]$

$\tau_z(\lambda)$ optical depth at the level z, which is a function of solar zenith angle.

The heat transport equations for the electrons, ions and neutrals are of the form

18) $$n_s k C_v \frac{\partial T_s}{\partial t} - \frac{\partial}{\partial z}\left(k_s(T_s) \frac{\partial T_s}{\partial z} \right) = Q_s - \sum_j L_{sj}$$

k : Boltzmann's constant

C_v: specific heat at constant volume

T_s: temperature of species s (K)

k_s: thermal conductivity of species s(ergs $cm^{-1}\ s^{-1}\ k^{-1}$)

Q_s: the heating rate of the species s(ergs $cm^{-1}\ s^{-1}\ K^{-1}$). For electrons the heating rate consists of both local and non local heating (see Geisler and Bowhill (1965)).

L_{sj}: the heat exchange rate due to collisions between the species s and j (ergs cm^{-1} s^{-1} K^{-1}).

For electrons:

19) $k_e = 2.6 \times 10^{-6} T_e^{5/2}$

20) $Q_e = \varepsilon_z \sum_j Q(X_j) + Q_{NL}$ (ergs cm^{-3} s^{-1})

ε_z : is the energy which an electron, just being stripped off from the atom (or molecule) j, has. It is a frunction of height z and is typically of the order of 1 .... 10 eV.

Q_{NL}: is the rate of non local heating due to unthermalized electrons passing through the plasma. The non local heating rate was calculated by a method similar to that given by Geisler and Bowhill (1965).

21) $L_{ei} = 8.2 \times 10^{-19} N_e n_i (T_e - T_i)/(A_i T_e^{3/2}) \ln \Lambda$

$A(H_2^+) = 2 A(H_4^+) = 4 A(H^+) = 1$

$$\ln \Lambda \simeq 15$$

(Herman et al. 1971)

The losses from electrons to the neutrals are given by

22) $L_{en} = 1.602 \times 10^{-12} N_e (T_e - T_N) \{6.43 \times 10^{-3} (T_e - T_n) + 1.8 \times 10^{-15} n(H_2) (1 + 4.3 \times 10^{-4} T_e) + 1.72 \times 10^{-14} n(H_2) T_e^{-\frac{1}{2}} + 2.46 \times 10^{-17} n(He) T_e^{\frac{1}{2}} + 9.63 \times 10^{-16} n(H) (1 - 1.35 \times 10^{-4} T_e) T_e^{\frac{1}{2}}\}$

(Herman et al. 1971)

The energy loss from H^+ to the neutral gas is given by

23) $L_{H^+n} = n(H^+)\ (T_H + - T_N)\ (4 \times 10^{-26}\ n(H)\ (T_{H^+} + T_N)^{\frac{1}{2}}$
$+ 1.4 \times 10^{-25}\ n(H_2) + 4.65 \times 10^{-26}\ n(He)$

The energy losses of H_2^+ and He^+ are neglected because of the small concentrations of these species.

The thermal conductivity of H^+ is given by

24) $k_{H^+} = 7.37 \times 10^{-8}\ T_{H^+}^{5/2}$

The heat conductivity of the neutrals is given by

25) $k_N = \dfrac{\sum_{s=1}^{3} F_s\ n\ (X_s)}{\sum_{s=1}^{3} n\ (X_s)}\ T_N^{\frac{1}{2}}$

$F_1 = F(H_2) = 1880$; $F_2 = F(He) = 875$; $F_3 = F(H) = 2080$ all in cgs units.

(see e.g. Herman et al. 1971)

The momentum and continuity equations have the general form in the steady state ($\frac{\partial}{\partial t} = 0$)

26) $V_s \dfrac{\partial V_s}{\partial z} = - \dfrac{\partial P_s}{\partial z} \quad m_s\ n\ (X_s)\ g + e\ n\ (X_s)\ E$

27) $\dfrac{\partial}{\partial z}\ (V_S\ n(X_s)) = Q(X_s) - L\ (X_s)$

with $N_e = \sum N_i$ (charge neutrality) which was used to derive (16) as a solution to the set of equations (15), and $P_s = n(X_s)\ k\ T_s$.